Dear Editor,

please find attached our modified version of the manuscript:

Validation of the Swiss Methane Emission Inventory by Atmospheric Observations and Inverse Modelling

S. Henne, D. Brunner, B. Oney, M. Leuenberger, W. Eugster, I. Bamberger, F. Meinhardt, M. Steinbacher, and L. Emmenegger

We uploaded a point-by-point reply to the referee comments.

We modified the manuscript largely following the suggestions by the referees. The comments of referee 1 largely added to the discussion of the obtained, whereas those of referee 2 helped to clarify the methodological description of our inverse modelling approach.

Since both referees requested minor changes no major changes to the manuscript where necessary so that the results remain largely unchanged, but the discussion is altered at some points according to the given suggestions. A track-changes version of the manuscript is attached, to highlight our minor modifications to the text.

We are confident that with the additional explanations given in the replies and in the modified text we can satisfy the requests of the referees and are looking forward to your response concerning publication of the manuscript in ACP.

Best regards,

Stephan Henne

Reply to Referee #1

Referee comment in bold, reply in plain text, *modified text for manuscript in italics*.

Henne et al. present a comprehensive analysis of 2013 Swiss methane emissions using atmospheric observations from the new CarboCount-CH measurement network. They perform a suite of inversions using different specifications of the uncertainty, definitions of the background, and inversion frameworks. Importantly, they find emissions that are consistent with the Swiss Greenhouse Gas Inventory (SGHGI). This is an excellent manuscript. It is well written, uses state-of-the-art inversion techniques, the figures are high quality, and demonstrates that well-informed bottom-up inventories can accurately represent the emissions. This manuscript should be published in ACP. The only comments I have are, seemingly, minor.

We would like to thank the referee for the positive review and will address all minor issues in the revised manuscript.

Best inversion?

It could be useful for the authors to suggest a "best" setup. This would help inform others doing similar atmospheric inversions. The authors may want to perform an additional inversion using the "best" setup. They currently say the best estimate is the mean over all sensitivity inversions (Page 35452, Lines 19-21). However, this seems a little odd because it means they don't actually have a map of their "best emissions". It seems like they could try one additional inversion using the setups that performed best (extKF, ML method, COSMO transport, seasonality, all sites, MAIOLICA, and Grid baseline).

Also, why don't the extended Kalman Filter inversions have Skill scores for FRU and GIM in Table 4?

Although there might be a best setup in the sense that its results are closest to the truth, this best setup is not known (as little as the truth is known). The ML method applied here is an objective method to tune the free parameters of an inversion but this doesn't necessarily correspond to the "best setup" since it cannot account for potential biases arising from transport errors or the problems in representing the release height of the particles. Our approach therefore was to provide a reference setup corresponding to our expert judgment of a best setup (as in many previous Bayesian inversion studies) but, in addition, to test a range of other setups and configurations that we consider similarly likely. We argue that the range of estimates from these individual setups provides a more realistic estimate of uncertainty than the analytical uncertainty of a single setup. We included these arguments more prominently at the beginning of the results section in the revised manuscript.

Our Kalman Filter inversion system is currently not able to consider additional validation sites and FRU and GIM would need to be validated manually. We did not consider this additional effort proportionate to the gained insights.

Unidentified source in north-eastern Switzerland

Page 35456, Lines 23-26: The authors mention that different manure management methods could lead to slight variations in emission factors. However, the differences due to manure management can be dramatic. Owen & Silver (2014) find orders of magnitude differences in the methane emission rate between anaerobic lagoons, slurry tanks, and manure piles (see their Fig. 3; Anaerobic lagoons emit at a rate about 35× larger than manure piles!). They also include a revised liquid manure slurry manure conversion factor that's about 2× larger than what's currently used by the European Union.

Have there been changes in the regional manure management practices (maybe due to a shift to more concentrated animal feeding operations)?

According to Daniel Bretscher from the Swiss institute Agroscope for agricultural research (which is responsible for collecting the information on Swiss GHG emissions from agriculture), no such changes in regional manure management practices occurred in Switzerland recently. Although different manure management methods may result in different emission factors, we have no indication that manure management practices vary strongly within Switzerland. Furthermore, the average emission rate for anaerobic lagoons given by Owen & Silver (2014) is associated with a rather large uncertainty as can be seen in their Fig. 3 but especially when comparing the range of individual values given in their table 2a. Considering this range the given average value should be taken with care. Most importantly, manure storage in anaerobic lagoons does not exist in Switzerland, where the largest contribution to CH_4 emissions originates from liquid/slurry manure (90 %, FOEN, 2015). The manure conversion factor given by Owen & Silver (2014) for liquid/slurry is about a factor of 2 larger than the one used in the Swiss inventory. However, the latter is based on country specific emission factors (Hiller et al., 2014) and some Swiss studies even suggest considerably lower emission factors (Zeitz et al., 2012). In addition, there seems to be no indication that liquid/slurry storage is more frequently used in Eastern Switzerland than elsewhere in the country. On the contrary, the discussed region can be characterised by more traditional farming practices, which may suggest a larger fraction of manure piles and, hence, smaller CH_4 emissions from manure storage. We included a reference to Owen & Silver (2014) in our revised discussion. The unidentified source will be subject of a follow-up project, which started earlier this year and will include additional CH_4 measurements to target this source.

Discussion of US ruminant and natural gas emissions

In Section 4.2 (Page 35454, Lines 23-25) and Section 5 (Page 35459, Lines 5-7), the authors mention that the findings of reduced ruminant emissions are in contrast to studies from the USA (Miller et al., 2013; Wecht et al., 2014; Turner et al., 2015). It's not clear to me that these results are actually inconsistent. Miller et al. (2013), Wecht et al. (2014), and Turner et al. (2015) all find that US methane emissions from ruminants are underestimated. However, the Turner et al. (2015) shows little-to-no change throughout Europe (see their Fig.3) in their coarse global inversion. Another paper (Alexe et al.,2015) also find a a large increase in US emissions and a decrease in the emissions across Europe (see their Fig. 6). This would imply that Swiss ruminant emissions are not underestimated (in agreement with the finding from Henne et al.). It seems

that it may just be different regional features, not something pervasive in inventories (which would make sense because countries have different reporting requirements).

We revised the text accordingly and included a reference Alexe et al. (2015). Note that the emission increments reported by Turner et al. (2015) and Alexe et al. (2015) for Europe and the US depend on the chosen a priori (EDGAR v4.2). While EDGAR v4.2 is somewhat lower than the official inventory in the US (Turner et al., 2015), it is about 35% higher than the total of all European inventories reported to UNFCCC (Bergamaschi et al., 2015). This needs to be taken into account when interpreting their results.

The authors present a similar argument in Section 4.2 (Page 35455, Lines 2-5) and Section 5 (Page 35459, Lines 16-20) for natural gas emissions from the distribution sector. The authors claim their findings are in contrast to studies from the USA, "This is in contrast to recent studies from the USA where a large underesimation of fugitive emissions was established in the inventories for different metropolitan areas (Wennberg et al., 2012; McKain et al., 2015) and fractional loss rates between 2.5 and 6% were established." However, the fractional loss rates from Wennberg et al. (2012) and McKain et al. (2015) are probably not representative of the average US leak rate. Wennberg et al. (2012) examined emissions from Los Angeles, a city with a lot of oil and gas activity (the Aliso Canyon leak is, anecdotal, evidence of this), and McKain et al. (2015) examined emissions from Boston, an old city with a lot of cast-iron pipes. So these studies are not necessarily indicative of a pervasive problem in the inventory, as implied by Henne et al.

We added a comment towards the lacking representativeness of the mentioned US studies. However, we still feel that this is a more general problem for the US. Even if Boston is a relatively old city (obviously not as old as Basel or Zurich, but maybe that is not true for the gas distribution network) it is also one of the wealthier cities in the US and one may therefore expect a certain degree of modernisation. The main point we wanted to raise it that findings such as an underestimation of gas leak emissions observed in one country cannot easily be transferred to another country. We think this is an important message for the community. Note that the national inventories are often applying the same emission estimation methods based on default equations and parameters provided by the IPCC guidelines (known as "Tier 1" method) and thus one may expect that results obtained in one country may also be applicable in other countries. For losses from the gas distribution network, however, Switzerland applies a country-specific "Tier 2" method. It accounts, for example, for the fact that cast-iron pipes have gradually been replaced by polyethylene pipes which is expected to have reduced CH4 emissions from gas transmission and distribution by 36%. There are thus significant differences between countries regarding infrastructure and emission estimation methodologies, which is a strong motivation for country-specific studies as the one presented here.

Consider adding a brief discussion of Zavala-Araiza et al.

I feel like one of the biggest strengths of this paper is demonstrating the consistency between a well-informed bottom-up inventory and the top-down estimates. This was the main point of the

recent paper: Zavala-Araiza et al. (2015). It seems that this paper could be another one that demonstrates this point.

We added the findings of Zavala-Araiza et al. (2015) in our conclusions emphasising the common reconciliation of top-down and bottom-up.

Implementation of the inversion

On Page 35430 the authors state, "In our implementation of the inverse of S = MBMT − R, a L × L matrix, was calculated using LU factorisation (function DGESVX in LAPACK)." This seems like it may be an inefficient implementation. The DGESVX routine in LAPACK is for dense linear algebra. However, the matrices in atmospheric inversions are typically sparse (usually less than 1% of the elements are non-zero). I've found that I get a 31× speedup and use 17× less memory by just switching from dense to sparse matrices for large atmospheric inversions (KE > 2, 000, 000). There are also routines that allow for efficient solutions to large inverse problems with covariance matrices that can be represented as a Kronecker product (cf. Yadav & Michalak, 2013; they provide source code for the routines). The authors could also look into some of the multi-scale state vector design methods from Bocquet et al. (2011).

Bocquet et al. (2011) presented methods for optimally designing a multi-scale state vector that allowed information to transfer across scales. These are merely suggestions for future code development that may allow the authors to expand the scale of the problem (Increase the number of observation sites? Estimate monthly emissions? Expand the inversion domain?). The implementation presented here is sufficient to tackle the problem they are interested in.

We thank the reviewer for these very interesting remarks on the technical aspects of the inverse algorithm and will certainly follow up on them during future code developments.

Specific comments

Pages 35421-35422, Lines 29-1: Should add a reference to Zhao et al. (2009), Jeong et al. (2012), Jeong et al. (2013), and Ganesan et al. (2015).

We added Zhao et al. (2009), Jeong et al. (2012) and Jeong et al. (2013) at this point in the manuscript.

The study by Ganesan et al. (2015) was not carried out at the high spatial resolution that we were referring to. They used a transport model at approximately 25 km horizontal resolution and also their inversion grid was rather coarse (estimating emissions for approximately 60 regions across the UK). Nevertheless, we added a reference to Ganesan et al. (2015) in our discussion of European agricultural emissions.

Page 35425, Line 9: Is this an issue if wind direction changes? 3hr seems like a long time.

We used 3-hourly aggregates to reduce the computation time for the transport model, which was also only started for 3-hourly intervals. However, the model is driven by hourly wind data, so changes in advection direction will still be reflected in the model result. Also particles are released continuously within each 3-hour interval, so that changes in advection are considered in the model. The aggregation certainly will smooth some of the observable variability but we feel that we don't have a strong loss of

information from the aggregation, especially since we also consider a temporal correlation length in the model/observation covariances of half a day, which adds additional smoothing of the contained information.

Page 35426, Lines 9-30: How are the PBL heights? I didn't see any mention of evaluating them.

PBL heights are a critical parameter in FLEXPART, since they are used as a scaling parameter for the turbulence parameterisation. We use the standard implementation within standard FLEXPART to diagnose PBL heights from a Bulk-Richardson method (Stohl et al., 2005;Vogelezang and Holtslag, 1996). In contrast to standard FLEXPART we did not use 2-metre temperatures from COSMO in the PBL estimation but the lowest model level temperature (~10 m above ground), since MeteoSwiss COSMO 2-meter temperatures are known to have a warm bias during convective conditions. COSMO internal and FLEXPART diagnosed PBL heights were compared by MeteoSwiss for the sounding site Payerne on the Swiss Plateau. The comparison showed a positive bias for COSMO and also for FLEXPART derived PBL heights when using 2-m temperatures. This bias mostly vanished when using the first level temperature as done in our simulations. We added this information to the manuscript.

Page 35428, Lines 8-13: Why are you using a fixed height? Shouldn't it be the mixed layer height? It seems that using a percentage of the PBL height would be more reasonable.

While we agree with the referee, FLEXPART does not allow a variable sampling height (yet). The chosen sampling heights agree with the minimal PBL used by the different model versions, therefore avoiding that the sampling height is ever larger than the mixing height. During convective mixing the particles should be homogeneously distributed throughout the PBL and a sampling height smaller than the PBL height should be valid. However, we agree that particle statistics might improve with a variable sampling(Zeitz et al., 2012). We did tests with doubled sampling heights that did not indicate systematic changes in simulated sensitivities. Therefore, we don't think that the current sampling height introduces systematic biases in the transport description.

Page 35429, Line 21: I think it should be "K_E _ 1000", not "J_E _ 1000".

Yes. We corrected this in the revised manuscript.

Page 35430, Line 9: How many observations? I'm assuming L < K since you're using the L-form.

Actually L > K (approximately L~3000 observations versus K~1400 elements in the state vector) for most of the presented inversions. We realise that under these conditions equation 5 may be solved more efficiently when reformulated. This will be subject of further code development as already mentioned above.

Page 35431, Line 17: What is f_E? I didn't see it in the table. What is the resulting grid-scale uncertainty? Is there a floor on the uncertainty?

f_E is the proportionally constant between prior emissions and prior uncertainties. f_E was set constant for all land grid cells with significant emissions and the value was chosen so that the country total emission uncertainty for Switzerland became 16 %. The resulting value for f_E was 0.3 and this information

was given on page 35437 line 1. We clarified this connection in the revised manuscript. To avoid very low uncertainties in grid cells with low emissions we adjusted the uncertainty for land grid cells with less than 10% of average land cell emissions and for ocean grid cells to a minimum uncertainty corresponding to 10 % of the average land cell uncertainty. This procedure was tested with several threshold values and did not at all affect the results for Switzerland and hence this information was not given in the manuscript.

Page 35432, Line 25: Are observations only correlated for a given site or all sites?

No correlations between sites were treated as mentioned on line 5 of page 35433.

Page 35435, Line 10: Spent a lot of time explaining the Bayesian, maybe give the equation for the extKF or explain how Q was specified.

We added the following lines at the end of Section 2.5.3:

Accordingly, uncertainties of the state vector are allowed to grow from one time step to the next which introduces an additional amount of prior uncertainty as compared to the Bayesian approach. The matrices B and R were parameterized according to equations (9) and (12), respectively. The chosen parameter values are listed in Table 3. The forecast uncertainty matrix Q was also parameterized according to equation (9), notably with the same spatial correlation length. The diagonal elements of Q were set to a relative forecast uncertainty of the emissions of 0.6% per 24 hours which resulted in fairly constant a posteriori emissions with only a small seasonal cycle.

Page 35437, Line 1: How? How is summing diagonals with 30% uncertainty giving you a smaller uncertainty (16%) at the national scale (without anti-correlations in the off-diagonal)?

The uncertainty of the sum (E) over two independent emission elements (a,b) with a relative uncertainty of 30% would only be 21 % if a=b. The following equations should illustrate this.

Total emissions:

$$E = a + b = 2a$$

Uncertainty:

$$\sigma_a = f_E a$$

Total uncertainty (Gaussian error propagation for uncorrelated uncertainties):

$$\sigma_E = \sqrt{\sigma_a^2 + \sigma_b^2} = \sqrt{2}\sigma_a \ = \sqrt{2} f_E a$$

Total relative uncertainty:

$$\frac{\sigma_E}{E} = \frac{\sqrt{2} f_E a}{2a} = \frac{1}{\sqrt{2}} f_E = 0.707 f_E$$

So the relative uncertainty of the sum is a factor of 0.707 smaller than the relative uncertainty of the each individual emission element. Hence, even in the case of positive covariances the relative uncertainty of the sum can be smaller than the relative uncertainty of the individual elements. This calculation is also reflected in equation 7.

Page 35438, Line 15: Should say “separated”, not “separating”.

Corrected

Page 35438, Line 16: Should say “ensure”, not “assure”.

Corrected

Page 35438, Line 19: Should say “ensures”, not “assures”.

Corrected

Page 35448, Line 15: Should say “distinct”, not “destinct”.

Corrected

Page 35448, Line 27: Should say “sensitivity”, not “sensititivy”.

Corrected

Page 35453, Line 15: Should cite Ganesan et al. (2014).

Added

Page 35454, Line 21: Should say “inferred”, not “infered”

Corrected

Additional References

Alexe, M., Bergamaschi, P., Segers, A., Detmers, R., Butz, A., Hasekamp, O., Guerlet, S., Parker, R., Boesch, H., Frankenberg, C., Scheepmaker, R. A., Dlugokencky, E., Sweeney, C., Wofsy, S. C., and Kort, E. A.: Inverse modelling of CH4 emissions for 2010–2011 using different satellite retrieval products from GOSAT and SCIAMACHY, Atmos. Chem. Phys., 15, 113-133, doi: 10.5194/acp-15-113-2015, 2015.

Bergamaschi, P., Corazza, M., Karstens, U., Athanassiadou, M., Thompson, R. L., Pison, I., Manning, A. J., Bousquet, P., Segers, A., Vermeulen, A. T., Janssens-Maenhout, G., Schmidt, M., Ramonet, M., Meinhardt, F., Aalto, T., Haszpra, L., Moncrieff, J., Popa, M. E., Lowry, D., Steinbacher, M., Jordan, A., O'Doherty, S., Piacentino, S., and Dlugokencky, E.: Top-down estimates of European CH4 and N2O emissions based on four different inverse models, Atmos. Chem. Phys., 15, 715-736, doi: 10.5194/acp-15-715-2015, 2015.

FOEN: Switzerland's greenhouse gas inventory 1990-2013, Submission of April 2015 under the United Nations Framework Convention on Climate Change and under the Kyoto Protocol, Federal Office for the Environment (FOEN), Bern, 2015.

Hiller, R. V., Bretscher, D., DelSontro, T., Diem, T., Eugster, W., Henneberger, R., Hobi, S., Hodson, E., Imer, D., Kreuzer, M., Künzle, T., Merbold, L., Niklaus, P. A., Rihm, B., Schellenberger, A., Schroth, M. H., Schubert, C. J., Siegrist, H., Stieger, J., Buchmann, N., and Brunner, D.: Anthropogenic and natural methane fluxes in Switzerland synthesized within a spatially explicit inventory, Biogeosciences, 11, 1941-1959, doi: 10.5194/bg-11-1941-2014, 2014.

Stohl, A., Forster, C., Frank, A., Seibert, P., and Wotawa, G.: Technical note: The Lagrangian particle dispersion model FLEXPART version 6.2, Atmos. Chem. Phys., 5, 2461-2474, doi: 10.5194/acp-5-2461-2005, 2005.

Turner, A. J., Jacob, D. J., Wecht, K. J., Maasakkers, J. D., Lundgren, E., Andrews, A. E., Biraud, S. C., Boesch, H., Bowman, K. W., Deutscher, N. M., Dubey, M. K., Griffith, D. W. T., Hase, F., Kuze, A., Notholt, J., Ohyama, H., Parker, R., Payne, V. H., Sussmann, R., Sweeney, C., Velazco, V. A., Warneke, T., Wennberg, P. O., and Wunch, D.: Estimating global and North American methane emissions with high spatial resolution using GOSAT satellite data, Atmos. Chem. Phys., 15, 7049-7069, doi: 10.5194/acp-15-7049-2015, 2015.

Vogelezang, D. H. P., and Holtslag, A. A. M.: Evaluation and model impacts of alternative boundary-layer height formulations, Bound. Lay. Met., 81, 245-269, doi: 10.1007/BF02430331, 1996.

Zeitz, J. O., Soliva, C. R., and Kreuzer, M.: Swiss diet types for cattle: how accurately are they reflected by the Intergovernmental Panel on Climate Change default values?, Journal of Integrative Environmental Sciences, 9, 199-216, doi: 10.1080/1943815X.2012.709253, 2012.

Reply to Referee #2

Referee comment in bold, reply in plain text, *modified text blocks for manuscript in italics*.

Please note that the line number given by the referee refer to the originally submitted manuscript and not the one published on ACPD.

The manuscript "Validation of the Swiss methane emission inventory by atmospheric observations and inverse modelling" by Henne et al. analyze an ensemble of atmospheric inversions of the Swiss methane emissions using continuous CH4 measurements from a ground based network of 4 to 6 sites. The study highlights the consistency between the results from the different inversion set-up and the SGHGI inventory. Finally, it attempts at interpreting the spatial and temporal distribution of the inverted emissions, linking it to the different types of sources and processes underlying the CH4 emissions in Switzerland.

In general the manuscript is very well structured and written. The inversion system and the experimental framework seem robust, and the results are highly encouraging for the use of atmospheric inversions as a mean to verify and potentially improve the GHG emission inventories. I do not see any major issue in this manuscript, which I strongly recommend for publication in ACP.

I still have some concerns regarding the text and the results as detailed below.

We would like to thank the reviewer for this very careful review that clearly helped to improve our manuscript.

There is a series of minor issues related to the "baseline treatment". The definition of the "baseline" and of what is targeted through the optimization of the "baseline" is unclear. The term baseline is not really self-explanatory. The definition of the baseline as "conditions without recent emission input" (l. 186) is vague even though it connects it to the concept of model boundary conditions. The different configurations of the state vector for the baseline are not really justified by a characterization of this baseline. Why could it be assumed to vary between the sites that are often quite close to each other compared to their distances to the boundaries of the inversion domain? Why could it have a full 3D structure in space? The impact of including the baseline in the state vector and the sensitivity to its configuration is important for such a regional configuration. When the inversion is allowed to optimize a different baseline for each site, it can easily make attribution errors between the baseline and the emissions, as illustrated by the results from experiments S-ML (there is a beginning of discussion on this topic at lines 459-462). Most of the inversion tests use low prior uncertainties in the baselines, which could limit the influence of the baseline on the inverted emissions, but which, on the other hand, may prevent from fully accounting for the uncertainties in the boundary conditions of the inversion domain. The baseline should thus be better defined and discussed, its weight on the inversion and the corresponding attribution errors should be better characterized.

The baseline concentration as seen by our regional scale LPDM can be understood as the average mole fraction at the individual particle locations at the end of the transport simulations (4 days before arrival at the sites or at a domain boundary). As such this baseline mole fraction is not simply the mole fraction at the domain boundary but may well contain contributions from within the domain in cases where our backward integration time was not sufficiently long for all particles to leave the domain. The justification for using an individual baseline for each site lies within this fact. In our most simple baseline treatment (used by various authors before) any information on the particle end points is neglected. Even though the baselines for nearby sites should be similar they may still vary considerably de-

pending on the elevation of the site. This is especially true for the sites with very different elevation JFJ, SSL versus BEO and LAE. The 3D structure of the baseline presents the attempt to deduce the mole fraction at the particle end points as one common baseline.

The potential for attribution errors was the reason why we introduced 3 different treatments of the baseline. Since these yielded similar results we had hoped to refute any concerns regarding this point. However, we see that it merits further discussion in the manuscript.

We extended the description of our baseline definition and highlighted the different considerations, given above, in the revised manuscript (sections 2.2, 2.3, 2.5.7).

We also point out the potential of attribution errors due to the baseline treatment. We discuss the results of two additional test inversions with factor of 2 lower or higher baseline prior uncertainty. Their result for total Swiss emissions was 210 Gg/yr and 160 Gg/yr for low and high baseline uncertainty, respectively, and low particle release height. This is within the range defined by all other sensitivity inversions. Given the fact that in neither case the obtained posterior baselines looked very realistic (too smooth in the case of small prior uncertainty and too closely following the observed variability in the case of large prior uncertainties), we did not include these cases as part of our sensitivity inversions but discuss them along with the alternative baseline inversions.

I feel that the authors go too fast in rejecting the assumptions that the positive corrections applied by the inversion in the north-east of Switzerland could be artifacts. The fact that those corrections could balance (through attribution errors or due to a lack of flexibility) the imperfect inversion of the baseline for north-east winds is quite ignored while this is a likely explanation. Furthermore, I do not agree with the sentences at line 908 "it seems unlikely that the same systematic bias would be inherent to both meteorological inputs" and at line 22 "which rules out an artefact of the transport model and the inversion system". Both meteorological forcings have a limited spatial resolution (which can be critical in this area) and errors inherent to FLEXPART would apply to both FLEXPART-ECMWF and FLEXPART-COSMO. Section 4.3 fails to identify a significant missing source. Therefore, my feeling is that the discussion attempting at linking the corrections in the north-east to specific processes in section 4.3 is a bit too long and a bit too ambitious. It could be shortened and the text should acknowledge that some limitations of the inversion system could explain such corrections. What is the weight of these corrections in the national budget of the emissions from the inversions? Considering that this is connected to a sector underestimated by the SGHGI, or to an artifact of the inversion, considering that the inversion decrease the emissions from agricultural lands compared to the SGHGI, and given that SGHGI is a purely bottom-up estimate, it seems that the fit between the national budgets from the inversion and from SGHGI could be seen as a coincidence without such a weigthing.

We understand the concerns of the referee. We hope that some of them were already addressed by the more detailed explanation of the baseline treatment and its uncertainties (see above). We followed the advice of the referee and don't rule out inversion artefacts in the manuscript anymore. However, we did not shorten the discussion on the potential source, especially since also referee 1 highlighted the potential role of different manure handling practices that could induce large spatial differences in this emission type.

The additional test inversions with factor of 2 different baseline uncertainty did not change the spatial pattern of emission changes in Switzerland significantly. The increase in north-eastern Switzerland was confirmed also for the inversion with large baseline uncertainty that resulted in considerably lower (160 Gg/yr) country total emissions than the base inversion (similar to results from S-ML).

One additional argument in favor of a true increase in north-eastern Switzerland is that it is also observed in summer time when pollution events with easterly advection are absent (see Figure 6).

The contribution of the gird cells in the north-eastern part of Switzerland (selected 4 grid cells with largest increase in posterior) to the national total emissions to total Swiss emissions was 16.3 Gg/yr or 9 %. In the posterior this was increased to 22.5 Gg/yr or 12.5 %. The change of 6.2 Gg/yr represents 3.4 % of the national total. This is not a negligible contribution to the national estimate, but does not

compromise our conclusion that the posterior estimate is in close agreement with the bottom-up inventory, even if the increase in the north-eastern area is ignored completely.

Several components of the inversion configuration need to be presented in a more explicit way and earlier than they are presently: the temporal resolution at which the emissions are estimated (it should be explained in section 2.3, and anticipated at the end of section 2.2 at lines 246-. . .), the transport modeling and inversion spatial domain (what are the COSMO-7 domain and Western Europe in section 2.2 ?). Section 2.3 should confirm the inversion period (Mar 2013-Feb 2014) even though it is implicitly defined near the end of section 2.1. Much of the model vs. data analysis are lead without stating whether they are based on 3-hourly timeseries with or without the data selection applied to the data assimilation (using 12:00-18:00 and 0:00-6:00 time windows only, and filtering the data according to the wind speed: line 77 states that it is used for the inversion, but we do not know whether it is used e.g. for the REBS analysis few lines later). Typically, the text does not say precisely what is plotted in figure 3 and 4 in terms of temporal resolution and temporal selection.

We followed the advice of the referee:
We included the information of the temporal resolution of the target emission estimate.
We added information on the meteorological domains.
We confirmed the target period in 2.3.
We clarified that only the 3-hourly filtered and aggregated time series were used in all inversions, analysis and discussion.
We added missing information on temporal resolution to Figure 3 and 4.

Minor comments

line 5 vs line 9 vs line 20: you should introduce the "reference" prior emissions at line 5
The reference prior emissions are now introduced first.

line 9 and elsewhere: use error (or uncertainty) covariance instead of covariance by itself; use something more self-explanatory than "baseline treatment" at line 10 ?

We use uncertainty covariance throughout the text now.
We replaced the term baseline in the abstract by “large-scale background mole fraction”. Later in the text baseline is explained in detail and we stick to this terminology.

line 8 vs 12 vs 15: you should use the same designation for the inventory, otherwise the reader can believe that you speak about 3 different inventories

We stick to SGHGI throughout the whole text now.

- line 11: I feel that "independent character" is a bit strong, even though I do not contest the robustness of the system. You still have large sensitivities to e.g. the prior uncertainty in the baseline which is a critical component of the system. Furthermore, here, you do not necessarily speak about the national budgets only, and the sensitivity of the spatial distribution of the emissions to the inversion set-up is also significant.

Although we used relatively small uncertainties for the prior, we established that different prior distributions and totals (MAIOLICA vs. EDGAR) did not result in significantly different posterior emissions. Also increasing the prior uncertainty as done in S-ML did not result in significantly different posterior

emissions. The same is true for the baseline. We investigated various baseline treatments in order to explore the range of possible baseline influences. Considering these results from the sensitivity inversions, we are confident about the independent character of the inverse estimate, which showed only small effects due to assumptions on the prior.

- line 58-59: "Methane emissions from individual sources are much more difficult to quantify than anthropogenic emissions of CO2" it's a too general statement to be true

We agree that for individual sources this is not generally true. We were rather referring to the fact that total national anthropogenic CO2 emissions can be derived relatively precisely because combustion is by far the most important anthropogenic CO2 source and fuel statistics, for a country like Switzerland, are very well know . In contrast, CH4 emissions stem from less well understood processes that may vary strongly on an individual basis (ruminants, manure handling, waste treatment). We revised the wording of this sentence to clarify this point.

- l. 71-72 : this raises some questions; inventories of CH4 emissions should be built on such an upscaling of site / process scale measurements or on highly uncertain emissions factors, so why would this be too difficult ? or why were the numbers from these specific studies difficult to upscale (because the sampling was too small ?) ?

These studies did not necessarily focus on an individual emission sources but rather on small regions. Therefore, they did not provide emission factors for a source process that could be up-scaled. Due to different source compositions within each analysed area and the small number of studies it is not easily possible to translate these results to the country scale. However, we revised the wording, removing the word up-scaling, to clarify this.

- line 75: the inversion delivers but does not "combine" an optimal estimate of the emissions
We revised the sentence accordingly.

- line 92 : evaluate instead of validate ?

We would like to stick to validate in this context (see also title of manuscript). The discussion about validation versus evaluation was raised by the modeling community due to the fact that a model can never be "validated" (it will always be wrong to some extent"), but it is possible to evaluate whether a model is fit for a given purpose. However, we are validating the inventory in the sense that we are checking whether the reported emission total is consistent with our (more or less) independent estimate *within the range of the combined uncertainty*.

- l. 95 give an idea about this high resolution
Information was added to the manuscript

- l.114: you do not target the Swiss Plateau in the following, but rather the national budgets which is thus something different (by 30%)

The sentence states that the sites are "mainly" sensitive to the Swiss Plateau, but not exclusively. Furthermore, we add two more sites in the inversion (JFJ and SSL) which are sensitive to larger areas than our Swiss Plateaus sites. Overall the combined sites should be sufficiently sensitive to the whole of Switzerland to derive national emissions. In addition, the inversion will account for the lack of sensitivity (for example south of the Alps) by not reducing uncertainties in these areas.

- l. 185, the justification for using nighttime data at JFJ and SSL goes too fast and should explain why the situation regarding the PBL and the local sources is different there compared to the other sites (otherwise it could seem in contradiction with lines 182-183).

We extended the explanation why we used night-time data from JFJ and SSL.

- l 185-198: this paragraph is not fully clear (is the baseline an annual mean, or a series of 60 day averages ?) and will generate some confusions in the following, where the baseline will rather be computed as an interpolation of "baseline nodes" and where only the REBS analysis for JFJ will be used. You should find a way to avoid this little issue either here or later when describing the inversion protocol. "reflecting different degrees of variability and frequency of air masses not influenced by recent surface contact and emissions." is not really clear.

We added some clarification, but refer to the REBS publication for further details on the method. We furthermore added a sentence on how the mole fractions at baseline nodes were derived from the REBS estimates in section 2.3.

- l. 206: why the spatial resolution of ECMWF is degraded outside the Alpine area ?

for computational issues ?

This is due to limited storage capacity and done in a similar way by many groups using similar modelling approaches). Away from the releases points and the steep topography the coarse ECMWF resolution still gives sufficiently accurate transport results.

l. 208-210 : can you explain the role (on the top of the analysis from MeteoSwiss) and horizontal resolution of COSMO ?

COSMO is the NWP system used to generate hourly meteorological fields using data assimilation of observed parameters. We did not run COSMO ourselves, but merely used the operational product of MeteoSwiss. The main advantage of this, as compared to doing independent COSMO simulations, is the benefit of the assimilation cycle and the continued validation efforts by MeteoSwiss in terms of meteorological variables. We use COSMO analysis at a 7 km by 7 km horizontal resolution to drive our transport simulations. Although this resolution is not entirely sufficient to describe all details of the complex, near-surface flow in mountainous terrain, it proved to be reliable for the elevated sites used in this study. This information is given in some detail in section 2.2, but we added additional COMOS domain information to the revised text.

- l. 214 "time-inverted" was not mentioned before

We now mention this when the FLEXPART versions are introduced.

- Table 1: the particle release heights are given for FLEXPART-COSMO only, not for FLEXPART-ECMWF unless the release heights at JFJ and SSL for the latter are based on the ground height in COSMO ? (the paragraph on the release heights is not fully clear about this).

We added this information to the table.

- l .244: for the mountaintop site JFJ during nighttime only ?

The cited publication evaluated simulations for all times of day and night-time separately and did not establish significant differences due to this selection.

- l. 258-259 : you speak about sensitivities, not about sensitivities multiplied by the emissions, so you should not write lines 257-259 (or you should speak about mi,j times Ei,j and defining Ei,j correctly)

We reformulated this sentence.

- l. 279-280 should be improved

We understand that the referee requests further details on how the grid box aggregation was done. We added these to the text.

- l. 284: can you give more details about the domains that were tested? it could be important for the discussion on the baseline and on the corrections in the North East of the Alpine area.

The current inversion domain has an eastward extent up to 21° East, this is also roughly the extent of the COSMO7 domain, which was used for the FLEXPART simulations. Reducing this eastward extent by 5 degrees did not show significant differences in the inversion (both in terms of baseline and emission adjustment). With a further reduction in the eastward extent, the under-prediction during the highlighted pollution events increased and emission increments towards the east were more emphasised. We did not include these experiments in the paper in more detail since the choice of a sufficiently large inversion domain seemed to be a prerequisite for a successful inversion. The CSOMO7 domain limits are now given in the text.

- l. 327 : you will correct the baseline differently for each site, so why using the REBS analysis at JFJ site as a prior for all sites ? see the main comment regarding the lack of characterization for the baseline which could help justify the way it is accounted for in the inversion state vector and the way priors and prior uncertainties are assigned to it.

We used the baseline from JFJ since this was most robustly obtained from the observations. The REBS method generally requires that about 50 % of the observations are baseline observations in the sense that they follow a normal distribution about a smoothed baseline curve. For the sites closer to emissions this condition is usually not met. While REBS still produces a reasonable baseline curve here, it is evident that it often lies above the lowest observed mole fractions: a clear indication that the method did not fully succeed. We did a test inversion using the REBS baselines obtained from each individual site that did not succeed in terms of bringing down the posterior baseline, resulting in simulated mole fractions that were generally too large during little polluted conditions.

- l. 303: "the vector f gives the fractional contribution of the region to each inversion grid cell" something is inverted in this sentence and it could be said better in order to mention that it is related to the surface area (see l. 303 vs. l. 306-307). l. 306-307: I am not sure to understand, you will thus derive xk in terms of emission per capita instead of per m2 to be consistent ? then will it impact the results ? The whole paragraph should be clarified.

The calculation of f_k in grid cells that span more than one region is based on high resolution population density and not simply on a by-area contribution. This is to avoid wrong allocation in cases where for example a large city of region A is situated in the same inversion grid cell as a sparsely populated area of region B. In the case of the current CH4 inversion the influence of this treatment is of minor importance. It was introduced in our system for application to halocarbon inversions.

We clarified the description in the manuscript.

- l. 317: the letter f is already used for eq. (7), you should use another letter to avoid confusion ?

Here it is f_E not f. However, we changed the letter f in equation 7 to g to avoid confusion.

- Equation 8 and associated parameters at lines 322-323: you do not discuss and justify this modeling of the spatial correlations. Ignoring the independence between the different types of sources of methane in such a definition could raise problems. The 14-day timescale for the errors on the baselines, which could miss the signal associated with synoptic events, is also given without justification. The set-up of the prior and observation/model error covariance parameters cannot be perfect but it could be supported by few explanations.

We are aware of the fact that this approach is a simplification, but it has been widely used in lack of more detailed information on the spatial correlation and in order to further constrain the posterior solution (e.g., Rödenbeck et al., 2003;Gerbig et al., 2006;Thompson and Stohl, 2014). Hiller et al. (2014) investigated the spatial correlation length scale by analysing differences between the MAIOLICA, EDGAR and TNO inventories in a variogram approach. Their estimate of 13 km and 8 km when comparing

to the EDGAR and TNO inventory is considerably lower than what we used in the inversion. When using a value around 10 in our inversion, emissions in individual grid cells become almost independent of each other and the prior did not provide sufficient constraint for a reasonable posterior solution, as indicated by seemingly arbitrary posterior adjustments and the introduction of dipole structures in the posterior field.

The chosen length scale for the baseline represents a compromise between something that would be closer to the synoptic time scale (~5 days) and the need for additional constraint on the baseline. Values lower than 14 days tend to give too much freedom to the baseline. In addition, we would argue that most of the synoptic-scale variability should be picked up by the advection changes within the domain (intensity and location of contact with the surface/emissions) and not the baseline, given the rather large extent of the inversion domain.

These considerations are not free of a certain degree of subjectivity. However, both parameters were evaluated in the ML method later in the manuscript and similar values were obtained, lending credibility to our choices.

We give additional motivation for the use of the chosen parameters in the manuscript.

- l. 321: if you use the vector 1, you will include emissions from all countries, while you aim at comparing it to the Swiss budget (line 323). Could you confirm that you scale uncertainties outside Switzerland based on the scaling factor derived in Switzerland?

Yes the same relative uncertainty is applied for grid cells outside Switzerland as can also be seen in figure S2.

- l. 330 add "at a given site"; and speak about the spatial correlations between errors on baselines at the different sites (some justifications may be needed). Line 333: then you apply the uncertainty diagnosed by the REBS for the annual baseline to the uncertainty in 5-day baseline nodes ? or does the number given by the REBS mean something else ?

We added the suggestion to the text and keep the assumption of no correlation between sites (see argumentation in reply to first question.

The uncertainty provided by REBS does not give an annual mean but the prediction uncertainty at every time step so that it should be appropriate to apply it to the 5-day baseline nodes.

- the paragraph regarding the model errors is quite confusing and should be improved; it is difficult to understand what exactly means "a constant contribution while the third term represents an uncertainty contribution relative to the prior simulation of above baseline concentrations". Through these computation aren't you attributing part of the prior uncertainty to R ? Lines 342-348 go too fast and are unclear. "Residual" is not a self-explicit term.

We improved the description of the concept. Generally, we agree with the reviewer that in our method the prior has some influence on the estimate of R. We added a note of caution to this extent:

*These methods have in common that the results of the prior simulation influence the estimation of **R** therefore somewhat violating the independence of prior and model/observation uncertainties assumed in the Bayesian approach.*

However, the choice of the method is a compromise driven by the lack of better information to characterise the model/observation uncertainty.

-l. 356: the selection of the data should remove this problem of the simulation of the diurnal cycle in the PBL ? furthermore, such an error sounds like a "bias" while 0.5 days is relatively short

We agree with the referee that by selecting only day-time (night-time) data the problem of the diurnal cycle is diminished in our inversion. However, we use two afternoon (or in case of SSL and JFJ nighttime) observations per site and day and therefore the correlation length scale is still appropriate

to take care of auto-correlated nature of the observation errors. Others have also determined the temporal correlation length scale from the auto-correlation function of the prior residuals. When we attempted this, values close to 0.5 and no significant changes on the inversion result were obtained.

- l. 362-363 : even if these assumptions were true, the set-up of the inversion would still be highly uncertain, which explains most of the sensitivity tests. What do you mean by "uncorrelated residuals" ?

To explain what we mean by "residuals" we changed line 342 to "were estimated separately for each site from the model residuals (differences between simulated and observed values) of the prior simulation" and changed "uncorrelated residuals" on line 362 to "temporally uncorrelated residuals". Most of our sensitivity tests are addressing potential systematic biases. If the assumptions listed on lines 362-363 were true, most of these tests would not be necessary.

- l. 385: could you define the seasons (the corresponding months) here ?

We included a definition in the text.

- l. 385 the text could mention here or even before (when defining the temporal resolution of the state vector) that the emissions may actually have significant variations in time (even though it will be discussed in section 4)

We included a statement at this location.

- l. 389: here as in section 2.5, you describe some new theoretical components faster than in section 2.3 while it could require the same level of detail (especially when presenting the extKF). I suggest to (1) generalize section 2.3, (2) detail the configuration for the base inversion (3) present the sensitivity tests by detailing each corresponding perturbation to this base inversion using the mathematical framework of 2.3.

We followed this suggestion and extended 2.3 at the expense of somewhat shortening 2.5. However, we tried avoiding duplication of information wherever possible.

-l. 390: 90 days is nearly one season, so the inversion might have a limited ability to increase the seasonal variations. Do you know whether decreasing this temporal correlation would have significantly increased the seasonal variations that are analyzed in 3.2 and discussed in section 4 ?

When reducing the temporal correlation length to 45 days changes in the seasonal posterior emissions were not more than +/- 4 Gg/yr compared to the setup with a correlation length of 90 days. We consider this a minor influence, but added this information to the text.

- Section 2.5.3 is a bit short given that many of the inversion parameters, concepts and underlying assumptions change when switching from the base method to extKF. And the text should explain which type of uncertainties are targeted by this sensitivity test. This section should better characterize what is the state vector for each (3-hourly ?) analysis of the sequential algorithm. What is the time resolution of the corrections to the emissions here ? L. 396: what is the tendency of the baseline value ? Are there some consistencies between the B and R matrices used here and that used in the base inversion ? Do you need the ML method to set-up these parameters (maybe switch the sections 2.5.4 and 2.5.3)? l. 403-405 is impossible to understand; how Q is set up ?

We kept the description of the Kalman Filter short on purpose, since it was recently published in full detail. This is in contrast to the implementation of our Bayesian approach, which we never published in as much detail as presented here. However, we added some additional information on the Kalman Filter approach to improve the understanding of this section, in particular regarding the design of the uncertainty covariance matrices **B**, **R** and **Q**.

- L. 408: based on the national emission uncertainty as estimated by SGHGI provides the best knowledge of the uncertainty in SGHGI, not of the uncertainty in the prior estimates (MAIOLICA and EDGAR) used here

We clarified this in the text. It now reads:
Our base inversion is based on the prior emission uncertainty as estimated by the SGHGI, which we consider to be the best knowledge of bottom-up uncertainty in Switzerland. Since Hiller et al. (2014) used the same by-category emissions as the SGHGI to spatially disaggregate total emissions for the MAIOLICA inventory (our prior), we extrapolated the SGHGI uncertainty information to the whole inversion domain.

- L. 415-416 : residuals and differences sound like shortcuts to me

We are following standard terminology: The term "residuals" is used strictly for differences between simulated and observed mole fractions. This is now explained in the revised text at the first place where "residuals" appears.

- L. 427: why ? in theory, the model/obs errors should be similar in the base and extKF inversions, even if the changes in the state vector can impact part of the model error (e.g. the aggregation errors related to the resolution of the state vector)

This is merely due to technical reasons. It simply was not implemented in the system yet. We added this information to the text.

- l. 435 : who reports to UNFCCC ? FOEN and thus MAIOLICA would be consistent with SGHGI ?

FOEN is the Swiss Office for the Environment which annually reports the SGHGI. The reference for the SGHGI is thus FOEN (2015). The total emissions in the MAIOLICA inventory for the anthropogenic sectors are identical to the SGHGI (reported in 2012). Natural emissions were added in MAIOLICA but estimated to be almost negligible. The total uncertainty of the SGHGI thus also applies to MAIOLICA. We clarified this in the text.

- l. 445-446: rewrite, it's hard to understand.

Indeed this was not well formulated. Actually we were referring to the total uncertainty of the country emissions. The revised text should make this clear now.

- Sections 2.5.5 and 2.5.6 define some critical components of the base inversion. So, in section 2.5, we are not just looking at perturbations to the base configuration. This supports my earlier suggestion to start giving a general framework for the inversion which could apply to both the base and sensitivity cases, and then to present the base and sensitivity configurations.

The information on prior emissions in the base inversion was moved to section 2.3.

The treatment of the baseline is now more generally introduced in section 2.3. However, the details of the alternative approaches are still detailed in section 2.5.6.

- L. 465 and 469: "initial" may be confusing here

Changed to *FLEPXART particle end points*.

- L. 463-465: I would rather discuss the link between the baseline and the boundary conditions (which can be derived from large scale transport models) earlier when defining the baseline.

We do this in the revised manuscript at the end of section 2.2

- L. 473 to 485: shouldn't the baseline rather be discretized in space over the inversion domain boundaries ? The concept of a 3D discretization of the baseline looks strange (see the general discussion about the baseline), but it's balanced in this inversion test by the fact that the same baseline is applied to all sites, and by the coarse resolution of the grid for this 3D baseline.

See general discussion above.

- L. 481-482: it is surprising to see that this level is at 3000magl. What is the typical PBL height during the afternoon in winter / summer ? One could have thought that most of the sensitivity for afternoon data lies in the PBL. Of note is that it could make sense to select a vertical separation close the PBLH.

The typical diurnal maximum boundary layer height is below this altitude (~1500. m agl in summer). We first used this as a threshold, but observed much larger sensitivities in the sub-column above 1500 m than for the sub-column below. This can be explained by the fact that we are looking at the particle end points (4 days before arrival at the sites) where particles were already more evenly mixed throughout the troposphere. The low sensitivities in the below 1500 m sub-column did then result in minor adjustments of the prior values, which seemed unreasonable. Hence, we chose a threshold that distributed the sensitivities more evenly in the vertical.

- l. 504-505: you do not explain this mapping so this is not straightforward

This mapping artefact is due to inversion grid cells covering more than one country and therefore emissions may be assigned to the wrong country. We tried to remedy this by using a by-population weighting in such grid cells (see discussion above), but could not get rid of this effect completely. Further steps could include an inversion grid design that is oriented along country borders or a higher resolution inversion grid. We extended the sentence to explain that the mapping artefacts are associated with grid cells along the Swiss border overlapping the neighbouring countries.

- l. 517, 519: this seems more frequent than induced by these sentences. Oct 2013 is an example comparable to March April 2013.

We added the Oct 2013 period to the text.

- L. 525-526 : we do not know (in the text; the figure gives the answer) if this prior baseline is a REBS analysis of the prior simulation, or the prior of the baseline state variable which should be equal, for all sites, to the REBS analysis at JFJ

We added this information also to the text.

- L. 527 and 543: Figure 4 does not necessary indicate a considerable improvement of the fit to the data after inversion. However, the inversion relies on corrections to the emissions and baseline at very low time resolution, so it has a limited potential for increasing the fit at high temporal resolution, which could explain why the posterior correlations hardly exceed 0.6. So would not it be more relevant to check the correlations between the model and the observations at a lower temporal resolution ?

Note that values of R^2 are shown in Figure 4, not of R. The posterior correlations at the sites BEO, LAE, SSL and JFJ used in the inversion reach values between 0.75 and 0.83 and not only of about 0.6. The reason for limited improvements can be seen in the good quality of the prior inversion both in terms of emission strength and spatial distribution. The improvement is still visible even if one does not want to call it considerable. However, we would argue that these improvements are considerable, since they explain an additional 15 % of the observed variability as compared to the prior simulation.

We already discuss correlations for above-baseline (high frequency) and complete signal and indicate that some of the improvement of the complete signal originates from the baseline adjustment. The

improvements in high frequency can still be significant in a grid cell inversion since a spatial redistribution of emissions can help improve also the simulated temporal variability.

Furthermore, the temporal correlation in the residuals is only about 0.5 days suggesting that we can extract independent information from the observations up to that frequency. It might thus make sense to reduce the temporal resolution of the comparison to 12-hourly means but not to anything longer. This would further improve the correlations somewhat but we prefer to stick to the full time resolution in the manuscript.

- l. 533: you have a major part of North Western and Central Europe in your domain

While we have large parts of North-Western and Central Europe in our domain, we did not claim here that the flow was from these regions. We said that the high pressure centre is over Central Europe that means that the flow towards Switzerland was from Eastern Europe and possibly originated outside our model domain.

- l 536: I don't really see it at JFJ

The statement was supposed to refer to the fact again that the baseline was derived for JFJ, but we agree that it is confusing and reworded it.

- l. 562-563: I'm not sure to understand what indicates the link between the correlation and "general flow to the site", and the link between the STD and the local processes

We assume that the temporal pattern of the variability is driven by transport, whereas the amplitude is driven by the emission strength and initial vertical mixing (in turn the PBL) height. The model captures the temporal variability well (correlation) but does not capture the amplitude (std), hence our suggestion. We clarified this in the revised text.

- l. 585: this study uses a higher resolution modeling so the scores should be better; but it also depends on the type of sites where these scores are derived (this study focuses on a complex area)

As the referee correctly states, we use high resolution transport modelling compared to the cited studies, but include sites in complex terrain close to emission sources, which means that these will show more complex variability than those used previously. The fact that our model system is still able to simulate the observations as well as more remote sites in other studies, documents the validity of our system. We emphasised this fact in the revised manuscript.

- l. 603: - 605: putting these 2 sentences together is quite confusing. In one hand you discuss the theoretical uncertainty reductions. On the other hand you have an estimate based on sensitivity studies exploring sources of errors ignored by the theoretical computation (here the uncertainty in the particle release height). Mixing these two numbers (you say "additional uncertainty range") is a bit confusing.

We understand the second sentence as a note of caution at this point that the purely analytical uncertainty should not be taken as the only uncertainty of the posterior estimate. We clarified this in the revised text.

- L. 640, 665, 697. . .. the maps of posterior emissions are systematically stated to be "similar" to that of the base inversion. It is sometimes difficult to assess the level of similarity since the supplementary material does not show these maps (it already shows a lot of material). But the maps of corrections to the prior emissions by the inversion sometimes strongly differ regionally (such as S5c), S8c) S17c) vs. 2c)). The uncertainties in the inverted emissions for some specific

areas may thus need to be more emphasized in the discussion sections when analyzing the spatial distribution of the emissions.

Since for most sensitivity inversion the same prior was used as for the base inversion it should be sufficient to look that the corrections (posterior differences).

For the S-K sensitivity inversion (Figure S5) we outline the similarities and differences to the base inversion in lines 642 to 645. For S-E (Figure S8) a different prior is used as explained in the text. Therefore, it is not enough to just compare the corrections in this case. However, the posterior distribution looks very similar to the base inversion as shown below. As the referee stated, there is already a lot of information in the supplement. Therefore, we did not want to include an additional figure at this point.

For inversion S-B2 we included an additional discussion of the differences in posterior distribution in the text.

- l. 647-648: as previously discussed, the low temporal scale of the state vector in the base inversion limits the potential for increasing the correlation to 3-hourly data. extKF correcting the emissions at a much (which one ?) higher temporal resolution, it definitely has a higher potential for increasing this correlation.

The Kalman filter corrects the emissions and baseline on a daily basis. We already state the fact that this is the cause of increased posterior model performance in the text but put more emphasis on this in the revised text. In the revised version of section 2.5.3 we describe the setup of the matrix Q (prediction uncertainty) in more detail and mention that the values chosen in Q only allow for very slow temporal changes in the emissions that do not even fully capture seasonal fluctuations. The higher skill scores are thus only to a small extent due to the temporal variations of the emissions but are mainly due to using 6-hourly averaged (instead of 3-hourly) values and a more flexible treatment of the baseline.

-l. 657-658: clarify and explain it earlier when presenting the extKF in section 2.5.3

We added this information also to section 2.5.3.

- l. 678: this is not straightforward; the theoretical computation of A can account for the model performance only through the set-up of R. Then this discussion should rather be based on the comparisons of the estimates of R for COSMO vs. ECMWF.

On second thought we agree with this statement and removed the sentence and replaced it with: *This can partly be attributed to the larger model uncertainty assigned in the ECMWF case (especially low particle release case) compared to the base inversion (compare Tab. 3).*

- l. 681-684 the link between smaller posterior emissions and the diffusivity is not fully straightforward and could be better explicited.

The explanation is given in the following sentence. Increased vertical and horizontal dispersion of an emission plume will lead to lower atmospheric mole fractions when the plume intercepts a receptor. If the model under-estimates the dispersion the plume will be more concentrated in the simulation as compared to the observations. In order to align model and observation a decrease in emissions would be necessary.

- l. 705-708: the high corrections and uncertainty reductions for urban centers should not be too surprising: since the prior uncertainty is proportional the prior map of the emissions, and since in EDGAR urban emissions are high, the inversion will naturally apply large corrections and derive large uncertainty reductions for urban centers when using EDGAR as a prior. Does it yield urban emissions that are similar to that when using MAIOLICA as a prior ?

Yes. The posterior emission distribution in urban areas is very similar for both S-E and base inversion.

- l. 712: rewrite "model/observation pairs of one site" ?

We reworded this sentence.

- l. 748-750: the text is quite confusing and could be improved. Discussing the influence areas of the different sites and linking it to specific patterns of the corrections could feed this discussion. It raises some doubts regarding the corrections in the North East of Switzerland in the base inversion (see the general comment about it).

We tried to clarify our argument here. As we outline in this section this kind of attribution error was exactly the reason to include the additional sites JFJ and SSL in the study, because they show a largely different sensitivity pattern as compared to LAE and BEO.

- l. 755: it will be critical to strongly support the assumption that the corrections driven by GIM are erroneous since biased by a high signature of the local emissions at this site. Otherwise one could also think that the "shadowing effect" impacted the results when removing GIM and that the best estimate of the national emissions from the inversions should be obtained when using all the data.

L 755 does not discuss GIM but the LAE only case.

L760 discusses the GIM inversion. As discussed here and earlier in the text, we strongly believe that a combination of large local emissions and potential biases of the model in vertical mixing act together and seem to introduce a general low bias in our model simulations. Our method of estimating the model/observation uncertainty partly accounts for this misfit by estimating larger uncertainties for the site GIM. However, a general model bias cannot be treated by a Gaussian uncertainty alone and therefore we decided to exclude the site from the base inversion.

- l. 765: it is a dangerous discussion; it sounds like paradoxical to analyze the theoretical positive uncertainty reduction brought by GIM and FRU and to use it to demonstrate that they only have a local footprint, while it was stated earlier that assimilating these data increase significantly the errors on national budgets

The uncertainty discussed here represents only the analytical uncertainty, whereas the statement that these observations bias the emission estimate was based on more general considerations and the failure of the inversion system for these locally influenced sites. What we wanted to express here is that these additional observations in S-O5 did not improve posterior uncertainties and that this is also partly due to their localised footprint. We agree that the statement was confusing and we reworded accordingly.

- l 770-774 and 995-999: this assumes that the best inversion case is the base inversion, which is contradicted somewhere else. Having similar results with one site only, despite the "shadowing effects" that have been mentioned earlier, is actually a bit preoccupying. You may have to be more careful about such a discussion. Figure 5 was already showing the dominant role of BEO. But on principle, other sites should have been necessary to ensure that the incoming ("baseline") CH4 from remote areas is well constrained and that gradients between BEO and these sites could be used to constrain the fluxes in the inversion domain without high attribution uncertainties.

Although we don't want to promote the base inversion as our best estimate, we varied the sensitivity inversions only for one aspect at a time. Given all sensitivity inversions with variable observations we still think the base inversion should be understood as the reference in the context of this paragraph. However, we reworded the sentence to being a little bit less optimistic of running an inversion with a single site.

- Table 5 and line 815: why don't you rather look at the inventory for the year 2013 ? your inversions apply to 2013; can you systematically use the same denomination for the SGHGI / FOEN / national inventory ?

As mentioned in the text (l811 to l816) by the time we started this analysis only the reporting for the year 2012 was available in the 2014 reporting. The 2015 reporting showed relatively large changes compared to previous reporting (as given in Table5) and also included an estimate for 2013, which varied little from the 2012 value reported in 2015.

The inventories referred to as SGHGI, FOEN, and national inventory are all the same. We were not very careful with the naming, but improved this in the revised manuscript, sticking to SGHGI.

- l. 787 : these expectations highly depend on the definition of the baseline. See the general discussion about it.

As explained above our definition of baseline is driven by the 4-day backward calculations used in the study. See discussion above.

- l 800-804: such a comparison is a bit unadapted; their problem sounds like too different from yours

Although their study focusses on another species, we still think that this comparison is valid as it puts our results in perspective and indicates that uncertainties associated with the choice of transport model may indeed be larger than what we could identify with our two FLEXPART versions.

- l 825-840: having optimistic theoretical posterior uncertainties is not surprising since they rely on assumptions that the errors have unbiased and gaussian distributions, and that the set-up of the error covariances in the inversion system is perfect. When using the ML method, the analytical computation of the prior and obs/model variances rely on such assumptions and on the optimization of a few parameters, which correspond to a simple approximation of the actual errors. l. 837-838 are unclear.

While this may not be surprising, we wanted to emphasize the fact again that analytical uncertainty obtained from an individual inversion will in most cases not be sufficient to characterise the posterior uncertainty.

We did not understand which part of l837-838 is unclear and did change them.

- l. 845-846: please clarify what you mean by "referred"

We replaced the word.

- l 865: does the inversion yield such a seasonal variations for all agricultural areas or are there large areas where this does not apply ?

The general seasonal cycle can be observed in all agricultural areas, even those in eastern Switzerland, where emission were increased. These increases were strongest during spring/summer as can be seen in Figure 6. We added this statement to the text.

- in the abstract and at line 969 you should remind that the value you provide from SGHGI is for 2012

We added this information in the text and abstract.

- l. 993: I missed the link with the biosphere CO2 fluxes; the problem of the inversion of CO2 bio fluxes is quite different from that of inverting CH4 emissions and such a link is rather weak.

The link is the transport model. If the transport model is insufficient for the complex terrain encountered in the study area, then any CO2 flux inversion is bound to fail. However, we weakened our statement so that it does not suggest that we can easily apply the current technique to CO2 as well.

Additional references

Gerbig, C., Lin, J. C., Munger, J. W., and Wofsy, S. C.: What can tracer observations in the continental boundary layer tell us about surface-atmosphere fluxes?, Atmos. Chem. Phys., 6, 539-554, doi: 10.5194/acp-6-539-2006, 2006.

Hiller, R. V., Bretscher, D., DelSontro, T., Diem, T., Eugster, W., Henneberger, R., Hobi, S., Hodson, E., Imer, D., Kreuzer, M., Künzle, T., Merbold, L., Niklaus, P. A., Rihm, B., Schellenberger, A., Schroth, M. H., Schubert, C. J., Siegrist, H., Stieger, J., Buchmann, N., and Brunner, D.: Anthropogenic and natural methane fluxes in Switzerland synthesized within a spatially explicit inventory, Biogeosciences, 11, 1941-1959, doi: 10.5194/bg-11-1941-2014, 2014.

Rödenbeck, C., Houweling, S., Gloor, M., and Heimann, M.: CO2 flux history 1982–2001 inferred from atmospheric data using a global inversion of atmospheric transport, Atmos. Chem. Phys., 3, 1919-1964, doi: 10.5194/acp-3-1919-2003, 2003.

Thompson, R. L., and Stohl, A.: FLEXINVERT: an atmospheric Bayesian inversion framework for determining surface fluxes of trace species using an optimized grid, Geosci. Model Dev., 7, 2223-2242, doi: 10.5194/gmd-7-2223-2014, 2014.

Manuscript prepared for Atmos. Chem. Phys. Discuss.
with version 2014/09/16 7.15 Copernicus papers of the LaTeX class copernicus.cls.
Date: 9 March 2016

Validation of the Swiss methane emission inventory by atmospheric observations and inverse modelling

S. Henne[1], D. Brunner[1], B. Oney[1], M. Leuenberger[2], W. Eugster[3], I. Bamberger[3,4], F. Meinhardt[5], M. Steinbacher[1], and L. Emmenegger[1]

[1]Empa Swiss Federal Laboratories for Materials Science and Technology, Überlandstrasse 129, Dübendorf, Switzerland
[2]Univ. of Bern, Physics Inst., Climate and Environmental Division, and Oeschger Centre for Climate Change Research, Bern, Switzerland
[3]ETH Zurich, Inst. of Agricultural Sciences, Zurich, Switzerland
[4]Institute of Meteorology and Climate Research Atmospheric Environmental Research (IMK-IFU), Karlsruhe Institute of Technology (KIT), Garmisch-Partenkirchen, Germany
[5]Umweltbundesamt (UBA), Kirchzarten, Germany

Correspondence to: S. Henne (stephan.henne@empa.ch)

Abstract

Atmospheric inverse modelling has the potential to provide observation-based estimates of greenhouse gas emissions at the country scale, thereby allowing for an independent validation of national emission inventories. Here, we present a regional scale inverse modelling study to quantify the emissions of methane (CH_4) from Switzerland, making use of the newly established CarboCount-CH measurement network and a high resolution Lagrangian transport model. In our reference inversion, prior emissions were taken from the "bottom-up" Swiss Greenhouse Gas Inventory (SGHGI) as published by the Swiss Federal Office for the Environment in 2014 for the year 2012. Overall we estimate national CH_4 emissions to be $196 \pm 18\,\mathrm{Gg\,yr^{-1}}$ for the year 2013 (1σ uncertainty). This result is in close agreement with the recently revised ~~"bottom-up"~~ SGHGI estimate of $206 \pm 33\,\mathrm{Gg\,yr^{-1}}$ ~~published by the Swiss Federal Office for the Environment as part of the Swiss Greenhouse Gas Inventory (SGHGI).~~ as reported in 2015 for the year 2012. Results from sensitivity inversions using alternative prior emissions, uncertainty covariance settings, ~~baseline treatments~~large-scale background mole fractions, two different inverse algorithms (Bayesian and extended Kalman Filter), and two different transport models ~~confirms~~ confirm the robustness and independent character of our estimate. According to the latest ~~"bottom-up" inventory~~ SGHGI estimate the main CH_4 source categories in Switzerland are agriculture (78 %), waste handling (15 %) and natural gas distribution and combustion (6 %). The spatial distribution and seasonal variability of our posterior emissions suggest an overestimation of agricultural CH_4 emissions by 10 to 20 % in the most recent ~~national inventory~~SGHGI, which is likely due to an overestimation of emissions from manure handling. Urban areas do not appear as emission hotspots in our posterior results suggesting that leakages from natural gas ~~disribution~~ distribution are only a minor source of CH_4 in Switzerland. This is consistent with rather low emissions of $8.4\,\mathrm{Gg\,yr^{-1}}$ reported by the SGHGI but inconsistent with the much higher value of $32\,\mathrm{Gg\,yr^{-1}}$ implied by the EDGARv4.2 inventory for this sector. Increased CH_4 emissions (up to 30 % compared to the prior) were deduced for the north-eastern parts of Switzerland. This feature was common to most sen-

sitivity inversions, which ~~rules out~~ is a strong indicator that it is a real feature and not an artefact of the transport model and the inversion system. However, it was not possible to assign an unambiguous source process to the region. The observations of the CarboCount-CH network provided invaluable and independent information for the validation of the national bottom-up inventory. Similar systems need to be sustained to provide independent monitoring of future climate agreements.

1 Introduction

Atmospheric methane (CH_4) acts as an important greenhouse gas (GHG) whose man-made increase from pre-industrial to present day levels (from $\approx 700\,\mathrm{nmol\,mol^{-1}}$ in 1750 to $1819\,\mathrm{nmol\,mol^{-1}}$ in 2012) directly and indirectly contributes 0.97 (0.74–1.20) $\mathrm{W\,m^{-2}}$ to present day global radiative forcing (Myhre et al., 2013). As such, its contribution to human-induced global warming is second only to carbon dioxide (CO_2). Globally, natural sources (wetlands, lakes, geological seeps, termites, methane hydrates, and wild animals) and anthropogenic sources (fossil fuel extraction, distribution and combustion, rice cultivation, ruminants, and waste) each contribute about half to CH_4 emissions to the atmosphere (Kirschke et al., 2013), but larger uncertainties are connected with the natural sources. Owing to increased research efforts in recent years, uncertainties associated with these fluxes have decreased on the global and continental scale (Kirschke et al., 2013, and references therein). However, there remain open questions about the contributing processes and their temporal and spatial distributions on the regional scale (Nisbet et al., 2014).

In many developed countries natural CH_4 sources are of limited importance (Bergamaschi et al., 2010) and anthropogenic emissions dominate. For example $\approx 98\,\%$ of Swiss CH_4 emissions are thought to be of anthropogenic origin (Hiller et al., 2014a). Owing to its comparatively short atmospheric lifetime ($\approx 10\,\mathrm{years}$) CH_4 has been classified as a short-lived climate pollutant, and reducing anthropogenic CH_4 emissions has become a promising target to lower near-term radiative forcing (Ramanathan and Xu, 2010; Shindell et al., 2012). However, the development of efficient mitigation strategies requires detailed knowl-

edge of the source processes and the success of the mitigation measures should be monitored once put into action. The Kyoto protocol sets legally binding GHG emission reduction targets for Annex-1 countries and the United Nations Framework Convention on Climate Change (UNFCCC) calls signatory countries to report their annual GHG emissions of CO_2, CH_4, nitrous oxide, sulphur hexafluoride, and halocarbons.

In Switzerland, the Federal Office for the Environment (FOEN) collects activity data and emission factors in the Swiss Greenhouse Gas Inventory (SGHGI) (FOEN, 2014, 2015) and annually reports emissions following IPCC guidelines (IPCC, 2006). According to this inventory, emissions from agriculture are the single most important source (161.5 $Gg\,yr^{-1}$) in Switzerland, followed by waste handling (32.3 $Gg\,yr^{-1}$) and fossil fuel distribution and combustion (12.1 $Gg\,yr^{-1}$, all values refer to the 2015 reporting for the year 2012). Estimates following IPCC guidelines are derived bottom-up from source-specific information combined with activity data and other statistical data, all of which may contain considerable uncertainties. ~~Methane emissions from individual sources~~ Anthropogenic CH_4 emissions in Switzerland originate from processes that may vary strongly on an individual basis (e.g., ruminants, manure handling, waste treatment). Hence, on the country level they are much more difficult to quantify than anthropogenic emissions of CO_2, which can be largely deduced from fuel statistics. As a consequence, the uncertainty assigned to total Swiss CH_4 emissions ($\pm$16 %) is much larger than that of CO_2 emissions ($\pm$3 %) (FOEN, 2015). According to the SGHGI, Swiss CH_4 emissions have decreased by about 20 % since 1990 (FOEN, 2015), but given the above uncertainties, these estimates require further validation, also in order to survey the effectiveness of the realised reduction measures. Furthermore, considerable differences exist between the SGHGI and other global and European scale inventories (e.g. EDGAR) both in terms of total amount and spatial distribution (Hiller et al., 2014a). Previous validation efforts of the Swiss CH_4 inventory were restricted to flux measurements either on the site scale focusing on a specific emission process (Eugster et al., 2011; Tuzson et al., 2010; Schroth et al., 2012; Schubert et al., 2012) or campaign based flight missions (Hiller et al., 2014b) and tethered balloon soundings (Stieger et al., 2015), mainly confirming estimates of the SGHGI on the local scale. In addition, mobile near-

surface measurements were used to verify emission hot spots in a qualitative way (Bamberger et al., 2014). However, due to the limited number of studies and the focus on rather small areas it is very difficult to ~~upscale the results of these studies to validate national annual~~ employ these results for the validation of national total emissions.

Such an independent validation of spatially resolved national inventory data can be achieved through inverse modelling yielding a top-down estimate that ~~combines~~ uses atmospheric observations of the target species together with transport modelling ~~and an optimal estimation of~~ in order to optimally estimate the underlying emissions (Enting, 2002; Bergamaschi et al., 2005). Early inverse modelling studies of CH_4 focused on the global scale budget and relied on global flask sampling observations (e.g. Hein et al., 1997; Houweling et al., 1999; Bergamaschi et al., 2000; Dentener et al., 2003; Mikaloff Fletcher et al., 2004). Later studies also included continuous surface and airborne observations (e.g. Vermeulen et al., 1999; Bergamaschi et al., 2005, 2010; Chen and Prinn, 2006; Kort et al., 2010; Manning et al., 2011; Miller et al., 2013) and provide country specific emissions. For data sparse regions, the additional use of satellite retrieved CH_4 data in atmospheric inversions has recently helped reducing uncertainties (Meirink et al., 2008; Bergamaschi et al., 2013) and increased the ability to deduce emissions with higher spatial resolution (Wecht et al., 2014; Turner et al., 2015). However, such top-down estimates were usually not made for small countries and regions like Switzerland (O(10 000 km^2)), owing to the coarse spatial resolution of the inversion systems. Recent studies from the USA have shown large differences between national and regional bottom-up estimates and inverse modelling, predominantly detecting large emission underestimations in the bottom-up inventories (Wecht et al., 2014; Turner et al., 2015; Miller et al., 2013; McKain et al., 2015; Wennberg et al., 2012). These were mainly attributed to three major source processes: oil and gas extraction, ruminants, and natural gas distribution to the end user.

Here, we validate the bottom-up estimate of Swiss CH_4 emissions as given in the SGHGI by analysing continuous, near surface observations of CH_4 from the newly established, dense CarboCount-CH measurement network in central Switzerland (Oney et al., 2015) and two neighbouring sites. For the first time, we apply an inverse modelling framework with

high spatial resolution (<10 km) to a relatively small area with considerable land surface heterogeneity and topographical complexity. Such modelling approaches have only recently become feasible through the use of high-resolution atmospheric transport simulations ~~(e.g. for CH_4, McKain et al., 2015)~~(e.g. for CH_4, Zhao et al., 2009; Jeong et al., 2012, 2013; McKa
The main aim of the study is to provide an independent validation of the SGHGI in terms of national total emissions (FOEN, 2015), geographical (Hiller et al., 2014a) and temporal distribution. Results in the spatio-temporal distribution shall be used to draw conclusions on the estimates of individual source processes.

2 Data and methods

2.1 Observations

The CH_4 observations used in this study are those of the CarboCount-CH[1] network (BEO, ~~LAE~~LHW, FRU, GIM) located on the Swiss Plateau and those from two additional mountain sites: Jungfraujoch and Schauinsland (see Fig. 1, S1 in the Supplement and Table 1). The Swiss Plateau, the relatively flat area between the Alps in the south and Jura mountains in the north, covers only about one third of the area of Switzerland but is home to two thirds of the Swiss population and is characterized by intensive agriculture and extended urban and suburban areas. Approximately two thirds of the Swiss CH_4 emissions are thought to stem from this area (Hiller et al., 2014a). Oney et al. (2015) characterised the transport to the ~~CarboCount-CH~~ CarboCountCH sites applying the same transport model as used here. They find that all four sites are mainly sensitive to emissions from most of the Swiss Plateau during summer day-time conditions, whereas sensitivities are more localised around the sites in winter, but still provide reasonable coverage of the targeted area of the Swiss Plateau.

The Beromünster (BEO) site is located on a hill in an intensively used agricultural area. It is surrounded mainly by croplands and to a smaller extent rangeland. The site itself consists

[1] http://www.carbocount.ch, last accessed 9 September 2015

of a 217 m high decommissioned radio transmission tower. Gas inlets and meteorological instrumentation are installed on the tower at 5 different heights above ground (12 to 212 m), whereas the gas analyser is located at the foot of the tower. A comprehensive description of the installation and the measurement system can be found in Berhanu et al. (2015). Here, only the observations from the topmost inlet height (212 m) were used, since this height showed the largest extent of the relative footprint and, hence, is least influenced by local sources (Oney et al., 2015).

Lägern Hochwacht (~~LAE~~LHW) is a mountain top site on a a very steep, west–east extending crest approximately 15 km north-west of and 400 m above the city centre of Zurich, the largest city in Switzerland. The site is surrounded by forest with average tree crown heights of 20 m close to the site. The gas inlet and meteorological instrumentation is mounted on a small tower of 32 m.

Früebüel (FRU) is another mountain site and located at 982 m a.s.l. above lake Zug on the south-eastern edge of the Swiss Plateau. Unlike Lägern-Hochwacht, the site is located on a mountain top plateau with a south-west aspect above lake Zug and with slightly more elevated areas to the south-east. The area around the site is used as rangeland and emissions from a local dairy farm may influence the observations. In contrast to the other sites, gas samples and meteorological observations are taken close to the surface (3 m above ground). A more detailed analysis of how the observations of this site are locally influenced and how they can be compared to observations from the close-by tall tower in BEO is given in Bamberger et al. (2015). Here we only note that the influence of local emissions that cannot be accounted for in the transport model needs to be filtered from the observational data before the use in inverse modelling. We did this by removing all data (10 min resolution) with low wind speeds ($< 3\,\mathrm{m\,s^{-1}}$) coming from the direction of the aforementioned farm (140 to 200°). These thresholds were determined by comparing differences between the observations of BEO (212 m), which exhibit less local influences, and FRU as a function of wind speed and direction at FRU.

At the Gimmiz site (GIM, 443 m a.s.l.) sample gases are drawn from a 32 m tall water tower. The surrounding area is flat and dominated by intensive agriculture, mostly veg-

etable farming and croplands. The area is a transformed wetland that used to be regularly flooded until the 1850s before the leveling of the river system (1868–1891) when also former wetlands were converted to agricultural lands (Schneider and Eugster, 2007). Although there are only two small farms in the direct vicinity, larger potential CH_4 sources are located in the town of Aarberg about 2.5 km to the south-east. Here a sugar refinery, operating a large-scale waste water treatment plant (250 000 person equivalent), a compost and soil recycling facility, and a biogas reactor for electrical power generation are located. These local sources may not be represented sufficiently well in model simulations. Therefore and as in the case of FRU, observations from GIM were filtered by wind speed and direction, excluding all 10 min averages for which wind speeds were either below 2 m s^{-1} or coming from directions between 90 and 150 °. Again these thresholds were estimated by comparison to the observations at BEO.

Schauinsland (SSL, 1205 m a.s.l.) is a mountain top site in the Black Forest, Germany, to the north of the Swiss Plateau. As such it is usually situated above the stable nocturnal boundary layer of the surrounding, but at day-time it is affected by boundary layer air (Schmidt et al., 1996). The site is surrounded by forests and rangeland and no large CH_4 source is known in the direct vicinity. While not part of CarboCount-CH network, the observations from SSL provide additional constraints for the atmospheric inversion especially at mid-distance from the Swiss Plateau.

The high-altitude observatory Jungfraujoch (JFJ, 3580 m a.s.l.) is located in the northern Swiss Alps on a steep mountain saddle between the two mountains Jungfrau (4158 m a.s.l.) and Mönch (4099 m a.s.l.). Altough JFJ is usually located in the free troposphere, it intermittently receives polluted boundary layer air both from sources north and south of the Alps (Zellweger et al., 2003; Henne et al., 2010; Tuzson et al., 2011). The intensity of these transport events from the boundary layer can vary strongly depending on the weather condition and the transport process responsible for lifting.

At all sites CH_4 measurements were carried out using PICARRO (Santa Clara, CA, USA) cavity ring-down spectrometers (Rella et al., 2012) which provide high frequency (approximately 0.5 to 1 Hz) observations of CO_2, CH_4, H_2O and (at BEO and ~~LAE~~LHW)

CO. All instruments were calibrated against the WMO X2004 CH_4 scale (Dlugokencky et al., 2005) and were reporting dry air mole fractions by either applying a water vapor correction accounting for dilution and spectroscopic effects (CarboCount-CH sites and SSL) or by using pre-sample drying of sample air (JFJ). At the CarboCount-CH sites, measurements of additional target gases, not used for the calibration, give an estimate of the instruments' non-random uncertainty for CH_4 of $\approx 0.5\,\mathrm{nmol\,mol^{-1}}$ (Oney et al., 2015). At SSL observations of three additional target gases yield a combined measurement uncertainty of $0.3\,\mathrm{nmol\,mol^{-1}}$. For JFJ a combined measurement uncertainty of $\sigma = \sqrt{0.31^2 + (3.61 \times 10^{-4} \times \chi)^2}\,\mathrm{nmol\,mol^{-1}}$ was reported for hourly aggregates, where χ is the observed mole fraction (Empa, 2015).

For the use in the inversion 3 hourly aggregates were produced from high frequency observations for the period 1 March 2013 to 28 February 2014, the first year with a complete set of measurements for all CarboCount-CH sites. Prior to aggregation, the data filtering as described above was applied to the sites GIM and FRU. Out of the dataset, only the afternoon values, covering 12:00 to 18:00 UTC (CarboCount-CH sites), were used in the atmospheric inversion. This was done in order to capture the time of day with the deepest planetary boundary layer (PBL) extent, which should also be best captured by the transport model and yield the smallest model bias (Kretschmer et al., 2014) and at the same time minimise the influence of local sources and sinks. For the ~~more remote~~ elevated sites JFJ and SSL, the night-time data from 00:00 to 06:00 UTC were used instead~~,~~. This is the time when the sites are least influenced by ~~transport in complex terrain.~~ small-scale, thermally induced flow systems in the complex topography around the sites. Since the sites are situated on mountain tops no development of a shallow night-time boundary layer is expected so that the influence of local sources (if at all present) remains negligible at night. All of the following analysis and discussion is based on this filtered and aggregated dataset. In addition to the absolute mole fraction, an estimate of ~~the baseline mole fraction, which is supposed to~~ larger-scale background mole fractions, which represent conditions without recent emission input, was generated using the "Robust Estimation of Baseline Signal" (REBS) method (Ruckstuhl et al., 2012). We refer to this term as baseline mole fraction

in the following. It represents a smooth curve fitted to the data, providing a baseline mole fraction for each observational time. The absolute mole fraction of the observations, χ_{o}, can then be given as the sum of the baseline, $\chi_{\mathrm{o,\,b}}$, and the contribution due to recent emissions, $\chi_{\mathrm{o,\,p}}$,

$$\chi_{\mathrm{o}} = \chi_{\mathrm{o,\,p}} + \chi_{\mathrm{o,\,b}}. \tag{1}$$

The REBS method iteratively fits a non-parametric local regression curve to the observations, successively excluding points outside a certain range around the baseline curve. REBS was applied separately to hourly data from each site using asymmetric robustness weights with a tuning factor of $b = 3.5$, a temporal window width of 60 days and a maximum of 10 iterations. An estimate of the baseline uncertainty is given by REBS as a constant value for the whole time series. For JFJ the baseline uncertainty was estimated to 17.4 nmol mol^{-1}, whereas uncertainties for the other sites ranged between 16.2 nmol mol^{-1} (SSL) and 18.9 nmol mol^{-1} (~~LAE), reflecting different degrees of variability and~~ LHW). The larger values generally reflect a larger degree of variability in the baseline and a reduced frequency of air masses not influenced by recent surface contact and emissions.

2.2 Transport models

Source sensitivities giving the direct influence of a mass emission from a source location onto the mole fraction at a receptor site were calculated with two different versions of the Lagrangian Particle Dispersion Model (LPDM) FLEXPART (Stohl et al., 2005), which can be run in time-inverted mode. The first represents the standard FLEXPART model (version 9.02) driven by analysis fields of the operational runs of the Integrated Forecast System (IFS) of the European Centre for Medium Range Weather Forecast (ECMWF). Input fields were available every 3 h with a horizontal resolution of 0.2° × 0.2° (≈ 15 km × ≈ 22 km) for the Alpine area ~~and~~ (-4°E to 16°E and 39°N to 51°N) and 1° × 1° elsewhere. The second FLEXPART version is the one adapted to the use of output from the COSMO regional numerical weather prediction (NWP) model (Baldauf et al., 2011). FLEXPART-COSMO was

driven by operational analysis fields as generated hourly by the Swiss national weather service, MeteoSwiss, for Western Europe (approx. -10°E to 20°E and 38°N to 55°N) with a horizontal resolution of ~~approximately~~ approx. 7 km × 7 km. Hourly analysis fields are produced applying an observational nudging technique (Schraff, 1997) to near surface and vertical profile observations of pressure, relative humidity and wind. The use of a high-resolution transport model in regional scale inversions based on point observations is a prerequisite to reduce the representation uncertainty of the model (Tolk et al., 2008; Pillai et al., 2011). Furthermore, the use of a time-inverted LPDM is highly beneficial to this purpose as it allows an accurate transport description in the near-field of the sites below the resolution of the driving meteorology.

The main differences between FLEXPART-COSMO and standard FLEXPART-ECMWF are the internal vertical grid representation and the parameterisation of convective transport. In FLEXPART-COSMO, the native vertical grid of the COSMO model is used as the main frame of reference, which, in this case, was a height-based hybrid coordinate system (Gal-Chen and Somerville, 1975). In contrast, standard FLEXPART uses a terrain-following vertical coordinate with constant level depths up to the model top, which requires an initial vertical interpolation from the pressure-based hybrid coordinate used in the IFS. In FLEXPART-COSMO, all interpolation to particle positions is done directly from the native COSMO grid, avoiding multiple interpolation errors. In FLEXPART-ECMWF sub-grid scale convection is treated by an Emanuel type scheme (Emanuel and Zivkovic-Rothman, 1999; Forster et al., 2007), whereas in FLEXPART-COSMO the same modified version of the Tiedtke convection scheme (Tiedtke, 1989) as used in COSMO was implemented.

PBL heights are a critical parameter in FLEXPART since they are used as a scaling parameter for the turbulence parameterisation. We use the default implementation within FLEXPART to diagnose PBL heights applying a Bulk-Richardson method (Stohl et al., 2005; Vogelezang and Holtslag, 1996). In contrast to standard FLEXPART we did not use 2-metre temperatures from COSMO in the PBL estimation but the lowest model level temperature (approx. 10 m above ground), because FLEXPART and COSMO PBL heights showed a positive bias when compared to PBL height observations from the

sounding site Payerne on the Swiss Plateau under convective conditions and when using 2-metre temperatures (Collaud Coen et al., 2014). This bias disappeared when using the first level temperatures instead.

With both model versions source sensitivities were calculated for each observation site and 3 hourly interval. For each interval and location a total of 50 000 particles was released and followed backward in time for 4 and 10 days in the COSMO and ECMWF version, respectively. Particles leaving the limited COSMO-7 domain were terminated prematurely. The limited horizontal model resolution and the complex terrain in the investigated domain lead to differences between the model surface altitude and the real site altitude. In such situations, the most representative height above model ground for particle releases in an LPDM is not well known. Therefore, we chose to release particles at two vertical locations for the CarboCount-CH sites to analyse the sensitivity of this choice. At BEO, where the model topography is relatively close to the site's altitude, these span the possible range of reasonable release altitudes by representing (1) the height above model surface as given by the inlet height of the observations and (2) the absolute altitude above sea level of the inlet. At the sites FRU and ~~LAE~~ LHW the lower release height was chosen 50 m and the higher 150 m above model ground because height deficiencies in the model were larger here. At GIM only one release height was used because the model topography was relatively close to the true surface altitude. Also for the more remote sites JFJ and SSL only one release height was simulated that represents the middle between the model surface and the site altitude. Previously it was shown that such an approach works best (independent of time of day) for the mountaintop site JFJ, which shows large model topography deficits (Brunner et al., 2013). Values for all release heights are given in Table 1. Note, that release heights were the same for all FLEXPART-ECMWF and FLEXPART-COSMO simulations except for JFJ and SSL were surface height differences between the models were large.

From both models, output was generated on a regular longitude/latitude grid with a horizontal resolution of $0.16^\circ \times 0.12^\circ$ (≈ 13 km) covering Western Europe and for a nested Alpine domain with a horizontal resolution of $0.02^\circ \times 0.015^\circ$ (≈ 1.7 km). The generated output represents the summed residence time, $\tau_{i,j}$, of particles in a given grid box, i, j, and

below a specific sampling height, h_s, divided by the density of dry air in this grid cell and has units $s\,m^3\,kg^{-1}\,gridcell^{-1}$. The sampling height was set to 50 and 100 m above ground in FLEXPART-COSMO and FLEXPART-ECMWF, respectively, coinciding with the minimal PBL height used in the models. Multiplication of $\tau_{i,j}$ with the volume of the sampling grid cell, $V_{i,j} = A_{i,j} \cdot h_s$, and the ratio of the molar weight of the species of interest, μ_s, and the molar weight of dry air, μ_d, yields the desired source sensitivity, $m_{i,j}$, in units $s\,kg^{-1}\,mol\,mol^{-1}$

$$m_{i,j} = \frac{\tau_{i,j}}{V_{i,j}} \frac{\mu_d}{\mu_s}. \tag{2}$$

$m_{i,j}$ ~~provides the effect~~ multiplied by a mass emission ~~, $E_{i,j}$ (),~~ in a ~~source~~ grid box (~~i,j~~)i,j), $E_{i,j}$ ($kg\,s^{-1}$) gives the effect this emission would have on the dry air mole fraction at the receptor. The sum over all grid boxes then yields the increase in mole fraction, χ_p, due to recent emissions~~.~~, whereas the baseline mole fraction, χ_b, can be obtained as the average mole fraction over all particles at their endpoints in the simulation

$$\chi = \underbrace{\sum_{i,j} m_{i,j} E_{i,j}}_{\chi_p} + \underbrace{\frac{1}{K} \sum_{k}^{K} \chi_k}_{\chi_b}, \tag{3}$$

where i, j are the horizontal grid indices, χ_k the mole fraction at each particle's end point, and K is the number of particles. In our FLEXPART-COSMO simulations particles were followed for 4 days backward in time. Not all particles leave the limited area model domain during this time, so that the baseline mole fraction as given in (3) cannot be directly translated to conditions at the domain boundaries, but may also contain contributions from within the domain and, therefore, may vary between different sites. For the inversion set-up it would be beneficial if the baseline mole fractions could be estimated from an external 3-dimensional model. However, such model input was not available at the time of analysis, and thus the prior baseline mole fraction was taken as the one estimated from the observations (REBS) and further optimised in the inversion.

2.3 Inversion framework

In our inversion system the source sensitivities calculated by the transport model can be used to give a direct relationship between the simulated mole fractions and the so called state vector, $\boldsymbol{x} = (x_1 \dots x_K)$ with a total of K elements, that primarily contains the desired gridded emissions. In matrix notation this can be expressed as

$$\boldsymbol{\chi} = \mathbf{M}\boldsymbol{x}, \tag{4}$$

where $\boldsymbol{\chi} = (\chi_1 \dots \chi_L)$ represents the simulated mole fractions at different times and locations, $l = 1, \dots, L$. The sensitivity matrix $\mathbf{M}$ (dimensioned $K \times L$) contains the sensitivities for each time/location towards the kth element of the state vector.

In our case, the state vector contained additional parameters characterising the baseline mole fractions χ_b at different times and for different sites. Hence, $\boldsymbol{x}$ contained K_E elements describing the emissions and $K_\mathrm{B} = K - K_\mathrm{E}$ elements giving baseline mole fractions, which were not estimated at each observation but at discrete time intervals (baseline nodes). Therefore, the sensitivity matrix $\mathbf{M}$ consists of two block matrices $\mathbf{M}^\mathrm{E}$ and $\mathbf{M}^\mathrm{B}$ giving the dependence on the emissions and baseline mole fractions, respectively. Similar to Stohl et al. (2009), elements of $\mathbf{M}^\mathrm{B}$ were set to represent temporal linear interpolation between the baseline mole fractions at the neighbouring baseline nodes. We estimate the baseline separately for each site in the inversion, since it does not necessarily just reflect the conditions at the boundary of the domain, but may also contain contributions from within the domain (see discussion above). Different sites may therefore have different levels of within-domain-influence. This is especially true for sites at different altitudes even if these are located at short distances as in our network. Since the baseline treatment is a critical part of the inversion system and may lead to attribution errors of the emissions, we present two alternative baseline estimation approaches as part of our sensitivity analysis (see Sect. 2.5.7). For our base inversion, baseline nodes were spaced equidistantly with a distance of $\tau_\mathrm{B} = 5$ days over the observation period and were optimised separately for each site, resulting in 73 baseline elements in the state vector for each site. Prior estimates

of the baseline mole fractions were REBS estimates for the site JFJ (see Sect. 2.1). Since the REBS estimate represents a smooth curve to the data, the REBS value at the time of a given baseline node was used as its prior value.

In our base set-up we target temporal average emission fluxes for the period of observations (March 2013 to February 2014) and optimise their spatial distribution. We include seasonality in the emission fluxes as part of our sensitivity analysis (see Sect. 2.5.2).

In order to reduce the size of the inversion problem, emissions were not optimised on a regular longitude/latitude grid as given by the FLEXPART simulations. Instead, a reduced grid was used that assigns finer (coarser) grid cells in areas with larger (smaller) average source sensitivities. Starting from the finest output grid resolution of $0.02^\circ \times 0.015^\circ$ ~~grid boxes up to a maximum size of $2.56^\circ \times 1.92^\circ$ were aggregated~~ four neighbouring grid cells were merged if their average residence time did not reach a specified threshold. ~~In this way~~ This procedure was iterated up to a maximum grid cell size of $2.56^\circ \times 1.92^\circ$. The residence time threshold was set manually in order to reduce the number of cells in the inversion ~~was reduced~~ to the order of ~~$J_E \approx 1000$~~ $K_E \approx 1000$. The overall extent of the emission grid was determined by (1) the extent of the COSMO-7 domain, (2) the existence of considerable CH_4 emissions (cut-off over the oceans) and (3) a minimum source sensitivity. Tests with larger and smaller inversion domains did not indicate significant influences on the deduction of Swiss emissions.

In Bayesian atmospheric inversion prior knowledge of the state vector, $\boldsymbol{x}_b$, and its probability distribution is used to guide the optimisation process. Mathematically this can be expressed by formulating a cost function J that penalises deviations from the prior state and differences between simulated and observed mole fractions (e.g. Tarantola, 2005)

$$J = \frac{1}{2}(\boldsymbol{x} - \boldsymbol{x}_\mathrm{b})^T \mathbf{B}^{-1}(\boldsymbol{x} - \boldsymbol{x}_\mathrm{b}) + \frac{1}{2}(\mathbf{M}\boldsymbol{x} - \boldsymbol{\chi}_\mathrm{o})^T \mathbf{R}^{-1}(\mathbf{M}\boldsymbol{x} - \boldsymbol{\chi}_\mathrm{o}), \quad (5)$$

where $\boldsymbol{x}$ describes the optimised and $\boldsymbol{x}_b$ the prior state vector, and $\mathbf{M}\boldsymbol{x} - \boldsymbol{\chi}_\mathrm{o}$ is the difference between simulated and observed mole fractions. $\mathbf{B}$ and $\mathbf{R}$ give the uncertainty covariance matrices of the prior state and the combined model-observation uncertainty. In Sect. 2.4

the structure of these matrices is discussed in more detail. Minimisation of J yields the posterior state

$$\boldsymbol{x} = \boldsymbol{x}_\mathrm{b} + \mathbf{B}\mathbf{M}^T \left(\mathbf{M}\mathbf{B}\mathbf{M}^T - \mathbf{R}\right)^{-1} (\boldsymbol{\chi}_\mathrm{o} - \mathbf{M}\boldsymbol{x}_\mathrm{b}). \tag{6}$$

In our implementation the inverse of $\mathbf{S} = \left(\mathbf{M}\mathbf{B}\mathbf{M}^T - \mathbf{R}\right)$, a $L \times L$ matrix, was calculated using LU factorisation (function DGESVX in LAPACK). In addition to the posterior state also its uncertainty expressed as ~~a~~ an uncertainty covariance matrix, $\mathbf{A}$, can be given (e.g. Tarantola, 2005)

$$\mathbf{A} = \mathbf{B} - \mathbf{B}\mathbf{M}^T\mathbf{S}^{-1}\mathbf{M}\mathbf{B}. \tag{7}$$

The total emissions and their uncertainty from a certain region or country can then be calculated as

$$E = \sum_k^{K_\mathrm{E}} x_k f_k g_k; \sigma_\mathrm{E}^2 = \boldsymbol{g}^T \mathbf{A}^\mathrm{E} \boldsymbol{g}, \tag{8}$$

where the vector ~~f~~ g gives the fractional contribution of ~~the region to each~~ a region to an inversion grid cell and $\mathbf{A}^\mathrm{E}$ is the part of $\mathbf{A}$ that contains the uncertainty covariance of the posterior emissions. ~~f_k~~ g_k takes a value of 1 for a grid cell that is completely within the region and 0 for grid cells outside the region. For coarse inversion grid cells ~~on the border of a region, f_k~~ containing more than one region, g_k was calculated from higher resolution population data, weighting per region contributions by population and not by land surface area. In the case of the present CH_4 inversion and the national estimates for Switzerland this treatment was of minor importance but is more crucial for other species that exhibit sharp emission gradients more closely following the population distribution (e.g., halocarbons).

In our base inversion, we used the Swiss MAIOLICA inventory (Hiller et al., 2014a), which is based on the total Swiss emissions estimated by FOEN (SGHGI) for the year 2011 and reported to UNFCCC in 2013. For areas outside Switzerland prior emissions were taken from the European scale inventory developed by TNO for the MACC-2 project (Kuenen et al., 2014) (TNO/MACC-2 hereafter) applying the same country-by-country scaling to 2011 values reported to UNFCCC in 2013.

2.4 Covariance design

This section details the construction of the uncertainty covariance matrices **B** and **R** as used in the base inversion. Parameters used to build the matrices were chosen based on experience and previous publications (see below). The sensitivity to these choices was investigated in a set of sensitivity inversions as described in Sect. 2.5.

Both uncertainty covariance matrices are symmetric block matrices. In the case of **B** one block, $\mathbf{B}^{\mathsf{E}}$, describes the uncertainty covariances of the emission vector and a second block, $\mathbf{B}^{\mathsf{B}}$, the uncertainty covariances of the baseline mole fractions. Within each block the off-diagonal elements were allowed to be non-zero. The diagonal elements of $\mathbf{B}^{\mathsf{E}}$ were set proportional (factor f_{E}) to the prior emissions in the respective grid cell $B^{\mathsf{E}}_{j,j} = (f_{\mathsf{E}} x_{b,j})^2$. For ~~the off-diagonal elements~~ land grid cells with low emissions (below 10 % of land average) and ocean grid cells the uncertainty was set to 10 % of the average land cell uncertainty in order to avoid near zero uncertainties. Lacking more detailed information of the spatial uncertainty covariance structure, a spatial correlation of the uncertainty was assumed for the off-diagonal elements that decays exponentially with the distance between two grid cells (e.g., Rödenbeck et al., 2003; Gerbig et al., 2006; Thompson and Stohl, 2014)

$$B^{E}_{i,j} = e^{-\frac{d_{i,j}}{L}} \sqrt{B^{\mathsf{E}}_{i,i}} \sqrt{B^{\mathsf{E}}_{j,j}}, \tag{9}$$

where $d_{i,j}$ is the distance between two grid cell centres and L the correlation length. In this ~~setup~~ set-up the total squared uncertainty of the prior emissions $\sigma^2_{\mathsf{E}} = 1^T \mathbf{B}^{\mathsf{E}} 1$, where 1 is a vector of all ones, only depends on the settings of L and f_{E}. For the base inversion L was fixed to 50 km and f_{E} was adjusted to yield fixed relative uncertainties of the national estimate for Switzerland ~~.~~ of 16 %, which is the uncertainty given for the Swiss bottom-up estimate (FOEN, 2015). The choice of 50 km was driven by the need for sufficient constraints for neighbouring grid cells, whereas Hiller et al. (2014a) suggested a shorter length scale around 10 km based on a comparison of the spatial structures of the MAIOLICA, TNO/MACC-2 and EDGAR CH_4 inventories.

~~For the base inversion baseline nodes were spaced equidistantly with a distance of $\tau_B = 5$ days over the observation period and individually for each site, resulting in 73 baseline elements in the state vector for each site. Prior estimates of the baseline mole fractions were REBS estimates for the site JFJ (see Sect. 2.1).~~ All diagonal elements of $\mathbf{B}^{\mathsf{B}}$ were set to a constant value, $B^{\mathsf{B}}_{i,i} = f_{\mathsf{b}}\sigma^2_{\mathsf{b}}$, where σ_{b} is an estimate of any given baseline uncertainty and f_{b} is a scaling factor. The off-diagonal elements were set assuming an exponentially decaying correlation of the baseline uncertainty between baseline nodes at a given site

$$B^{\mathsf{B}}_{i,j} = e^{-\frac{T_{i,j}}{\tau_{\mathsf{b}}}} \sqrt{B^{\mathsf{B}}_{i,i}} \sqrt{B^{\mathsf{B}}_{j,j}}, \tag{10}$$

where $T_{i,j}$ is the time difference between two nodes and τ_{b} is the temporal correlation length. In the base inversion, σ_{b} was obtained from the REBS fit of the JFJ observations (17.4 nmol mol^{-1}), f_{b} was set to unity, and τ_{b} to 14 days. As for L, the choice of τ_{b} is somewhat arbitrary but governed by the need for sufficient constraints on the posterior solution without restricting adjustments too strongly .

In the case of temporally variable emissions (see Sect. 2.5.2) the state vector x, the sensitivity matrix and the prior uncertainty matrix have to be extended. $\mathbf{B}^{\mathsf{E}}$ now should treat spatial and temporal covariance of the state vector. Individual diagonal elements of $\mathbf{B}^{\mathsf{E}}$, $B^{\mathsf{E}}_{i,i}$, now refer to different emission locations and time, with the index i running over both of them. The off-diagonal elements can then be given by

$$B^{E}_{i,j} = e^{-\frac{T_{i,j}}{\tau_{\mathsf{t}}}} e^{-\frac{d_{i,j}}{L}} \sqrt{B^{\mathsf{E}}_{i,i}} \sqrt{B^{\mathsf{E}}_{j,j}}, \tag{11}$$

where in addition to equation (9), $T_{i,j}$ gives the time difference between two emission sets and τ_{t} is the temporal correlation length scale of the prior emissions.

The block matrix $\mathbf{R}$ contains one block for each site used in the inversion. In its diagonal elements both the observation and the model uncertainty were considered by quadratic

addition

$$R_{i,i} = \sigma_{\mathrm{o}}^2 + \sigma_{\mathrm{min}}^2 + \sigma_{\mathrm{srr}}^2 \chi_{\mathrm{p},i}^2, \tag{12}$$

where σ_o is the observation uncertainty as estimated for each 3 hourly CH_4 average (see Sect. 2.1) and the second and third term are contributions of the model uncertainty. σ_{min} represents a constant contribution while the third term represents an uncertainty contribution relative to the prior simulation of ~~above baseline~~ above-baseline concentrations, $\chi_{\mathrm{p},i}$ (Brunner et al., 2012). For the base inversion, σ_{min} and σ_{srr} were estimated separately for each site from the model residuals (difference between simulated and observed mole fraction) of the prior simulation, $\chi_{\mathrm{p},i}$, by fitting a ~~linear regression through binned RMSEs calculated~~ straight line through RMSEs calculated for separate bins along $\chi_{\mathrm{p,\,o}}$. The choice of this method was motivated by the observation that prior model residuals tend to increase with prior mole fractions. Estimating the model uncertainty from the ~~residuals of the prior simulation~~ prior model residuals has been suggested before by Stohl et al. (2009), where σ_{min} was estimated ~~from all residuals~~as the RMSE from the prior simulation, whereas σ_{srr} was set to 0. In an additional step this constant value was then forced to yield a normal distribution of the normalised model residuals. Furthermore, Stohl et al. (2009) applied their ~~residual~~ uncertainty estimation in an iterative way using the model residuals from successive inversion runs. In our experience this may lead to underestimated model uncertainties and we did not iterate our procedure. These methods have in common that the results of the prior simulation influence the estimation of R, therefore somewhat violating the independence of prior and model/observation uncertainties assumed in the Bayesian approach. Finally, off-diagonal elements of the model-observations uncertainty covariance matrix were assumed to follow an exponentially decaying correlation structure.

$$R_{i,j} = e^{-\frac{T_{i,j}}{\tau_{\mathrm{o}}}} \sqrt{R_{i,i}} \sqrt{R_{j,j}}, \tag{13}$$

where $T_{i,j}$ is the time difference between two measurements and τ_{o} is the temporal correlation length that describes the auto-correlation in the model-observation uncertainty. In

the base inversion τ_o was set to 0.5 days, a value previously used by other authors (e.g. Thompson et al., 2011) and associated with the inability of atmospheric transport models to correctly simulate the diurnal cycle in the PBL. The uncertainty covariances between observations from different sites were set to 0.

2.5 Sensitivity inversions

The Bayesian inversion provides an estimate of the posterior uncertainty of the state vector, which in itself should be sufficient to give an estimate of the combined top-down uncertainty. However, this analytical uncertainty tends to underpredict the true uncertainty. Optimality of the Bayesian approach requires normally distributed probability density functions, temporally uncorrelated residuals, and non-systematic uncertainties~~—~~; requirements that are difficult to meet exactly in practice. In particular, potential systematic uncertainties in model transport, which may contribute importantly to the overall uncertainty (e.g. Gerbig et al., 2008), are not accounted for. To explore the range of uncertainty beyond the analytically derived posterior uncertainty and to test the robustness of the results to different assumptions, it has therefore been proposed to perform additional sensitivity inversions (e.g. Bergamaschi et al., 2010, 2015). To this end, we set up a series of sensitivity inversions that vary different aspects of the inversion (transport simulations, inversion algorithm, uncertainty covariance design, prior emissions, observation selection, seasonality of emissions). An overview of these sensitivity inversions is given in Table 2 and details are described in the following.

2.5.1 Transport simulation

One important source of uncertainty when using observational data from elevated sites is the potential mismatch between model and real topography. The choice of the particle release height in the model can considerably change the model's performance and may lead to systematic biases in simulated concentrations. Therefore, we quantified the effect of the release height by using a "low" and "high" release case for each of the sensitivity

inversions in Table 2. One is always using the lower release heights for the CarboCount-CH stations as introduced in Sect. 2.2, whereas the other uses the higher release heights. The release heights of the more remote sites JFJ and SSL were not varied because of their less direct influence on the Swiss emissions. In addition to the release height, two different versions of the atmospheric transport model were used. The base inversion was based on FLEXPART-COSMO and a sensitivity run used the results of FLEXPART-ECMWF (S-EC).

2.5.2 Seasonal variability

In the base inversion emissions were assumed to be constant in time. However, considerable seasonal variability of the emissions especially from the agricultural sector can be expected. To test the implication of this assumption, a sensitivity run extending the state vector to separately hold emissions for each season (S-V) was set up ~~. The number of emission elements in the state vector increased by a factor of four in this case and the sensitivity matrix **M** had to be extended accordingly~~following the common definition of winter spanning the months December, January and February (DJF) and so forth (spring: MAM, summer: JJA, fall: SON). The prior emissions and their uncertainty were set identical for all seasons. ~~In addition, temporal correlation in the uncertainty covariance matrix of the prior state was treated analogously to the temporal correlation of the observation uncertainty by an exponentially decaying correlation with a time constant of 90 days~~ The correlation length scale between different emission times was set to $\tau_t = 90$ days (see equation 11). Reducing this time constant to 45 days had only a minor influence on the inverse emission estimate.

2.5.3 Inversion algorithm

An additional sensitivity test, replacing the Bayesian method by an extended Kalman Filter (extKF) inversion as described in Brunner et al. (2012), was conducted (case S-K). Similar to the Bayesian inversion a prior state vector is used by the extKF. In contrast to the Bayesian approach, the extKF assimilates the observations sequentially from time step to time step. In the extKF approach one baseline value and its tendency for each site are part

of the state vector. In each step observations from different sites but not from different times are incorporated. This allows for a more flexible temporal evolution of the emissions and the baseline values as for the Bayesian approach. Another important difference is that the extKF method of Brunner et al. (2012) estimates the logarithm of the emissions rather than the emissions themselves to enforce positive fluxes. This renders the problem non-linear and requires the use of an extended Kalman Filter. As in the Bayesian inversion the extKF describes the uncertainties of the prior state and the model-observation uncertainty through the respective uncertainty covariance matrices **B** and **R**. In addition to these, the extKF requires ~~a~~ an uncertainty covariance matrix **Q** that describes the uncertainty with which the state vector can change from one time step to the next.

Accordingly, uncertainties of the state vector are allowed to grow from one time step to the next, which introduces an additional amount of prior uncertainty as compared to the Bayesian approach. The matrices **B** and **R** were parameterised according to equations (9) and (12), respectively. The chosen parameter values are listed in Tab. 3. The forecast uncertainty matrix **Q** was also parameterised according to equation (9), notably with the same spatial correlation length. The diagonal elements of **Q** were set to a relative forecast uncertainty of the emissions of 0.6 % per 24 hours, which resulted in fairly constant posterior emissions in time with only a small seasonal cycle.

2.5.4 Covariance parameters

The next set of sensitivity inversions was designed to analyse the effect of different uncertainty covariance matrices. Our base inversion is based on the prior emission uncertainty as estimated by the ~~bottom-up inventory~~SGHGI, which we consider to be the best knowledge of ~~prior uncertainty~~bottom-up uncertainty in Switzerland. Since Hiller et al. (2014a) used the same by-category emissions as the SGHGI to spatially disaggregate total emissions for the MAIOLICA inventory (our prior), we extrapolated the SGHGI uncertainty information to the whole inversion domain. Next to the base inversion a set of uncertainty covariance parameters as estimated by the method of maximum likelihood (ML, Michalak et al., 2005) were used (S-ML). We estimated the covariance parameters (L, f_E, τ_b, and individually for each

site f_b, σ_{min}, σ_{srr}) by minimising the negative logarithm of the likelihood estimator (Michalak et al., 2005)

$$L_\theta = \frac{1}{2} \ln \left| \mathbf{MBM}^T + \mathbf{R} \right| + \frac{1}{2} (\boldsymbol{\chi}_o - \mathbf{M} x_b)^T \left(\mathbf{MBM}^T + \mathbf{R} \right)^{-1} (\boldsymbol{\chi}_o - \mathbf{M} x_b). \quad (14)$$

As a consequence of the ML optimisation posterior model residuals and posterior emission differences should follow a χ^2 distribution. To find the minimum of L_θ a multivariate optimisation routine was used. We applied the Broyden, Fletcher, Goldfarb and Shanno (BFGS) algorithm that is widely used for optimisation problems (see for example Nocedal and Wright, 2006). Initial parameter values were set equal to those used in the base inversion, but giving all sites the same σ_{min} of 20 nmol mol^{-1} and σ_{srr} of 1. To assess the robustness of the ML optimisation results an alternative algorithm was tested (Nelder–Mead), yielding very similar parameter sets.

Another sensitivity run varied the design of the model/observation uncertainty covariance by estimating the diagonal elements of the matrix from the prior RMSE at each site $\sigma_{min} = \mathrm{RMSE}(\chi_b - \chi_o)$ and applying a correction for extreme residual values according to Stohl et al. (2009) (S-S). Such extreme residuals only occurred for two observations at ~~LAE~~LHW, so that essentially a constant model uncertainty was used for each site. The off-diagonal elements were calculated in the same way as in the base inversion. For the extKF inversion it was only possible to use a fixed set of parameters σ_{min} and σ_{srr} for all sites, because by-site treatment was not yet implemented in the current version of the code. They were selected to be close to the average values used in the reference inversion. All covariance parameters used in the base, these two alternative and also the extKF inversion are compared in Table 3. In case of the Bayesian inversions, the covariance parameters differed between the two release heights with the high release showing larger values of σ_{min} for the sites BEO and ~~LAE~~ LHW and all applied estimation techniques.

2.5.5 Prior emissions

The sensitivity of the inversion result to the prior emissions was tested by using different prior inventories. In ~~our base inversion we used the Swiss MAIOLICA~~

inventory (Hiller et al., 2014a) reflecting the total Swiss emissions for the year 2011 as reported to UNFCCC in 2013. For areas outside Switzerland prior emissions were taken from the European scale inventory developed by TNO for the MACC-2 project (Kuenen et al., 2014) (TNO/MACC-2 hereafter) applying the same country-by-country scaling to 2011 values reported to UNFCCC in 2013. In a sensitivity inversion we replaced the MAIOLCIA emissions within Switzerland with those given by TNO/MACC-2 (S-T). A third sensitivity run was set up using the EDGAR (v4.2 FT2000) inventory for the base year 2010 (JRC/PBL, 2009) (S-E). In all three cases the prior uncertainty was set so that a value of $\sigma_E = 16\,\%$ was reached for the Swiss emissions, which is the uncertainty given for the Swiss bottom-up estimate SGHGI (FOEN, 2015). For individual grid cells the resulting prior uncertainty was ≈ 30proportionality factor was $f_E \approx 30\,\%$. However, the off-diagonal elements in $\mathbf{B}^E$ contributed considerably to the total uncertainty country uncertainty since they were especially large for small grid cells (see Fig. S2 in the Supplement).

2.5.6 Selection of observations

Another series of sensitivity inversions was set up using different parts of the observational data (runs S-01 to S-05, Table 2). The number and combination of sites used in each inversion was varied from using individual sites to using all six sites. For each of these sensitivity cases the inversion grid was adjusted according to the total source sensitivity of the selected sites, thereby assuring that small grid cells only occurred in areas with large sensitivities. In the base inversion the two CarboCount-CH sites BEO and LAE LHW and the two more remote sites JFJ and SSL were used, whereas the observations of FRU and GIM served for validation only.

2.5.7 Baseline treatment

As described above, the baseline mole fractions were treated as a linear interpolation between mole fractions at designated baseline nodes, the latter being optimised as part of the state vector in the inversion. However, The treatment of the baseline in this regional

scale inversion is critical and may introduce attribution errors in the posterior emissions. Therefore, we explored two alternative methods that address certain shortcomings of our main approach. For example, there were times when the simulated smooth baseline was not able to follow apparent fast changes in the observed baseline signal. ~~For example, this~~ This was the case when the general advection direction towards Switzerland quickly changed from west to east, with mole fractions often being considerably elevated during easterly advection. At such transition times using the smooth baseline may lead to attribution errors in the emission field. Instead of a smooth baseline it would have been desirable to take the baseline directly from an unbiased state of a global scale model, sampling the mole fractions at the ~~initial FLEXPART particle positions~~FLEXPART particle end points. However, such model output was not available for the investigation period at the time of the analysis.

~~Alternatively and to analyse the sensitivity of our set-up to these limitations, two additional baseline treatments were tested. The first~~ The first alternative method (S-B1) was based on two baseline estimations – one for the eastern and one for the western part of the inversion domain – which were combined using a weighted mean depending on the ~~initial location~~ end points of the model particles (here 4 days before arrival at the site). Since the initial location of the particles were available for every 3 h interval, this approach allows for more flexible variations of the simulated baseline signal. As in the standard baseline treatment, prior baseline mole fractions were taken from the REBS baseline at JFJ, applied here to both the eastern and western baselines. The second alternative baseline method (S-B2) extended the approach to a three-dimensional grid of baseline mole fractions accounting not only for east–west but also for north–south and vertical gradients. Again, the initial positions of the model particles within the grid as obtained from each FLEXPART simulation were used to determine the baseline concentration at the site as a weighted average. Different from methods B and S-B1, however, only one common set of gridded baseline mole fractions was estimated and applied to all sites. Only a very coarse ($3 \times 3 \times 2$) grid, covering the inversion domain, with a 15-daily temporal resolution was used in order to limit the size of the state vector. In the vertical, the grid was ~~separating~~ separated between heights 3000 m below and above ground level. The latter was chosen to ~~assure~~ ensure that average initial sensitivities

were similar for both vertical layers. Prior baseline values in the upper vertical layer were again taken from the REBS baseline at JFJ, whereas the lower layer was initialised with the REBS baseline at BEO. This ~~assures~~ ensures a negative vertical gradient in CH_4 baseline mole fractions, since estimates for BEO were generally larger than those for JFJ.

3 Results

In the following the results of the emission inversions are presented, first in a more detailed fashion for the base inversion and second in a less exhaustive way for the sensitivity inversions highlighting the differences from the base case. Note that the base inversion does not necessarily represent the best inversion set-up and most likely or best estimate of the posterior emissions. Rather, it is used as a starting point to analyse the sensitivity to different inversion settings. Although there might be a best inversion set-up in the sense that its results are closest to the truth, this best set-up is not known (as little as the true emissions are known). The ML method applied as an alternative is an objective method to tune the free parameters of an inversion, but this does not necessarily correspond to the best set-up since it cannot account for potential biases arising from transport errors or the problem in representing the release height of the particles.

3.1 Base inversion

Average source sensitivities as calculated with FLEXPART-COSMO on the reduced grid are shown in Fig. 1 for the base inversion as the combined sensitivity of the four sites BEO, ~~LAE~~LHW, SSL, and JFJ. Source sensitivities were largest close to the sites and in general for the Swiss Plateau (see Oney et al. (2015) for a detailed discussion of source sensitivities of the CarboCount-CH sites). The pronounced south-west to north-east orientation of the maximal source sensitivities is a result of the flow channeling between the Alps and the Jura mountains (Furger, 1990). South of the Alps and outside Switzerland source sensitivities quickly declined with generally larger values for westerly compared with easterly directions.

Source sensitivities towards the south-east were especially small, reflecting the shielding effect of the Alps.

In Switzerland prior emissions amounted to 178 $Gg\,yr^{-1}$. After mapping the high resolution emission data to the reduced inversion grid (Fig. 2a) and applying Eq. (8), Swiss prior emissions were quantified at 183 $Gg\,yr^{-1}$. The difference of 2 % can be explained by mapping artefacts along the Swiss border where inversion grid cells are overlapping with neighbouring countries, wrongly attributing some emissions from these to the Swiss total. The distribution of the prior emissions (Fig. 2a) in Switzerland clearly emphasises the dominating role of emissions from the agricultural sector. Emission maxima are located in the Canton of Lucerne in close vicinity to BEO and in the north-eastern part of the country towards Lake Constance in the Cantons of Thurgau and Saint Gallen. All these areas are characterised by intensive agriculture with a focus on cattle farming. Emissions from the urban centres of Zurich, Basel, Bern and Geneva, in contrast, are not especially pronounced in the MAIOLICA inventory. Within the high Alpine area, and to a smaller degree within the Jura mountains, MAIOLICA emissions are significantly smaller, but are large again in the north Italian Po Valley and also in south-western Germany.

Simulated CH_4 time series for the sites used in the base inversion with low model release heights (B low) are compared with the observations in Fig. 3. Most of the time the prior simulations were closely following the observed variability, underlining the very good performance of the transport model. However, during some periods the prior simulations considerably underestimated the observed mole fractions. This was especially true for the BEO and ~~LAE~~ LHW sites and a period in March/April ~~-~~as well as during episodes in October and November 2013. Some of the observed temporal variability was common for all sites suggesting an important influence from large-scale weather systems, whereas at other times the signals from different sites were little correlated. The two sites on the Swiss Plateau showed the most common behaviour, while, as expected, the high altitude observations at JFJ were most decoupled from the other observations. Also as expected, peak mole fractions were larger for the sites closer to the emissions (BEO, ~~LAE~~LHW) and smaller for the higher altitude sites (SSL and especially JFJ). The transport model captured this general

tendency very well. Except for JFJ, prior baseline mole fractions (based on the JFJ REBS estimate) were smaller than most observed mole fractions.

The model's skill considerably improved for the posterior simulations showing greater correlations and lower biases. The simulations more closely followed the observed variability and the bias was reduced (Fig. 3). Partly, this was achieved through changes in the baseline mole fractions. Posterior baselines were generally greater than the prior at the BEO, ~~LAE~~ LHW and SSL sites, whereas they were lower than the prior at JFJ. Largest baseline increases occurred during extended periods of elevated CH_4 (e.g. March 2013). These periods were characterised by easterly advection on the south-easterly side of high pressure systems with centres over north-western to central Europe. In these situations the limited model domain and the relatively short backward integration time of four days were likely insufficient to capture all recent emission accumulation above the baseline~~as observed at JFJ~~. As a consequence, the inversion adjusted the baseline upward.

The quality of the simulated time series is summarised in Fig. 4 where coefficients of determination, R^2, are given for all sites, for both prior and posterior simulations and separately for the complete (Fig. 4a) and above-baseline signal (Fig. 4b). The performance in the prior simulations ranged from $R^2 = 0.25$ for the site FRU to $R^2 = 0.5$ for the site GIM and the complete signal. The coefficients of determination for the above baseline signal were slightly lower, but showed the same ranking between the sites: largest at GIM followed by the sites SSL, ~~LAE~~LHW, BEO and JFJ and smallest for FRU. Posterior coefficients of determination considerably increased for all sites used in the inversion ($R^2 = 0.58$–0.69), slightly increased for FRU, but slightly decreased for GIM. Improvements were seen both for the complete signal as well as for the above-baseline signal. The ranking between the sites remained similar after the inversion.

An overall quality indicator, which not only accounts for the correlation but also for a correct representation of the amplitude of the variability, is the Taylor skill score (Taylor, 2001)

$$S = \frac{4(1+R)}{\left(\sigma_f + \sigma_f^{-1}\right)^2 (1+R_0)}, \tag{15}$$

where R is the Pearson correlation coefficient, R_0 the maximal attainable Pearson correlation of a "perfect" simulation, which is still limited by factors such as observation and representativeness uncertainty and was set to 0.9. $\sigma_f = {}^{\sigma_m}/_{\sigma_o}$ is the simulated standard deviation normalised by the observed standard deviation. S takes the value of 1 for a perfect simulation, but would take a value of 0.65 for perfectly correlated simulations that under/overestimate the observed variability by a factor of 2. The prior value of σ_f was well below 1 for all sites (0.43 to 0.71), indicating generally under-predicted peak heights, but increased in the posterior simulation to values between 0.65 to 0.8, except for GIM where it remained at 0.44. Posterior values of S for all sensitivity inversions and all sites are given in Table 4. For the base inversion S ranged from 0.78 to 0.91 for the sites used in the inversion and was smaller for the sites FRU and GIM (0.77 and 0.50). Note however, that for the latter two sites the baseline was not adjusted by the inversion, which may explain part of the weaker posterior performance. In the case of GIM it is remarkable that the correlation was comparatively large but the normalised standard deviation was very small. This may indicate that the general ~~flow~~ transport to the site was well captured by the ~~transport model~~ model (correlation), but that either local boundary layer heights or local emissions were overestimated or underestimated, respectively, so that the model was not able to simulate the observed amplitudes correctly. Taylor skill scores were very similar for posterior simulations of the base inversion using the high particle releases (B high in Table 4). Also, the prior simulation's performance was similar for low and high release heights, with lower release heights usually performing slightly better in terms of amplitude of the simulated variability and higher release heights showing slightly improved correlations. No clear preference for the lower or higher release height could be deduced from these results.

As an additional validation parameter the root mean square error (RMSE) and its reduction from prior to posterior simulations are shown in Fig. 4c and d. For sites used in the inversion the prior RMSE was between 20 and 40 $\mathrm{nmol\,mol^{-1}}$ and decreased by 15 to 25 % in the posterior simulations. For the near-surface sites FRU and GIM the RMSE did not significantly decrease after the inversion. At both sites simulated mole fractions were smaller than observed, especially at GIM. Even when using only afternoon values and when filtering for wind conditions with possibly large local influences (as done here), the transport model was not able to reproduce the amplitude of the observed variability at these sites. A reason for this poor model performance in FRU is most likely the inlet height very close to the surface and the associated high sensitivity to local emissions that cannot be captured at the resolution of the transport model. In GIM local emissions or mismatches in the local boundary layer height seem to be the main problem since the timing of the temporal variability was captured very well. The effect of including the sites GIM and FRU in the inversion is further discussed in Sect. 3.7.

~~Our model performance parameters are well within the range reported by~~ We used observations from sites in more complex terrain and closer to emission sources than used in other regional scale inversion studies of CH_4 surface fluxes for the European and East Asian domain ~~using continuous observations and applying similar transport models as in our study (Bergamaschi et al., 2015; Manning et al., 2011; Thompson et al., 2015)~~(Bergamaschi et al., 201 This should result in more complex variability at the sites. Nevertheless, our model performance parameters are well within the range reported previously by the above studies.

The posterior CH_4 emissions and their differences from the prior emissions are shown in Fig. 2b–d. The largest, though still modest, absolute changes (Fig. 2c) were estimated for the region south-west of BEO. In this region with large prior emissions from agriculture, reductions were in the order of 25 %. Further reductions were estimated east of the site ~~LAE~~ LHW in the canton of Thurgau (please refer to Fig. S1 for a map of the Swiss cantons) and in large parts of western Switzerland. In contrast, larger than prior emissions were obtained for north-eastern Switzerland in the Cantons of Saint Gallen and Appenzell and also

beyond the border in south-western Bavaria. Emissions in northern Italy were increased but due to the weak sensitivity for this region these posterior results are subject to larger uncertainties than those on the Swiss Plateau. Relative emission increases (Fig. 2d) of up to 30 % were detected for the Appenzell region and the bordering Vorarlberg region in Austria. On the contrary, relative emission reductions appeared for the southern Black Forest. Similar patterns emerged for the base inversion when using the high release heights (see Fig. S3 in the Supplement), but posterior emissions were generally larger in this case.

In this base inversion Swiss total emissions were estimated at $179 \pm 7\,\mathrm{Gg\,yr^{-1}}$ (1σ) and $195.0 \pm 7.3\,\mathrm{Gg\,yr^{-1}}$ for the low and high particle release heights, respectively. Both values are not significantly (two-sided Welch t test) different from their prior value, indicating a high level of consistency between the bottom-up estimate of the MAIOLICA inventory and our top-down estimate. Furthermore, analytical uncertainties of the posterior were considerably reduced by about 75 %. However, ~~an additional uncertainty range of~~ the difference $\pm 15\,\mathrm{Gg\,yr^{-1}}$ ~~is introduced by~~ in total Swiss emissions resulting from the choice of the particle release height suggests a relatively large additional contribution to the overall uncertainty due to the inversion set-up that is not included in the analytical uncertainty.

Next to an improved reproduction of the measurement time series, the reduction of uncertainty in the emission field provides information on the quality of the inversion. Uncertainty reductions were largest close to the observation sites (Fig. 5). For the sites with larger surface sensitivities (~~LAE~~ LHW and BEO), uncertainty reductions in their vicinity were larger than for the more remote sites (SSL and JFJ). It is interesting to note that uncertainty reductions were largest in the area around and west of BEO, where also emission reductions were the largest. Uncertainty reductions were smaller for the area east of ~~LAE~~LHW, where also considerable emission reductions were established. For north-eastern Switzerland, where the inversion produced large emission increases, uncertainty reductions were relatively small. The associated emission increases are thus less well constrained, which in turn may indicate temporally variable emissions or increased transport uncertainties for the associated flow direction.

3.2 Seasonal cycle

When allowing seasonal variability of the emission fluxes (S-V), distinct differences between the seasons are visible, although no seasonal variability was included in the prior (Figs. 6 and S4 in the Supplement). Winter-time posterior emissions were strongly reduced especially in agricultural areas. Posterior emissions during the other seasons tended to be slightly larger than their prior values.

Also the estimated emission patterns changed from season to season. In spring and summer increased posterior emissions were estimated for eastern Switzerland, the Canton of Lucerne (around BEO) and generally the pre-alpine area, whereas there was a tendency for smaller than prior emissions in western Switzerland. The strong increase around the station FRU (not used in the inversion) is consistent with the observation that the posterior model performance for the site FRU was considerably enhanced compared to the prior simulation. Performance was also enhanced compared to the posterior simulation of the base inversion both in terms of correlation and RMSE reduction, although Taylor skill scores were similar in both inversions (see Table 4). On the contrary, during fall higher than prior emissions were present in north-western and eastern Switzerland, and for small areas south of BEO and east of ~~LAE~~ LHW posterior emissions were below prior estimates.

For the low model release height, total Swiss emission rates were smallest during winter (152.2 ± 9.7 Gg yr^{-1}) but were relatively similar and close to the prior estimates during the other seasons (206.5 ± 12, 182.1 ± 13, and 202.7 ± 11 Gg yr^{-1} for spring, summer and autumn, respectively). The annual total Swiss emissions for S-V were 185.9 ± 6.5 Gg yr^{-1}, very close to those of the base inversion. Winter-time emission rates were 18 % smaller than the annual mean. For the high model release heights, a similar but less pronounced annual cycle was derived, which featured total annual emissions of 197 ± 7 Gg yr^{-1} and winter-time emission rates of 171 ± 10 Gg yr^{-1} (13 % lower than annual mean).

3.3 Extended Kalman Filter inversion

The extended Kalman filter inversion using low particle release heights (S-K low) yielded similar annual mean posterior emissions as the base inversion (Figs. 7 and S5 in the Supplement). Several features of the posterior emission differences obtained by the base inversion are also visible in the extKF inversion: reductions west of BEO, increases in north-eastern Switzerland, small changes in the Alpine area, small increase in the region close to GIM (shifted south-westerly as compared to base inversion). No emission reductions were, however, deduced for the area east of ~~LAE~~LHW. Overall the posterior model performance using the extKF inversion was superior (S between 0.84 and 0.95) compared to the base inversion (Table 4), which ~~may be~~ is most likely related to the time variable posterior emission field and ~~/or~~ to a smaller degree to the different treatment of baseline mole fractions.

Total Swiss emissions were estimated at 193 ± 13 and $217 \pm 14\,\mathrm{Gg\,yr^{-1}}$ by the extKF inversion for the low and high particle release height, respectively. These values are considerably larger (8 and 15 %) than those of the base inversion but fall well within the range of values reported by the other sensitivity inversions using the Bayesian approach. The difference in total emissions between the low and high release case of $24\,\mathrm{Gg\,yr^{-1}}$ was considerably larger than in the base inversion (Table 4). Uncertainty estimates of the posterior emissions remained larger in the extKF case than in the base inversion, despite the fact that similar prior uncertainties and model/observation uncertainties were used in both systems. The main reason for this observation is that the uncertainties of the state vector are allowed to grow in the extKF from one time step to the next accounting for the forecast uncertainty, which introduces an additional amount of prior uncertainty.

3.4 Influence of transport model

In the sensitivity case S-EC the source sensitivities were derived from FLEXPART-ECMWF instead of FLEXPART-COSMO (see Sect. 2.2). On the one hand, FLEXPART-ECMWF may be less suitable to resolve the complex flow in the Swiss domain due to its coarser horizontal resolution. On the other hand, FLEXPART-ECMWF is a well validated model code and has

been widely used for inverse modelling (e.g. Stohl et al., 2009; Thompson and Stohl, 2014; Thompson et al., 2015). Using the same inversion settings, FLEXPART-ECMWF simulations yielded generally similar posterior emissions as the base inversion (Figs. 8 and S6 in the Supplement). Common features were again the decrease west of BEO and east of ~~LAE~~ LHW and the increase in north-eastern Switzerland with respect to the prior emissions. In contrast to the base inversion, large emission reductions were also assigned to most of the western part of the country towards lake Geneva. For the low release height, the model performance at the observation sites was only slightly lower compared to the base inversion as indicated by the posterior Taylor skill scores (Table 4). In contrast, posterior Taylor skill scores were slightly larger in the high release case than in the base inversion. An exception was the GIM site, for which skill scores were strongly reduced using FLEXPART-ECMWF. This may reflect the growing inability of a coarser transport model to simulate the local CH_4 contribution to the site.

Although FLEXPART-ECMWF's performance at the sites was of similar quality as for the base inversion, the uncertainty reductions of the posterior emissions (Fig. 8b) were not as pronounced in the S-EC cases (low and high) as compared to the base inversion. ~~Again, this is a hint that the coarser model 's transport simulations are not as accurate and therefore lead to a less clear identification of the emission sources.~~This can partly be attributed to the larger model uncertainty assigned in the ECMWF case (especially low particle release case) compared to the base inversion (compare Tab. 3). Total Swiss posterior emissions in the S-EC case were 171.1 ± 8.0 and 182.1 ± 7.6 Gg yr^{-1} in the low and high particle release case, respectively, slightly smaller than in the base inversion. One possible explanation may be the coarser and, hence, potentially less dispersive behaviour of FLEXPART-ECMWF. Mesoscale flow patterns in complex terrain may contribute to effective dispersion (Rotach et al., 2013). The coarser resolution of FLEXPART-ECMWF likely results in larger under-representation of mesoscale flow in the complex Swiss terrain.

3.5 Influence of prior emissions

Two additional spatially explicit sets of prior emissions were used to explore the effect of the prior emissions on the inversion results. The sensitivity run based on EDGAR (S-E) starts off from considerably larger prior emissions for Switzerland (228 $Gg\,yr^{-1}$) and also deviates strongly in the spatial allocation of these emissions, putting more emphasis on the population centers than the MAIOLICA inventory (Hiller et al., 2014a). This can be traced back to EDGARv4.2 containing about 25 $Gg\,yr^{-1}$ larger emissions from the gas distribution network (IPCC category 1B2: fugitive emissions from oil and gas; 32 vs. 8 $Gg\,yr^{-1}$ in MAIOLICA), while other emission categories are similar. However, also the remaining emissions are more closely following the distribution of population density when compared with the MAIOLICA inventory, which is due to less detailed geographical information in the EDGARv4.2 inventory (Hiller et al., 2014a). Differences between the TNO inventory (S-T) and the MAIOLICA inventory are more subtle and amount to only 5 $Gg\,yr^{-1}$ for the Swiss total.

In all three inversions (B, S-E and S-T) posterior emissions were very similar both in their distribution (see Figs. S3, S7, S8 in the Supplement) and also in the national total. The latter only differed by 5 $Gg\,yr^{-1}$ for S-T and 10 $Gg\,yr^{-1}$ for S-E despite the fact that prior emissions were 45 $Gg\,yr^{-1}$ larger in the latter (Table 4). This indicates that the posterior emissions were well constrained by the observations and not solely governed by the prior emissions for which relatively small uncertainties were assigned. The strong posterior emission increase in north-eastern Switzerland was also prominent in S-E. The posterior to prior differences for S-E showed a strong emission reduction in the larger urban areas (mainly Basel, Zurich, but also Lucerne, Bern and Geneva) suggesting that the strong attribution of emissions to urban centers in the EDGAR inventory is unrealistic (Fig. 9a). In contrast to the base inversion, uncertainty reductions in the S-E case were also large for the urban areas (Fig. 9b), lending credibility to the associated emission reductions.

3.6 Influence of uncertainty covariance treatment

The inversion results using the model/observation uncertainty as estimated by the method of Stohl et al. (2009) (S-S) were smaller than in the base inversion in the low release case but differed only slightly in the high release case (see Table 4). In S-S an almost constant ~~uncertainty~~ value (see Sect. 2.4) was given to ~~all~~ the model/observation ~~pairs of one~~ uncertainty of each site, while in the base inversion uncertainties tended to be larger for large above-baseline mole fractions. However, model uncertainties were mostly smaller for the base inversion except for 10 to 20 % of the observations in the "low" and less than 10 % in the "high" release case. Despite these differences in the applied model uncertainty, the distribution of posterior fluxes was similar to that of the base inversion with two exceptions: emission reductions were more pronounced in the area west of BEO and east of ~~LAE~~ LHW in the S-S case and additional reduction occured around the BEO site itself (see Fig. S9 in the Supplement). The ~~destinct~~ distinct posterior increase in north-eastern Switzerland was also present in S-S.

In comparison with the base inversion, all parameters describing the uncertainty covariance matrices showed increased values when they were estimated by the maximum likelihood method (Table 3). Especially the uncertainty of the baseline, as described by parameter f_{b}, was strongly increased for all sites, but also the model uncertainties were generally larger (parameters σ_{min} and σ_{srr}). In addition, the ML method yielded an increased uncertainty of the prior emissions, resulting in a total uncertainty for Switzerland of about 30 %, indicating that the bottom-up estimate of 16 % may be too optimistic. The spatial correlation length of the prior emissions remained very close to the $L = 50\,\mathrm{km}$ used in the base inversion. The resulting posteriori emissions were distributed similarly as in the base inversion. However, emission reductions were more pronounced (see Fig. S10 in the Supplement). As for the S-S ~~sensititivy~~sensitivity, emission reductions were also estimated for the region between BEO and ~~LAE~~ LHW and only a small local increase around the BEO site remained. The total posterior emissions for Switzerland were only 158 ± 13 and $169 \pm 13\,\mathrm{Gg\,yr^{-1}}$ for the low and high particle release case, respectively. Due to the larger baseline uncertainty

as estimated by the ML optimisation, adjustments of the posterior baseline were larger than in the base inversion. As a result baseline mole fractions were raised for the sites BEO and ~~LAE~~ LHW during periods of increased CH_4 observations, hence, reducing the need for increased emissions at these times and lowering the overall posterior emissions. The increased prior and model uncertainties resulted in relatively large posterior uncertainties as compared with the base inversion. The overall posterior model performance was similar to that of the base inversion. However, a larger part of the ~~the~~ simulated variability was ~~atrributed~~ attributed to variations in baseline signal.

3.7 Influence of observation selection

For almost all sensitivity inversions with different subsets of observational data (S-O1 to S-O5 in Table 2) the emission reduction west of BEO could be confirmed (see Figs. S11, S12, S13, S14, S15 in the Supplement). In contrast, the reduction east of ~~LAE~~ LHW was only evident in those runs that also used the observations from ~~LAE~~LHW. Similarly, the increase in north-eastern Switzerland was more pronounced if the observations from BEO were used. Relatively large emission changes were obtained at mid range (100 to 500 km) from the sites on the Swiss Plateau when the more remote sites SSL and JFJ were not used in the inversion (S-O1 to S-O3). The larger emission changes in S-O1 to S-O3 were likely the result of ~~shadowing effects: the BEO and LAE~~ attribution errors. The BEO and LHW sites were only sensitive to these more distant areas when they were also sensitive to closer emission sources~~resulting in a false attribution of emissions to~~ . Hence, the inversion assigned increased emissions to these distant areas located behind the real emission sources. Using observations from additional sites with a different sensitivity pattern can solve this problem as it did in our base inversion, where the elevated sites JFJ and SSL with distinctly different sensitivity patterns were included.

Swiss CH_4 emissions for this set of sensitivity inversions were larger than in the base inversion (Table 4). Largest emissions (214.3 ± 11 Gg yr^{-1} in the low release case) were obtained when only the site ~~LAE~~ LHW was used (S-O2), resulting in large emission increases in western Switzerland, whereas posterior emissions remained similar to the base inver-

sion close to the BEO and ~~LAE~~ LHW sites. This pattern is most likely due to the problem of shadowing effects.

S-O5, the inversion using all six sites, resulted in comparatively large total emissions for Switzerland as well ($208.8 \pm 6\,\mathrm{Gg\,yr^{-1}}$ in the low release case). Emissions were largely increased around the site GIM and further west as a result of the large mole fractions observed at GIM. As discussed earlier, it seems likely that large local emissions around GIM could not properly be accounted for by the inversion system and were spread out over a larger area, resulting in overall larger national emissions.

It is interesting to note that including the additional observations from GIM and FRU only slightly reduced the overall uncertainty of the national emission estimate in comparison to the base inversion (from 7.0 to $6.0\,\mathrm{Gg\,yr^{-1}}$ for the low release case). In contrast, using the two sites ~~LAE~~ LHW and BEO in combination instead of either one of them individually, reduced the uncertainty from about 11 to $7.9\,\mathrm{Gg\,yr^{-1}}$. Hence, the additional gain in terms of uncertainty reduction was relatively small when adding the sites GIM and FRU~~, which is another indication of~~ . which would have been expected from their more localised sensitivity ~~and, hence, reduced value in the inversion~~as compared to the other sites.

Of the sensitivity inversions with differing observation data the results of the case using only observations from BEO (S-O1) was closest to those of the base inversion, both in terms of total emissions and of geographic distribution. This supports the expectation that a tall tower site should be best suited for inverse modelling ~~and may allow the~~ (as can also be seen by the dominating role of BEO in the uncertainty reduction; Fig. 5). However, the estimation of other Swiss GHG fluxes using observations from this site alone will strongly depend on our ability to correctly assign baseline values and the question if shadowing effects can be neglected.

3.8 Influence of baseline treatment

As mentioned above, the treatment of baseline mole fractions is critical in order to avoid attribution errors in the emission field. When varying the prior baseline uncertainty in our base inversion, considerable changes in posterior emissions indicated this sensitivity.

Doubling (halving) the prior baseline uncertainty results in -19 $Gg\,yr^{-1}$ (+31 $Gg\,yr^{-1}$) total Swiss emissions as compared to the base inversion (low particle release height). In both cases the obtained posterior baselines did not seem very reasonable (too smooth, too closely following the observed short term variability), so that these cases can be seen as the extreme range of the baseline influence. Nevertheless, by exploring different baseline treatments, the sensitivity to baseline assumptions was further documented. Comparing the inversion results of the two inversions with alternative baseline treatment (S-B1 and S-B2; see Sect. 2.5 for details) with the base inversion did not reveal any large differences in terms of geographical distribution (see Figs. S16 and S17 in the Supplement). In the case of S-B2 the reductions in the western part of Switzerland were confined to the area between GIM and BEO and also the reductions north of BEO (as seen in the base inversion) were turned into increases. Especially S-B2 yielded enhanced model performance that was mainly due to a more detailed description of the temporal variability of the baseline (Table 4). Total Swiss emissions for S-B1 remained very similar to the base inversion but were considerably larger for S-B2 (195.1 ± 6.9 and $223.6 \pm 6.9\,Gg\,yr^{-1}$ for low and high particle release height, respectively). In S-B2, where a coarse three-dimensional grid of baseline mole fractions was optimised, their posterior values were largest for the eastern and low grid cells and during the previously highlighted period in March 2013 and again in the winter 2013/14. Furthermore, vertical gradients were smaller during the summer months than during the winter (see Fig. S18 in the Supplement). This general distribution is in line with our expectations (higher mole fractions towards surface and more continental areas) and lends credibility to this kind of baseline estimation. One further advantage of analysing a common baseline grid for all sites is its possible use for the validation sites as well. Indeed, a larger improvement in posterior performance at the sites FRU and GIM can be seen for S-B2 than in any other sensitivity inversion in which the sites were used for validation only.

4 Discussion

4.1 National total emissions

The main result of the present study is summarised in Fig. 10 in terms of a histogram of total Swiss CH_4 emissions for the investigation period March 2013 to February 2014 taken from all sensitivity inversions. The estimates from the individual sensitivity inversions almost follow a normal distribution. A clear average difference between sensitivity runs using the high and low particle release heights of 20 $Gg\,yr^{-1}$ is apparent. This difference is larger than the one between the results taken from the two employed transport models FLEXPART-ECMWF and FLEXPART-COSMO (12 $Gg\,yr^{-1}$, 5 %). The latter supports the large degree of consistency between the two transport models and the underlying meteorology. In an inverse estimate of HFC-134a emissions from the continental USA, Hu et al. (2015) had observed a somewhat larger emission difference (20 %) when using source sensitivities obtained from two different dispersion models (HYSPLIT-NAM12, STILT-WRF) with similar horizontal resolution.

To derive an average national emission over all sensitivity inversions, we assigned the same weight to each sensitivity run and calculated a straightforward mean over all sensitivity inversions. This is a rather pragmatic approach, since some sensitivity inversions using, for example, only one site cannot be expected to be equally good as the base inversion with four sites. However, we are lacking a more objective measure that would allow us to assign quantitative weights to the different runs. Our estimates can be compared to the bottom-up estimates that the Swiss Federal Office for the Environment reported to the UNFCCC in the years 2014 and 2015 (Table 5). Please note that Swiss emissions are reported annually for the reporting period 1990 to two years before the submission date. Methodological updates from one year to another usually influence the whole reporting period (FOEN, 2014, 2015). We refer here to the emissions reported for the year 2012, since estimates for this year are available from the 2014 and 2015 reporting. According to the 2015 reporting, emission changes from 2012 to 2013 were small ($-0.14\,Gg\,yr^{-1}$) (FOEN, 2015). The estimate of CH_4 emissions submitted to the UNFCCC in 2014 for the year 2012 was $176 \pm 28\,Gg\,yr^{-1}$.

Our prior was based on these estimates plus a small contribution from natural emissions of 3 $Gg\,yr^{-1}$. Our posterior estimates were slightly but not significantly larger. This is true for the mean obtained from the two base inversions ($187 \pm 10\,Gg\,yr^{-1}$) as well as for the mean over all sensitivity inversions ($196 \pm 18\,Gg\,yr^{-1}$). The latter value should be seen as our best estimate of the Swiss CH_4 emissions. It is closer to the bottom-up estimate of $206 \pm 33\,Gg\,yr^{-1}$ reported in 2015 (FOEN, 2015) as to the one reported previously. The differences in the reporting are due to updated emission factors and methodologies in the national inventory. Our inversion results support these updates.

Our overall uncertainty estimate is based on the standard deviation of all sensitivity inversions and is considerably larger than any of the uncertainty estimates of the individual inversions (Table 4). Despite this fact, the overall posterior uncertainty remains smaller than the prior uncertainty. One possible reason for the relatively small posterior uncertainty of individual inversions may be seen in the small prior uncertainty of 16 % for the national total. Similarly, when applying the ~~the~~ ML method, considerably larger prior uncertainties in the range of 30 % were suggested (see Sect. 3.6). However, posterior uncertainties of the ML sensitiviy runs (S-ML in Table 4) were still considerably smaller than our overall uncertainty. Another reason for small posterior uncertainties could be an underestimated model/observation uncertainty, lending too much trust to the simulation of the observations and in turn reducing posterior uncertainties. However, model/observation uncertainties were optimised in the same step as prior uncertainties with the ML method and were not estimated to be considerably different from the base ~~setup~~ set-up (see Table 3). These considerations lead to the conclusion that the enhanced posterior uncertainty over all sensitivity runs needs to be seen as the contribution of systematic uncertainties that are introduced by the specific ~~setup~~ set-up of the inversion system and cannot be fully covered by the analytical estimate of the Bayesian analysis, a result that has also been obtained in previous inversion studies ~~(e.g. Bergamaschi et al., 2010, 2015)~~(e.g., Bergamaschi et al., 2010, 2015; Ganesan et al., 2014

4.2 Spatio-temporal emission patterns

Considerable emission differences were observed between the seasons, with winter-time emissions being 13 to 18 % lower than the annual average. Since the largest winter-time reduction was deduced for areas with large cattle density, it seems very likely that the estimated reductions are connected with the agricultural sector. ~~When referred~~ This observation was also true for the north-eastern part of Switzerland were, though annual emissions were increased, these increases were largest in spring and summer (see Fig. 6). When compared to the prior emissions from the agricultural sector only (150 $Gg\,yr^{-1}$, FOEN, 2014), the estimated seasonal posterior variability would be around 22 %. The latter is well in line with Gao et al. (2011) who estimated the seasonal variability of CH_4 emissions from a dairy cow farmstead in northern China. A major contribution to the annual variability may stem from CH_4 emissions from manure handling and storage, which strongly depends on temperature. Zeitz et al. (2012) speculated that Swiss CH_4 emissions from manure handling should be lower than estimated by FOEN (2014), since their observed emission factors were significantly smaller than those suggested by IPCC and used by FOEN (2014). However, their results were based on laboratory experiments that yet need to be validated in the field. Furthermore, Zeitz et al. (2012) suggest that emissions from manure handling should be significantly reduced or even cease during winter, considering the average temperatures in Switzerland. Accounting for the temperature of the manure storage, which may be well above the ambient temperature, in the emission calculation, a 50 % wintertime reduction was estimated in the bottom-up inventory (FOEN, 2015). Furthermore, seasonal variability in emissions from ruminants may be induced by seasonal variability of productivity, especially of dairy cows. In Switzerland it is common practice to time the calving date in the spring so that the cows reach their largest productivity at the point of largest feed availability (spring/summer). Since productivity and CH_4 emissions are roughly proportional, direct ruminant emissions should also follow a seasonal cycle with a minimum in the winter months (FOEN, 2015). The temporal variability in our inversion results largely agrees with these considerations and, hence, fits well

to our understanding of the main agricultural emission processes in Switzerland. Furthermore, we had seen that mean annual posterior emissions were about 10 to 20 % lower in agricultural areas in our base inversion (B low). Taking the mean over all sensitiviy inversions this reduction is around 5 to 15 % as compared to the prior, which was based on the 2014 reporting. Considering the larger emissions from agriculture in the 2015 reporting, our mean posterior emissions in agricultural areas suggest that the revised bottom-up inventory (FOEN, 2015) overestimates agricultural emissions by 10 to 20 %. From the ~~infered~~ inferred seasonality we conclude that this is most likely because emissions from manure handling are overestimated. Our findings are in ~~contrast to recent , somewhat controversial studies in the USA that find a~~ line with recent inversion results (covering the period 2009 to 2011) for Europe that indicate similar to lower emissions as compared to EDGAR (Alexe et al., 2015; Turner et al., 2015; Ganesan et al., 2015), whereas for the USA a number of studies suggest a significant underestimation of ruminant emissions in the EDGAR-v4.2 and USA EPA inventories (Miller et al., 2013; Wecht et al., 2014; Turner et al., 2015).

Our posterior results depend little on the prior emission distribution (B vs. S-E and S-T) and corrected the large emissions in urban areas given by the EDGARv4.2 inventory downwards. Hence, we conclude that the emissions from natural gas distribution and use in the SGHGI/MAIOLICA inventory is more realistic than in EDGARv4.2. The SGHGI emissions from natural gas distribution of 8 $\mathrm{Gg\,yr^{-1}}$ correspond to < 0.4 % of the Swiss natural gas consumption (FOEN, 2015). This is in contrast to recent studies from the USA where a large underestimation of fugitive emissions was established in the inventories for different metropolitan areas (Wennberg et al., 2012; McKain et al., 2015) and fractional loss rates between 2.5 and 6 % were established. However, these results may not be representative for the USA as a whole. According to the SGHGI, fugitive emissions were reduced in Switzerland by 36 % since 1990 mainly due to a gradual replacement of cast-iron pipes by polyethylene pipes (FOEN, 2015). Our results support the reductions documented in the SGHGI and, thus, the success of this emission reduction measure. This also highlights that large

reduction potentials can be expected for other countries as well when modernisation of the infrastructure is promoted.

CH_4 emissions from composting and anaerobic digestion (IPCC 5B), mainly in the conversion of biogenic waste to biogas in small scale facilities, were amended from 5 to 16 $Gg\,yr^{-1}$ from the 2014 to the 2015 reporting (Table 5). In our prior inventory, these emissions were not explicitly localised (Hiller et al., 2014a). Since our prior was based on the earlier 5 $Gg\,yr^{-1}$ estimate, an increase in regions with intensive biogas production should have been detectable. However, the biogas and composting plants are approximately evenly distributed across the Swiss Plateau in areas of dominating agricultural use. Hence, it is impossible to finally attribute any of the observed posterior emission differences to this emission process. Similarly and as already indicated by Hiller et al. (2014a), emissions from waste water treatment were probably underestimated in previous FOEN estimates. In the most recent reporting from 2015, these emissions were 6.77 $Gg\,yr^{-1}$, which is an increase by a factor of 15 compared to previous reports. The spatial distribution of CH_4 emissions from waste water treatments should mainly follow the population density. Although, our inversion results do not support increased emissions in densely populated areas, the relatively small emission revision (compared to the total emissions) may be very difficult to detect.

4.3 Unidentified source in north-eastern Switzerland

The largest emission changes that were localised by the inversion and were present in almost all sensitivity inversions were those in the north-eastern part of Switzerland in the Cantons of Saint Gallen and Appenzell. These areas are also dominated by agriculture and the estimated increase, hence, contradicts the reductions in other agricultural regions. The area contributed about 16.3 % to the national emssions in our prior inventory. This contribution was increased to 22.5 % in the posterior estimate of the base inversion, an increase of 6.2 $Gg\,yr^{-1}$. One possible reason for the increase could be systematic biases in the transport simulations and in the balance between baseline and emission adjustment. One argument against this possibility is that the increase was observed also when using

FLEXPART-ECMWF instead of FLEXPART-COSMO (see Sect. 3.4) and it seems unlikely that the same systematic bias would be inherent to both meteorological inputs. Furhtermore, FLEXPART-ECMWF calculations were not as restricted by the limited model domain as FLEXPART-COSMO simulations (see discussion above). However, all inversions using either one of the three different methods to adjust the baseline did yield similar increases in north-eastern Switzerland. Another possible reason for the increased emissions could be an emission source close to the observational sites that could not be described correctly by the limited model resolution and whose contributions were wrongly assigned to the respective area. Again, this seems unlikely, since the increase was present in sensitivity inversions using either one of the sites on the Swiss Plateau (S-O1, S-O2). In conclusion and although we cannot completely rule out inversion artefacts, it seems likely that the estimated increase represents a real emission source that is not present or under-estimated in our prior inventory.

This raises the question which processes may be responsible for the detected emissions. A possible candidate is an erroneous spatial distribution of ruminant emissions within Switzerland. However, in Switzerland the number of ruminants by animal species needs to be reported at the farm level and this information, aggregated to communities, was used for distributing agricultural emissions in the prior inventory (Hiller et al., 2014a). Different cow breeds may have different CH_4 emissions factors. The dominating breeds in Switzerland are Brown Swiss and Holstein, for which similar emissions factors have been reported (Felber et al., 2015, and references therein). Different ~~management methods~~ manure management methods (e.g., Owen and Silver, 2015) and diet types (e.g., Klevenhusen et al., 2011) may also lead to ~~slight variations in the~~ variations in per head emission factors. To our knowledge, detailed investigations of emission factors under real Swiss farming conditions and their spatial variability are currently not available. The large emission factors given by (Owen and Silver, 2015) for manure storage in anaerobic lagoons do not apply to Switzerland, since this storage type does not exist here (FOEN, 2015). Therefore, effects of spatial variability of herd composition and management cannot be excluded, although it seems unlikely that these could fully explain the differences estimated by the inversion.

A typical farming practice in Switzerland is moving grassing cows towards elevated Alpine pastures during the summer months. This was considered in the prior by redistributing 4 % of the national ruminant emissions to Alpine pastures (Hiller et al., 2014a). Altough there are extended areas of Alpine pastures present in north-eastern Switzerland, these are not more prominent than in other Alpine areas where we did not observe increased posterior emissions. Furthermore, increased emisisons in north-eastern Switzerland were also observed by the inversion for the winter and spring periods, when the Alpine pastures are unoccupied. Possible additional sources of anthropogenic CH_4 in north-eastern Switzerland may stem from biological treatment of waste in composting and anaerobic digestion facilities, solid waste disposal, waste water treatment, and natural gas distribution. Currently we have no indication that either of these processes shows a specifically high density in the given area.

This leaves the possibility of an underestimated or unaccounted natural CH_4 source. The net natural emissions accounted for by Hiller et al. (2014a) were very small ($\approx 3\,\mathrm{Gg\,yr^{-1}}$) compared to their anthropogenic counterpart ($\approx 180\,\mathrm{Gg\,yr^{-1}}$). Emissions from wetlands and lakes are thought to be the largest natural source in Switzerland ($4.6\,\mathrm{Gg\,yr^{-1}}$). Although there are a number of small wetlands and lakes situated in the Cantons of Appenzell, their fractional coverage and total area is not larger than in other areas (for example Entlebuch south-west of BEO). Furthermore, we have no indication that climate variability within the domain could have impacted the drivers of wetland emissions (precipitation, temperature) in an inhomogeneous way to explain large regional differences. Aerobic soils (forest and agricultural) are generally thought to be CH_4 sinks and were estimated to contribute a negative CH_4 flux of -4.3 to $-2.8\,\mathrm{Gg\,yr^{-1}}$ (Hiller et al., 2014a). Nevertheless, under anerobic conditions methanogensis may dominate in deep organic soils, which can be found in wetland or peatland areas. When former peatlands are re-wetted (either due to accidental flooding or renaturation) they have been shown to become a significant CH_4 source depending on water table depth, the abundance of vascular vegetation transporting CH_4 from the root space to the atmosphere and the amount of available carbon in plant litter (Couwenberg and Hooijer, 2013). Organic soils were not considered as CH_4 sources in our prior. One large area

of deep organic soils in Switzerland is located in the Alpine Rhine valley (Wüst-Galley et al., 2015), only slightly east of the area of our largest posterior increase. This possible source though remains uncertain since the area in question is used for agriculture and should be well drained throughout most of the year. The only other large area of converted peatland in Switzerland is the Seeland region around the GIM site, possibly contributing to the large CH_4 concentrations observed there (see Sects. 2.1 and 3.1). Admittedly, river re-routing and drainage systems should keep the water table low in this area. In conclusion, we cannot explicitly determine which process may have caused the increased posterior emissions in north-eastern Switzerland. Additional studies using data from more recent observations and/or additional sites will be needed to clarify these open questions.

5 Conclusions

We applied a high resolution atmospheric transport model to simulate the CH_4 observations of the CarboCount-CH network and used inversion techniques to estimate total Swiss CH_4 emissions and their geographical distribution for the period March 2013 to February 2014. A series of sensitivity inversions (varying the treatment of temporal variability of the emissions, the transport model, the inversion algorithm, the prior emissions, the uncertainty covariance matrices, the selected observations, and the baseline treatment) confirm the robustness and independent character of our results.

Our best estimate of total Swiss CH_4 emissions ($196 \pm 18\,\mathrm{Gg\,yr^{-1}}$) largely supports the bottom-up estimate as reported by the Swiss Federal Office for the Environment ($206 \pm 33\,\mathrm{Gg\,yr^{-1}}$, reported to UNFCCC in 2015 for the year 2012). The overall uncertainty as obtained from all sensitivity inversions (10 %) was larger than the analytical uncertainty of any individual sensitivity inversion, but still considerably reduced the uncertainty associated with the bottom-up estimate (16 %). Our results support the effectiveness of a well informed bottom-up inventory, calibrated to local to regional emission processes. A similar conclusion was drawn by Zavala-Araiza et al. (2015) who desinged an updated bottom-up inventroy for a gas production area in Texas, using locally observed emission factors. Although their

bottom-up estiamtes were at least two times larger than convential bottom-up estimates, they largely agreed with top-down estiamtes in the same area.

The inversion results indicate a redistribution of CH_4 as compared to the spatially explicit bottom-up inventory. Large winter time posterior emission reductions in regions dominated by agricultural emissions suggest that these are overestimated on an annual basis by 10 to 20 % in the most recent bottom-up inventory and that manure handling may be the responsible process. Our findings ~~are in~~ agree with recent inverse modelling of European scale CH_4 emsissions that suggest a similar to lower emission rates as in the EDGAR inventory. This is in contrast to recent studies from the USA that suggested considerably larger emissions from ruminants than reported in bottom-up inventories (Miller et al., 2013; Wecht et al., 2014; Turner et al., 2015). An area of increased posterior emissions in north-eastern Switzerland could not be assigned to a single most likely source process. Emissions from previously drained peatlands may be responsible for this observation. However, this suggestion needs further investigation.

Bottom-up estimates indicate that Swiss national emissions decreased by about 20 % since the 1990s, mainly due to a reduction in livestock numbers and improvements in the gas distribution network (FOEN, 2015). The latter can be supported by our study, which did not assign large emissions to densely populated areas and strongly corrected such emissions when present in the prior estimate (EDGAR inventory). This again is in contrast to recent studies from the USA that showed, at least for two metropolitan areas, larger than expected emissions from natural gas distribution (Wennberg et al., 2012; McKain et al., 2015) and provides evidence for the efficiency of comparatively simple modernisation efforts to reach greenhouse gas reduction targets.

Our results also demonstrate the feasibility of using high-resolution transport models and continuous atmospheric observations to deduce regional scale surface fluxes with a horizontal resolution required to retrace the underlying emission/uptake processes. This conclusion is especially encouraging when considering the complex topography of the study area ~~. Furthermore, it is a prerequisite for studying the more complex exchange of carbon dioxide between the terrestrial biosphere and the atmosphere~~and for future inverse

modelling studies of the two other trace gases observed within CarboCount-CH: carbon dioxide and carbon monoxide. Inversion results using data from two sites on the Swiss Plateau and two elevated sites (base inversion) were consistent with a sensitivity inversion that used only the tall tower observations of Beromünster (212 m a.g.l.). The latter emphasizes the special value of tall tower observations in deriving regional scale fluxes. Sustaining a dense observational network like CarboCount-CH will allow for independent monitoring of future climate agreements.

The Supplement related to this article is available online at doi:10.5194/acpd-0-1-2016-supplement.

Acknowledgements. This study was funded by the Swiss Federal Office for the Environment (FOEN) and by the Swiss National Science Foundation (SNSF) as part of the "~~CarboCount CH~~CarboCount-CH" Sinergia Project (Grant Number: CRSII2_136273). We thank the International Foundation High Altitude Research Stations Jungfraujoch and Gornergrat (HFSJG) for the opportunity to perform experiments on the Jungfraujoch, MeteoSwiss for providing meteorological observations at the site Lägern Hochwacht and COSMO model analysis, and Swiss FLUXNET for the meteorological observations at Früebüel. Measurements at Jungfraujoch were partly performed as part of the Swiss contribution to ICOS (www.icos-infrastructure.eu).

References

Alexe, M., Bergamaschi, P., Segers, A., Detmers, R., Butz, A., Hasekamp, O., Guerlet, S., Parker, R., Boesch, H., Frankenberg, C., Scheepmaker, R. A., Dlugokencky, E., Sweeney, C., Wofsy, S. C., and Kort, E. A.: Inverse modelling of CH4 emissions for 2010-2011 using different satellite retrieval products from GOSAT and SCIAMACHY, Atmos. Chem. Phys., 15, 113–133, doi:10.5194/acp-15-113-2015, 2015.

Baldauf, M., Seifert, A., Förstner, J., Majewski, D., Raschendorfer, M., and Reinhardt, T.: Operational Convective-Scale Numerical Weather Prediction with the COSMO Model: description and Sensitivities, Mon. Weather Rev., 139, 3887–3905, doi:10.1175/MWR-D-10-05013.1, 2011.

Bamberger, I., Stieger, J., Buchmann, N., and Eugster, W.: Spatial variability of methane: attributing atmospheric concentrations to emissions, Environ. Pollut., 190, 65–74, doi:10.1016/j.envpol.2014.03.028, 2014.

Bamberger, I., Oney, B., Brunner, D., Henne, S., Leuenberger, M., Buchmann, N., and Eugster, W.: Observation of atmospheric methane and carbon dioxide: tall tower or mountain top stations?, Bound. Lay. Meteorol., in review, 2015.

Bergamaschi, P., Bräunlich, M., Marik, T., and Brenninkmeijer, C. A. M.: Measurements of the carbon and hydrogen isotopes of atmospheric methane at Izaña, Tenerife: seasonal cycles and synoptic-scale variations, J. Geophys. Res.-Atmos., 105, 14531–14546, doi:10.1029/1999JD901176, 2000.

Bergamaschi, P., Krol, M., Dentener, F., Vermeulen, A., Meinhardt, F., Graul, R., Ramonet, M., Peters, W., and Dlugokencky, E. J.: Inverse modelling of national and European CH_4 emissions using the atmospheric zoom model TM5, Atmos. Chem. Phys., 5, 2431–2460, doi:10.5194/acp-5-2431-2005, 2005.

Bergamaschi, P., Krol, M., Meirink, J. F., Dentener, F., Segers, A., van Aardenne, J., Monni, S., Vermeulen, A. T., Schmidt, M., Ramonet, M., Yver, C., Meinhardt, F., Nisbet, E. G., Fisher, R. E., O'Doherty, S., and Dlugokencky, E. J.: Inverse modeling of European CH4 emissions 2001–2006, J. Geophys. Res.-Atmos., 115, D22309, doi:10.1029/2010JD014180, 2010.

Bergamaschi, P., Houweling, S., Segers, A., Krol, M., Frankenberg, C., Scheepmaker, R. A., Dlugokencky, E., Wofsy, S. C., Kort, E. A., Sweeney, C., Schuck, T., Brenninkmeijer, C., Chen, H., Beck, V., and Gerbig, C.: Atmospheric CH4 in the first decade of the 21st century: inverse modeling analysis using SCIAMACHY satellite retrievals and NOAA surface measurements, J. Geophys. Res.-Atmos., 118, 7350–7369, doi:10.1002/jgrd.50480, 2013.

Bergamaschi, P., Corazza, M., Karstens, U., Athanassiadou, M., Thompson, R. L., Pison, I., Manning, A. J., Bousquet, P., Segers, A., Vermeulen, A. T., Janssens-Maenhout, G., Schmidt, M., Ramonet, M., Meinhardt, F., Aalto, T., Haszpra, L., Moncrieff, J., Popa, M. E., Lowry, D., Steinbacher, M., Jordan, A., O'Doherty, S., Piacentino, S., and Dlugokencky, E.: Top-down estimates of European CH_4 and N_2O emissions based on four different inverse models, Atmos. Chem. Phys., 15, 715–736, doi:10.5194/acp-15-715-2015, 2015.

Berhanu, T. A., Satar, E., Schanda, R., Nyfeler, P., Moret, H., Brunner, D., Oney, B., and Leuenberger, M.: Measurements of greenhouse gases at Beromünster tall tower station in Switzerland, Atmos. Meas. Tech. Discuss., 8, 10793–10822, doi:10.5194/amtd-8-10793-2015, 2015.

Brunner, D., Henne, S., Keller, C. A., Reimann, S., Vollmer, M. K., O'Doherty, S., and Maione, M.: An extended Kalman-filter for regional scale inverse emission estimation, Atmos. Chem. Phys., 12, 3455–3478, doi:10.5194/acp-12-3455-2012, 2012.

Brunner, D., Henne, S., Keller, C. A., Vollmer, M. K., and Reimann, S.: Estimating European Halocarbon Emissions Using Lagrangian Backward Transport Modeling and in Situ Measurements at the Jungfraujoch High-Alpine Site, in: Lagrangian Modeling of the Atmosphere, edited by Lin, J. C., Gerbig, C., Brunner, D., Stohl, A., Luhar, A., and Webley, P., vol. 200 of Geophysical Monographs V, 207–221, AGU, Washington, DC, 2013.

Chen, Y. H. and Prinn, R. G.: Estimation of atmospheric methane emissions between 1996 and 2001 using a three-dimensional global chemical transport model, J. Geophys. Res.-Atmos., 111, D10307, doi:10.1029/2005JD006058, 2006.

Collaud Coen, M., Praz, C., Haefele, A., Ruffieux, D., Kaufmann, P., and Calpini, B.: Determination and climatology of the planetary boundary layer height above the Swiss plateau by in situ and remote sensing measurements as well as by the COSMO-2 model, Atmos. Chem. Phys., 14, 13 205–13 221, doi:10.5194/acp-14-13205-2014, 2014.

Couwenberg, J. and Hooijer, A.: Towards robust subsidence-based soil carbon emission factors for peat soils in south-east Asia, with special reference to oil palm plantations, Mires and Peat, 12, 1–13, 2013.

Dentener, F., van Weele, M., Krol, M., Houweling, S., and van Velthoven, P.: Trends and inter-annual variability of methane emissions derived from 1979-1993 global CTM simulations, Atmos. Chem. Phys., 3, 73–88, doi:10.5194/acp-3-73-2003, 2003.

Dlugokencky, E. J., Myers, R. C., Lang, P. M., Masarie, K. A., Crotwell, A. M., Thoning, K. W., Hall, B. D., Elkins, J. W., and Steele, L. P.: Conversion of NOAA atmospheric dry air CH4 mole fractions to a gravimetrically prepared standard scale, J. Geophys. Res.-Atmos., 110, D18306, doi:10.1029/2005jd006035, 2005.

Emanuel, K. A. and Zivkovic-Rothman, M.: Development and evaluation of a convection scheme for use in climate models, J. Atmos. Sci., 56, 1766–1782, doi:10.1175/1520-0469(1999)056<1766:DAEOAC>2.0.CO;2, 1999.

Empa: Technischer Bericht zum Nationalen Beobachtungsnetz für Luftfremdstoffe (NABEL) 2015, Tech. Rep. http://www.empa.ch/web/s503/nabel, Empa, available at: http://www.empa.ch/documents/56101/246436/Nabel-technischer-bericht-15/, last access: 14 December 2015.

Enting, I. G.: Inverse Problems in Atmospheric Constituent Transport, Cambridge University Press, 2002.

Eugster, W., DelSontro, T., and Sobek, S.: Eddy covariance flux measurements confirm extreme CH_4 emissions from a Swiss hydropower reservoir and resolve their short-term variability, Biogeosciences, 8, 2815–2831, doi:10.5194/bg-8-2815-2011, 2011.

Felber, R., Münger, A., Neftel, A., and Ammann, C.: Eddy covariance methane flux measurements over a grazed pasture: effect of cows as moving point sources, Biogeosciences, 12, 3925–3940, doi:10.5194/bg-12-3925-2015, 2015.

FOEN: Switzerland's greenhouse gas inventory 1990–2012, Submission of April 2014 under the United Nations Framework Convention on Climate Change and under the Kyoto Protocol, Tech. rep., Federal Office for the Environment (FOEN), 2014.

FOEN: Switzerland's greenhouse gas inventory 1990–2013, Submission of April 2015 under the United Nations Framework Convention on Climate Change and under the Kyoto Protocol, Tech. rep., Federal Office for the Environment (FOEN), 2015.

Forster, C., Stohl, A., and Seibert, P.: Parameterization of convective transport in a Lagrangian particle dispersion model and its evaluation, J. Appl. Meteorol. Clim., 46, 403–422, doi:10.1175/JAM2470.1, 2007.

Furger, M.: Die Radiosondierungen von Payerne: dynamisch-klimatologische Untersuchungen zur Vertikalstruktur des Windfeldes, Ph. D. thesis, University of Bern, zugl. Diss., Univ. Bern, 1990, 1990.

Gal-Chen, T. and Somerville, R. C. J.: On the use of a coordinate transformation for the solution of the Navier–Stokes equations, Journal of Computational Physics, 17, 209–228, doi:10.1016/0021-9991(75)90037-6, 1975.

Ganesan, A. L., Rigby, M., Zammit-Mangion, A., Manning, A. J., Prinn, R. G., Fraser, P. J., Harth, C. M., Kim, K. R., Krummel, P. B., Li, S., Mühle, J., O'Doherty, S. J., Park, S., Salameh, P. K., Steele, L. P., and Weiss, R. F.: Characterization of uncertainties in atmospheric trace gas inversions using hierarchical Bayesian methods, Atmos. Chem. Phys., 14, 3855–3864, doi:10.5194/acp-14-3855-2014, 2014.

Ganesan, A. L., Manning, A. J., Grant, A., Young, D., Oram, D. E., Sturges, W. T., Moncrieff, J. B., and O'Doherty, S.: Quantifying methane and nitrous oxide emissions from the UK and Ireland using a national-scale monitoring network, Atmos. Chem. Phys., 15, 6393–6406, doi:10.5194/acp-15-6393-2015, 2015.

Gao, Z., Yuan, H., Ma, W., Li, J., Liu, X., and Desjardins, R. L.: Diurnal and Seasonal Patterns of Methane Emissions from a Dairy Operation in North China Plain, Advances in Meteorology, 2011, 190234, doi:10.1155/2011/190234, 2011.

Gerbig, C., Lin, J. C., Munger, J. W., and Wofsy, S. C.: What can tracer observations in the continental boundary layer tell us about surface-atmosphere fluxes?, Atmos. Chem. Phys., 6, 539–554, doi:10.5194/acp-6-539-2006, 2006.

Gerbig, C., Körner, S., and Lin, J. C.: Vertical mixing in atmospheric tracer transport models: error characterization and propagation, Atmos. Chem. Phys., 8, 591–602, doi:10.5194/acp-8-591-2008, 2008.

Hein, R., Crutzen, P. J., and Heimann, M.: An inverse modeling approach to investigate the global atmospheric methane cycle, Global Biogeochem. Cy., 11, 43–76, doi:10.1029/96GB03043, 1997.

Henne, S., Brunner, D., Folini, D., Solberg, S., Klausen, J., and Buchmann, B.: Assessment of parameters describing representativeness of air quality in-situ measurement sites, Atmos. Chem. Phys., 10, 3561–3581, doi:10.5194/acp-10-3561-2010, 2010.

Hiller, R. V., Bretscher, D., DelSontro, T., Diem, T., Eugster, W., Henneberger, R., Hobi, S., Hodson, E., Imer, D., Kreuzer, M., Künzle, T., Merbold, L., Niklaus, P. A., Rihm, B., Schellenberger, A., Schroth, M. H., Schubert, C. J., Siegrist, H., Stieger, J., Buchmann, N., and Brunner, D.: Anthropogenic and natural methane fluxes in Switzerland synthesized within a spatially explicit inventory, Biogeosciences, 11, 1941–1959, doi:10.5194/bg-11-1941-2014, 2014a.

Hiller, R. V., Neininger, B., Brunner, D., Gerbig, C., Bretscher, D., Künzle, T., Buchmann, N., and Eugster, W.: Aircraft-based CH4 flux estimates for validation of emissions from an agriculturally dominated area in Switzerland, J. Geophys. Res.-Atmos., 119, 4874–4887, doi:10.1002/2013JD020918, 2014b.

Houweling, S., Kaminski, T., Dentener, F., Lelieveld, J., and Heimann, M.: Inverse modeling of methane sources and sinks using the adjoint of a global transport model, J. Geophys. Res.-Atmos., 104, 26137–26160, doi:10.1029/1999JD900428, 1999.

Hu, L., Montzka, S. A., Miller, J. B., Andrews, A. E., Lehman, S. J., Miller, B. R., Thoning, K., Sweeney, C., Chen, H., Godwin, D. S., Masarie, K., Bruhwiler, L., Fischer, M. L., Biraud, S. C., Torn, M. S., Mountain, M., Nehrkorn, T., Eluszkiewicz, J., Miller, S., Draxler, R. R., Stein, A. F., Hall, B. D., Elkins, J. W., and Tans, P. P.: U. S. emissions of HFC-134a derived for 2008–2012 from an extensive flask-air sampling network, J. Geophys. Res.-Atmos., 120, 801–825, doi:10.1002/2014JD022617, 2015.

IPCC: 2006 IPCC Guidelines for National Greenhouse Gas Inventories, available at: http://www.ipcc-nggip.iges.or.jp/public/2006gl/index.html, last access: 9 September 2015, 2006.

Jeong, S., Zhao, C., Andrews, A. E., Bianco, L., Wilczak, J. M., and Fischer, M. L.: Seasonal variation of CH4 emissions from central California, J. Geophys. Res. Atmos., 117, doi:10.1029/2011JD016896, 2012.

Jeong, S., Hsu, Y.-K., Andrews, A. E., Bianco, L., Vaca, P., Wilczak, J. M., and Fischer, M. L.: A multitower measurement network estimate of California's methane emissions, J. Geophys. Res. Atmos., 118, 11 339–11 351, doi:10.1002/jgrd.50854, 2013.

JRC/PBL: Emission Database for Global Atmosphere Research (EDGAR), release version 4.0, Tech. rep., available at: http://edgar.jrc.ec.europa.eu, last access: 9 September 2015, 2009.

Kirschke, S., Bousquet, P., Ciais, P., Saunois, M., Canadell, J. G., Dlugokencky, E. J., Bergamaschi, P., Bergmann, D., Blake, D. R., Bruhwiler, L., Cameron-Smith, P., Castaldi, S., Chevallier, F., Feng, L., Fraser, A., Heimann, M., Hodson, E. L., Houweling, S., Josse, B., Fraser, P. J., Krummel, P. B., Lamarque, J.-F., Langenfelds, R. L., Le Quere, C., Naik, V., O'Doherty, S., Palmer, P. I., Pison, I., Plummer, D., Poulter, B., Prinn, R. G., Rigby, M., Ringeval, B., Santini, M., Schmidt, M., Shindell, D. T., Simpson, I. J., Spahni, R., Steele, L. P., Strode, S. A., Sudo, K., Szopa, S., van der Werf, G. R., Voulgarakis, A., van Weele, M., Weiss, R. F., Williams, J. E., and Zeng, G.: Three decades of global methane sources and sinks, Nat. Geosci., 6, 813–823, doi:10.1038/ngeo1955, 2013.

Klevenhusen, F., Bernasconi, S. M., Kreuzer, M., and Soliva, C. R.: Experimental validation of the Intergovernmental Panel on Climate Change default values for ruminant-derived methane and its carbon-isotope signature, Animal Production Science, 51, 974–167, doi:10.1071/AN09112_CO, 2011.

Kort, E. A., Andrews, A. E., Dlugokencky, E., Sweeney, C., Hirsch, A., Eluszkiewicz, J., Nehrkorn, T., Michalak, A., Stephens, B., Gerbig, C., Miller, J. B., Kaplan, J., Houweling, S., Daube, B. C., Tans, P., and Wofsy, S. C.: Atmospheric constraints on 2004 emissions of methane and nitrous oxide in North America from atmospheric measurements and a receptor-oriented modeling framework, Journal of Integrative Environmental Sciences, 7, 125–133, doi:10.1080/19438151003767483, 2010.

Kretschmer, R., Gerbig, C., Karstens, U., Biavati, G., Vermeulen, A., Vogel, F., Hammer, S., and Totsche, K. U.: Impact of optimized mixing heights on simulated regional atmospheric transport of CO_2, Atmos. Chem. Phys., 14, 7149–7172, doi:10.5194/acp-14-7149-2014, 2014.

Kuenen, J. J. P., Visschedijk, A. J. H., Jozwicka, M., and Denier van der Gon, H. A. C.: TNO-MACC_II emission inventory; a multi-year (2003–2009) consistent high-resolution European emission in-

ventory for air quality modelling, Atmos. Chem. Phys., 14, 10963–10976, doi:10.5194/acp-14-10963-2014, 2014.

Manning, A. J., O'Doherty, S., Jones, A. R., Simmonds, P. G., and Derwent, R. G.: Estimating UK methane and nitrous oxide emissions from 1990 to 2007 using an inversion modeling approach, J. Geophys. Res.-Atmos., 116, D02305, doi:10.1029/2010JD014763, 2011.

McKain, K., Down, A., Raciti, S. M., Budney, J., Hutyra, L. R., Floerchinger, C., Herndon, S. C., Nehrkorn, T., Zahniser, M. S., Jackson, R. B., Phillips, N., and Wofsy, S. C.: Methane emissions from natural gas infrastructure and use in the urban region of Boston, Massachusetts, P. Natl. Acad. Sci. USA, 112, 1941–1946, doi:10.1073/pnas.1416261112, 2015.

Meirink, J. F., Bergamaschi, P., and Krol, M. C.: Four-dimensional variational data assimilation for inverse modelling of atmospheric methane emissions: method and comparison with synthesis inversion, Atmos. Chem. Phys., 8, 6341–6353, doi:10.5194/acp-8-6341-2008, 2008.

Michalak, A. M., Hirsch, A., Bruhwiler, L., Gurney, K. R., Peters, W., and Tans, P. P.: Maximum likelihood estimation of covariance parameters for Bayesian atmospheric trace gas surface flux inversions, J. Geophys. Res.-Atmos., 110, D24107, doi:10.1029/2005JD005970, 2005.

Mikaloff Fletcher, S. E., Tans, P. P., Bruhwiler, L. M., Miller, J. B., and Heimann, M.: CH4 sources estimated from atmospheric observations of CH4 and its 13C/12C isotopic ratios: 2. Inverse modeling of CH4 fluxes from geographical regions, Global Biogeochem. Cy., 18, GB4005, doi:10.1029/2004GB002224, 2004.

Miller, S. M., Wofsy, S. C., Michalak, A. M., Kort, E. A., Andrews, A. E., Biraud, S. C., Dlugokencky, E. J., Eluszkiewicz, J., Fischer, M. L., Janssens-Maenhout, G., Miller, B. R., Miller, J. B., Montzka, S. A., Nehrkorn, T., and Sweeney, C.: Anthropogenic emissions of methane in the United States, P. Natl. Acad. Sci. USA, 110, 20018–20022, doi:10.1073/pnas.1314392110, 2013.

Myhre, G., Shindell, D., Bréon, F., Collins, W., Fuglestvedt, J., Huang, J., Koch, D., Lamarque, J., Lee, D., Mendoza, B., Nakajima, T., Robock, A., Stephens, G., Takemura, T., and Zhang, H.: Anthropogenic and Natural Radiative Forcing, in: Climate Change 2013: The Physical Science Basis. Contribution of Working Group I to the Fifth Assessment Report of the Intergovernmental Panel on Climate Change, edited by: Stocker, T., Qin, D., Plattner, G., Tignor, M., Allen, S., Boschung, J., Nauels, A., Xia, Y., Bex, V., and Midgley, P., Cambridge University Press, Cambridge, UK and New York, NY, USA, 659–740, 2013.

Nisbet, E. G., Dlugokencky, E. J., and Bousquet, P.: Methane on the Rise-Again, Science, 343, 493–495, doi:10.1126/science.1247828, 2014.

Nocedal, J. and Wright, S. J.: Numerical optimization, Springer series in operation research and financial engineering, Springer-Verlag, New York, 2006.

Oney, B., Henne, S., Gruber, N., Leuenberger, M., Bamberger, I., Eugster, W., and Brunner, D.: The CarboCount CH sites: characterization of a dense greenhouse gas observation network, Atmos. Chem. Phys. Discuss., 15, 12911–12956, doi:10.5194/acpd-15-12911-2015, 2015.

Owen, J. J. and Silver, W. L.: Greenhouse gas emissions from dairy manure management: a review of field-based studies, Global Change Biology, 21, 550–565, doi:10.1111/gcb.12687, 2015.

Pillai, D., Gerbig, C., Ahmadov, R., Rödenbeck, C., Kretschmer, R., Koch, T., Thompson, R., Neininger, B., and Lavrié, J. V.: High-resolution simulations of atmospheric CO_2 over complex terrain – representing the Ochsenkopf mountain tall tower, Atmos. Chem. Phys., 11, 7445–7464, doi:10.5194/acp-11-7445-2011, 2011.

Ramanathan, V. and Xu, Y.: The Copenhagen Accord for limiting global warming: criteria, constraints, and available avenues, P. Natl. Acad. Sci. USA, 107, 8055–8062, doi:10.1073/pnas.1002293107, 2010.

Rella, C. W., Chen, H., Andrews, A. E., Filges, A., Gerbig, C., Hatakka, J., Karion, A., Miles, N. L., Richardson, S. J., Steinbacher, M., Sweeney, C., Wastine, B., and Zellweger, C.: High accuracy measurements of dry mole fractions of carbon dioxide and methane in humid air, Atmos. Meas. Tech. Discuss., 5, 5823–5888, doi:10.5194/amtd-5-5823-2012, 2012.

Rödenbeck, C., Houweling, S., Gloor, M., and Heimann, M.: CO2 flux history 1982-2001 inferred from atmospheric data using a global inversion of atmospheric transport, Atmos. Chem. Phys., 3, 1919–1964, doi:10.5194/acp-3-1919-2003, 2003.

Rotach, M. W., Wohlfahrt, G., Hansel, A., Reif, M., Wagner, J., and Gohm, A.: The World is Not Flat: implications for the Global Carbon Balance, B. Am. Meteorol. Soc., 95, 1021–1028, doi:10.1175/BAMS-D-13-00109.1, 2013.

Ruckstuhl, A. F., Henne, S., Reimann, S., Steinbacher, M., Vollmer, M. K., O'Doherty, S., Buchmann, B., and Hueglin, C.: Robust extraction of baseline signal of atmospheric trace species using local regression, Atmos. Meas. Tech., 5, 2613–2624, doi:10.5194/amt-5-2613-2012, 2012.

Schmidt, M., Graul, R., Sartorius, H., and Levin, I.: Carbon dioxide and methane in continental Europe: a climatology, and 222 Radon-based emission estimates, Tellus B, 48, 457–473, doi:10.3402/tellusb.v48i4.15926, 1996.

Schneider, N. and Eugster, W.: Climatic impacts of historical wetland drainage in Switzerland, Climatic Change, 80, 301–321, doi:10.1007/s10584-006-9120-8, 2007.

Schraff, C. H.: Mesoscale data assimilation and prediction of low stratus in the Alpine region, Meteorol. Atmos. Phys., 64, 21–50, doi:10.1007/BF01044128, 1997.

Schroth, M. H., Eugster, W., Gómez, K. E., Gonzalez-Gil, G., Niklaus, P. A., and Oester, P.: Above- and below-ground methane fluxes and methanotrophic activity in a landfill-cover soil, Waste Manage., 32, 879–889, doi:10.1016/j.wasman.2011.11.003, 2012.

Schubert, C. J., Diem, T., and Eugster, W.: Methane Emissions from a Small Wind Shielded Lake Determined by Eddy Covariance, Flux Chambers, Anchored Funnels, and Boundary Model Calculations: a Comparison, Environ. Sci. Technol., 46, 4515–4522, doi:10.1021/es203465x, 2012.

Shindell, D., Kuylenstierna, J. C. I., Vignati, E., van Dingenen, R., Amann, M., Klimont, Z., Anenberg, S. C., Muller, N., Janssens-Maenhout, G., Raes, F., Schwartz, J., Faluvegi, G., Pozzoli, L., Kupiainen, K., Höglund-Isaksson, L., Emberson, L., Streets, D., Ramanathan, V., Hicks, K., Oanh, N. T. K., Milly, G., Williams, M., Demkine, V., and Fowler, D.: Simultaneously Mitigating Near-Term Climate Change and Improving Human Health and Food Security, Science, 335, 183–189, doi:10.1126/science.1210026, 2012.

Stieger, J., Bamberger, I., Buchmann, N., and Eugster, W.: Validation of farm-scale methane emissions using nocturnal boundary layer budgets, Atmos. Chem. Phys. Discuss., 15, 21765–21802, doi:10.5194/acpd-15-21765-2015, 2015.

Stohl, A., Forster, C., Frank, A., Seibert, P., and Wotawa, G.: Technical note: The Lagrangian particle dispersion model FLEXPART version 6.2, Atmos. Chem. Phys., 5, 2461–2474, doi:10.5194/acp-5-2461-2005, 2005.

Stohl, A., Seibert, P., Arduini, J., Eckhardt, S., Fraser, P., Greally, B. R., Lunder, C., Maione, M., Mühle, J., O'Doherty, S., Prinn, R. G., Reimann, S., Saito, T., Schmidbauer, N., Simmonds, P. G., Vollmer, M. K., Weiss, R. F., and Yokouchi, Y.: An analytical inversion method for determining regional and global emissions of greenhouse gases: Sensitivity studies and application to halocarbons, Atmos. Chem. Phys., 9, 1597–1620, doi:10.5194/acp-9-1597-2009, 2009.

Tarantola, A.: Inverse Problem Theory and Methods for Model Parameter Estimation, SIAM, Philadelphia, PA, 2005.

Taylor, K. E.: Summarizing multiple aspects of model performance in a single diagram., J. Geophys. Res.-Atmos., 106, 7183–7192, 2001.

Thompson, R. L. and Stohl, A.: FLEXINVERT: an atmospheric Bayesian inversion framework for determining surface fluxes of trace species using an optimized grid, Geosci. Model Dev., 7, 2223–2242, doi:10.5194/gmd-7-2223-2014, 2014.

Thompson, R. L., Gerbig, C., and Rödenbeck, C.: A Bayesian inversion estimate of N_2O emissions for western and central Europe and the assessment of aggregation errors, Atmos. Chem. Phys., 11, 3443–3458, doi:10.5194/acp-11-3443-2011, 2011.

Thompson, R. L., Stohl, A., Zhou, L. X., Dlugokencky, E., Fukuyama, Y., Tohjima, Y., Kim, S. Y., Lee, H., Nisbet, E. G., Fisher, R. E., Lowry, D., Weiss, R. F., Prinn, R. G., O'Doherty, S., Young, D., and White, J. W. C.: Methane emissions in East Asia for 2000–2011 estimated using an atmospheric Bayesian inversion, J. Geophys. Res.-Atmos., 120, 4352–4369, doi:10.1002/2014JD022394, 2015.

Tiedtke, M.: A Comprehensive Mass Flux Scheme for Cumulus Parameterization in Large-Scale Models, Mon. Weather Rev., 117, 1779–1800, doi:10.1175/1520-0493(1989)117<1779:ACMFSF>2.0.CO;2, 1989.

Tolk, L. F., Meesters, A. G. C. A., Dolman, A. J., and Peters, W.: Modelling representation errors of atmospheric CO_2 mixing ratios at a regional scale, Atmos. Chem. Phys., 8, 6587–6596, doi:10.5194/acp-8-6587-2008, 2008.

Turner, A. J., Jacob, D. J., Wecht, K. J., Maasakkers, J. D., Lundgren, E., Andrews, A. E., Biraud, S. C., Boesch, H., Bowman, K. W., Deutscher, N. M., Dubey, M. K., Griffith, D. W. T., Hase, F., Kuze, A., Notholt, J., Ohyama, H., Parker, R., Payne, V. H., Sussmann, R., Sweeney, C., Velazco, V. A., Warneke, T., Wennberg, P. O., and Wunch, D.: Estimating global and North American methane emissions with high spatial resolution using GOSAT satellite data, Atmos. Chem. Phys., 15, 7049–7069, doi:10.5194/acp-15-7049-2015, 2015.

Tuzson, B., Hiller, R. V., Zeyer, K., Eugster, W., Neftel, A., Ammann, C., and Emmenegger, L.: Field intercomparison of two optical analyzers for CH_4 eddy covariance flux measurements, Atmos. Meas. Tech., 3, 1519–1531, doi:10.5194/amt-3-1519-2010, 2010.

Tuzson, B., Henne, S., Brunner, D., Steinbacher, M., Mohn, J., Buchmann, B., and Emmenegger, L.: Continuous isotopic composition measurements of tropospheric CO_2 at Jungfraujoch (3580 m a.s.l.), Switzerland: real-time observation of regional pollution events, Atmos. Chem. Phys., 11, 1685–1696, doi:10.5194/acp-11-1685-2011, 2011.

Vermeulen, A. T., Eisma, R., Hensen, A., and Slanina, J.: Transport model calculations of NW-European methane emissions, Environ. Sci. Policy, 2, 315–324, doi:10.1016/S1462-9011(99)00021-0, 1999.

Vogelezang, D. H. P. and Holtslag, A. A. M.: Evaluation and model impacts of alternative boundary-layer height formulations, Boundary-Layer Meteorology, 81, 245–269, doi:10.1007/BF02430331, 1996.

Wecht, K. J., Jacob, D. J., Frankenberg, C., Jiang, Z., and Blake, D. R.: Mapping of North American methane emissions with high spatial resolution by inversion of SCIAMACHY satellite data, J. Geophys. Res.-Atmos., 119, 7741–7756, doi:10.1002/2014JD021551, 2014.

Wennberg, P. O., Mui, W., Wunch, D., Kort, E. A., Blake, D. R., Atlas, E. L., Santoni, G. W., Wofsy, S. C., Diskin, G. S., Jeong, S., and Fischer, M. L.: On the Sources of Methane to the Los Angeles Atmosphere, Environ. Sci. Technol., 46, 9282–9289, doi:10.1021/es301138y, 2012.

Wüst-Galley, C., Grünig, A., and Leifeld, J.: Locating Organic Soils for the Swiss Greenhouse Gas Inventory, Tech. rep., Agroscope, 2015.

Zavala-Araiza, D., Lyon, D. R., Alvarez, R. A., Davis, K. J., Harriss, R., Herndon, S. C., Karion, A., Kort, E. A., Lamb, B. K., Lan, X., Marchese, A. J., Pacala, S. W., Robinson, A. L., Shepson, P. B., Sweeney, C., Talbot, R., Townsend-Small, A., Yacovitch, T. I., Zimmerle, D. J., and Hamburg, S. P.: Reconciling divergent estimates of oil and gas methane emissions, Proceedings of the National Academy of Sciences, 112, 15 597–15 602, doi:10.1073/pnas.1522126112, 2015.

Zeitz, J. O., Soliva, C. R., and Kreuzer, M.: Swiss diet types for cattle: how accurately are they reflected by the Intergovernmental Panel on Climate Change default values?, Journal of Integrative Environmental Sciences, 9, 199–216, doi:10.1080/1943815X.2012.709253, 2012.

Zellweger, C., Forrer, J., Hofer, P., Nyeki, S., Schwarzenbach, B., Weingartner, E., Ammann, M., and Baltensperger, U.: Partitioning of reactive nitrogen (NO_y) and dependence on meteorological conditions in the lower free troposphere, Atmos. Chem. Phys., 3, 779–796, doi:10.5194/acp-3-779-2003, 2003.

Zhao, C., Andrews, A. E., Bianco, L., Eluszkiewicz, J., Hirsch, A., MacDonald, C., Nehrkorn, T., and Fischer, M. L.: Atmospheric inverse estimates of methane emissions from Central California C8 - D16302, J. Geophys. Res. Atmos., 114, D16 302, doi:10.1029/2008JD011671, 2009.

Table 1. Overview of the location of the observational sites used in the study, including particle release heights as used in FLEXPART simulations. See text for details on release height selection.

Station	ID	Longitude (° E)	Latitude (° N)	Altitude (m a.s.l.)	COSMO-7 height (m a.s.l.)	Inlet height (m)	low release (m)	high release (m)
Beromünster	BEO	8.1755	47.1896	797	615	212	212 a.g.l.	1014 a.s.l.
Lägern Hochwacht	LHW	8.3973	47.4822	840	492	32	150 a.g.l.	250 a.g.l.
Schauinsland	SSL	7.9167	47.9000	1205	750	10	980 a.s.l.[a]	–
Jungfraujoch	JFJ	7.9851	46.5475	3580	2650	3	3100 a.s.l.[b]	–
Früebüel	FRU	8.5378	47.1158	982	711	5	50 a.g.l.	982 a.s.l.
Gimmiz	GIM	7.2480	47.0536	443	496	32	32 a.g.l.	–

[a] 920 m a.s.l. in FLEXPART-ECMWF
[b] 3000 m a.s.l. in FEXPART-ECMWF

Table 2. ~~Setup~~ Set-up of the base (B) and sensitivity inversions (S-X).

Inversion	Method	FLEXPART version	Sites	Baseline method	Seasonality	Prior emissions	Model/Observation uncertainty
B	Bayesian	COSMO	BEO, LHW, JFJ, SSL	Single	N	MAIOLICA	standard
S-V	Bayesian	COSMO	BEO, LHW, JFJ, SSL	Single	Y	MAIOLICA	standard
S-K	extKF	COSMO	BEO, LHW, JFJ, SSL	Single	Y	MAIOLICA	standard
S-EC	Bayesian	ECMWF	BEO, LHW, JFJ, SSL	Single	N	MAIOLICA	standard
S-T	Bayesian	COSMO	BEO, LHW, JFJ, SSL	Single	N	TNO/MACC-2	standard
S-E	Bayesian	COSMO	BEO, LHW, JFJ, SSL	Single	N	EDGAR	standard
S-S	Bayesian	COSMO	BEO, LHW, JFJ, SSL	Single	N	MAIOLICA	Stohl
S-ML	Bayesian	COSMO	BEO, LHW, JFJ, SSL	Single	N	MAIOLICA	ML
S-O1	Bayesian	COSMO	BEO	Single	N	MAIOLICA	standard
S-O2	Bayesian	COSMO	LHW	Single	N	MAIOLICA	standard
S-O3	Bayesian	COSMO	BEO LHW	Single	N	MAIOLICA	standard
S-O4	Bayesian	COSMO	BEO, LHW, JFJ, SSL, FRU	Single	N	MAIOLICA	standard
S-O5	Bayesian	COSMO	BEO, LHW, JFJ, SSL, FRU, GIM	Single	N	MAIOLICA	standard
S-B1	Bayesian	COSMO	BEO, LHW, JFJ, SSL	Gradient	N	MAIOLICA	standard
S-B2	Bayesian	COSMO	BEO, LHW, JFJ, SSL	Grid	N	MAIOLICA	standard

Table 3. Overview of parameters used for the construction of the uncertainty covariance matrices: contributions to model/observation uncertainty σ_{min} and σ_{srr}, baseline uncertainty factor f_{b}, baseline correlation length τ_{b}, prior correlation length L and prior Swiss emission uncertainty σ_{E}.

	σ_{min} (nmol mol^{-1})				σ_{srr} (–)				f_{b} (–)				τ_{b} (d)	L (km)	σ_{E} (%)
	BEO	LHW	SSL	JFJ	BEO	LHW	SSL	JFJ	BEO	LHW	SSL	JFJ			
Base inversion (B-B)															
low	11	16	11	17	0.53	0.47	0.34	0.36	1	1	1	1	14	50	16
high	22	23	11	17	0.45	0.46	0.35	0.36	1	1	1	1	14	50	16
ECMWF inversion (S-EC)															
low	1	21	11	17	0.76	0.45	0.34	0.35	1	1	1	1	14	50	16
high	14	22	11	17	0.52	0.45	0.35	0.35	1	1	1	1	14	50	16
Stohl09 (S-S)															
low	40	41	22	20	0	0	0	0	1	1	1	1	14	50	16
high	41	44	22	20	0	0	0	0	1	1	1	1	14	50	16
Maximum likelihood (S-ML)															
low	25	24	19	20	0.78	0.76	0.54	1.24	3.6	5.1	2.1	2.0	19	50	31
high	39	35	19	20	0.64	0.63	0.54	1.23	4.2	5.5	2.4	2.4	23	51	30
Extended Kalman Filter (S-K)															
low	14	14	14	14	0.5	0.5	0.5	0.5	–	–	–	–	–	50	16
high	14	14	14	14	0.5	0.5	0.5	0.5	–	–	–	–	–	50	16

Table 4. Overview of results of sensitivity inversions. E_A and E_B are the total Swiss CH_4 prior and posterior emissions (Gg yr^{-1}), respectively, and S is the posterior Taylor skill score for the individual sites. The settings of the sensitivity inversions are given in Table 2.

Inversion	Emissions		Skill score (S)					
	prior E_A	posterior E_B	BEO	LHW	SSL	JFJ	FRU	GIM
B low	183.0 ± 29.3	179.0 ± 7.0	0.83	0.89	0.91	0.78	0.77	0.50
B high	183.0 ± 29.3	195.0 ± 7.3	0.84	0.86	0.91	0.78	0.74	0.51
S-V low	183.0 ± 29.3	185.9 ± 6.5	0.84	0.89	0.91	0.77	0.77	0.51
S-V high	183.0 ± 29.3	197.3 ± 6.7	0.85	0.86	0.91	0.78	0.75	0.53
S-K low	179.6 ± 28.7	193.1 ± 13	0.92	0.94	0.94	0.84	–	–
S-K high	179.6 ± 28.7	216.7 ± 14	0.93	0.95	0.94	0.85	–	–
S-EC low	184.4 ± 28.0	171.1 ± 8.0	0.79	0.87	0.91	0.77	0.74	0.29
S-EC high	184.5 ± 29.0	182.1 ± 7.6	0.88	0.87	0.92	0.77	0.74	0.31
S-T low	188.1 ± 30.1	180.3 ± 7.2	0.82	0.89	0.91	0.78	0.74	0.44
S-T high	187.7 ± 29.7	199.1 ± 7.4	0.83	0.87	0.91	0.78	0.69	0.46
S-E low	228.2 ± 36.5	184.3 ± 7.9	0.84	0.89	0.90	0.77	0.75	0.43
S-E high	227.4 ± 36.4	207.1 ± 7.9	0.83	0.88	0.90	0.77	0.69	0.46
S-S low	183.3 ± 29.3	169.3 ± 7.5	0.79	0.84	0.89	0.77	0.70	0.39
S-S high	183.3 ± 29.3	197.6 ± 8.0	0.81	0.84	0.89	0.77	0.70	0.51
S-ML low	183.0 ± 37.3	158.4 ± 13	0.84	0.92	0.90	0.78	0.73	0.44
S-ML high	183.0 ± 65.6	168.7 ± 13	0.85	0.91	0.89	0.78	0.66	0.44
S-O1 low	184.9 ± 29.2	183.3 ± 10	0.85	0.83	0.84	0.62	0.78	0.40
S-O1 high	184.6 ± 29.5	200.8 ± 11	0.87	0.81	0.84	0.63	0.78	0.38
S-O2 low	185.8 ± 29.7	214.3 ± 11	0.77	0.90	0.83	0.66	0.77	0.57
S-O2 high	184.5 ± 29.6	229.6 ± 11	0.75	0.88	0.82	0.66	0.76	0.64
S-O3 low	183.3 ± 29.3	198.5 ± 7.9	0.85	0.91	0.84	0.66	0.79	0.49
S-O3 high	183.5 ± 29.4	221.3 ± 8.3	0.86	0.89	0.83	0.66	0.78	0.51
S-O4 low	183.3 ± 28.3	191.2 ± 6.2	0.84	0.90	0.91	0.78	0.82	0.46
S-O4 high	183.3 ± 29.2	207.7 ± 6.5	0.85	0.88	0.91	0.79	0.85	0.48
S-O5 low	181.9 ± 29.1	208.8 ± 6.0	0.84	0.90	0.92	0.79	0.83	0.66
S-O5 high	181.9 ± 29.1	224.3 ± 6.1	0.85	0.88	0.91	0.79	0.85	0.69
S-B1 low	183.0 ± 29.3	194.0 ± 6.9	0.83	0.89	0.92	0.79	0.77	0.49
S-B1 high	183.0 ± 29.3	211.7 ± 7.2	0.84	0.87	0.92	0.79	0.74	0.51
S-B2 low	183.0 ± 29.3	195.1 ± 6.9	0.88	0.89	0.92	0.83	0.82	0.62
S-B2 high	183.0 ± 29.3	223.6 ± 6.9	0.88	0.88	0.92	0.83	0.75	0.69

Table 5. Swiss CH_4 emissions ($Gg\,yr^{-1}$) by most relevant source process as reported by FOEN to UNFCCC for the year 2012 and total emissions as estimated by this study. Uncertainties denote 1σ confidence levels.

Source	~~FOEN~~ SGHGI 2014	~~FOEN~~ SGHGI 2015	This study
Total	176 ± 28	206 ± 33	197 ± 19
1A Fuel combustion	4.1	3.7	
1B Fugitive emissions from fuels	8.1	8.4	
2 Industrial processes	0.1	0.1	
3A Enteric fermentation	118.9	130.5	
3B Manure management	30.8	31.0	
5A Solid waste disposal on land	7.5	8.5	
5B Biological treatment of waste[a]	5.4	16.7	
5C Waste incineration[b]	0.3	0.3	
5D Waste water handling	0.4	6.8	

[a] composting and anaerobic digestion.
[b] without municipal solid waste incineration.

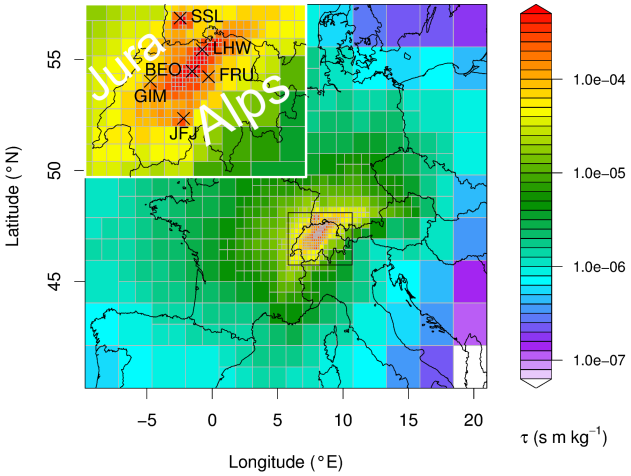

Figure 1. Total source sensitivity for the period March 2013 to February 2014 and the 4 sites used in the base inversion (crosses and labels in subplot; BEO: Beromünster, ~~LAE~~LHW: Lägern, JFJ: Jungfraujoch, SSL: Schauinsland). Source sensitivities are displayed on the reduced resolution grid that is used in the inversion. The units of the source sensitivity are given as residence times divided by atmospheric density and surface area. The locations of the two validation sites (FRU: Früebüel and GIM: Gimmiz) are given in the subplot as well.

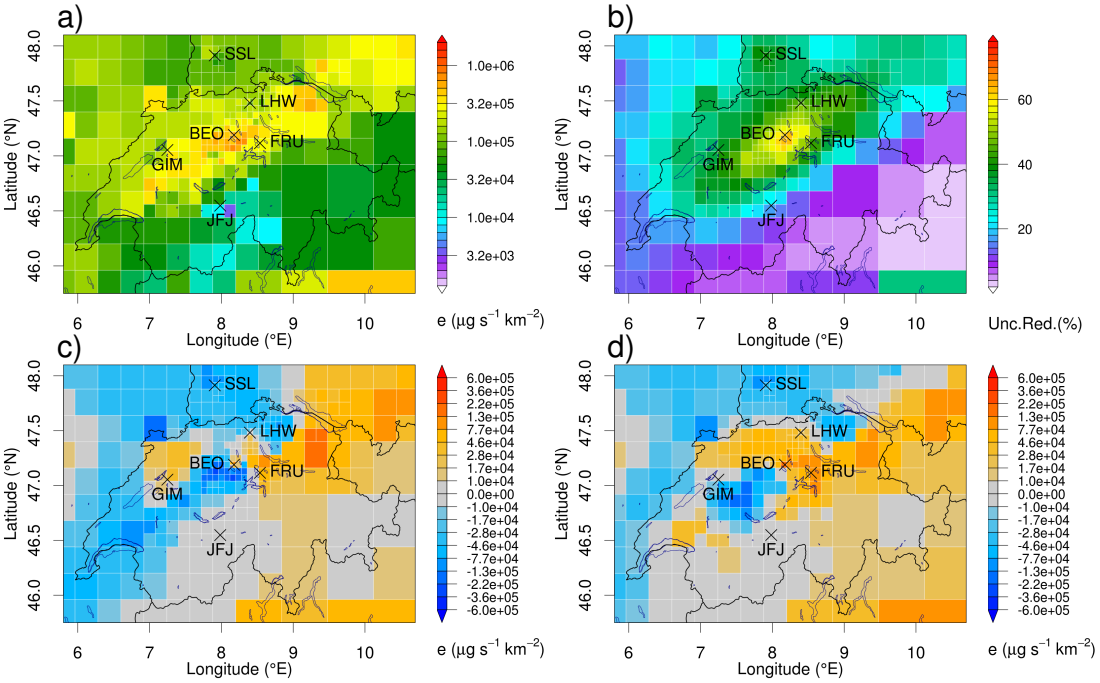

Figure 2. (a) prior and **(b)** posterior surface fluxes of CH_4 in the base inversion and low particle release heights (B low). **(c)** absolute and **(d)** relative (to prior) difference between posterior and prior emission fluxes. For panels c and d red (blue) colors indicate higher (lower) posterior than prior emissions.

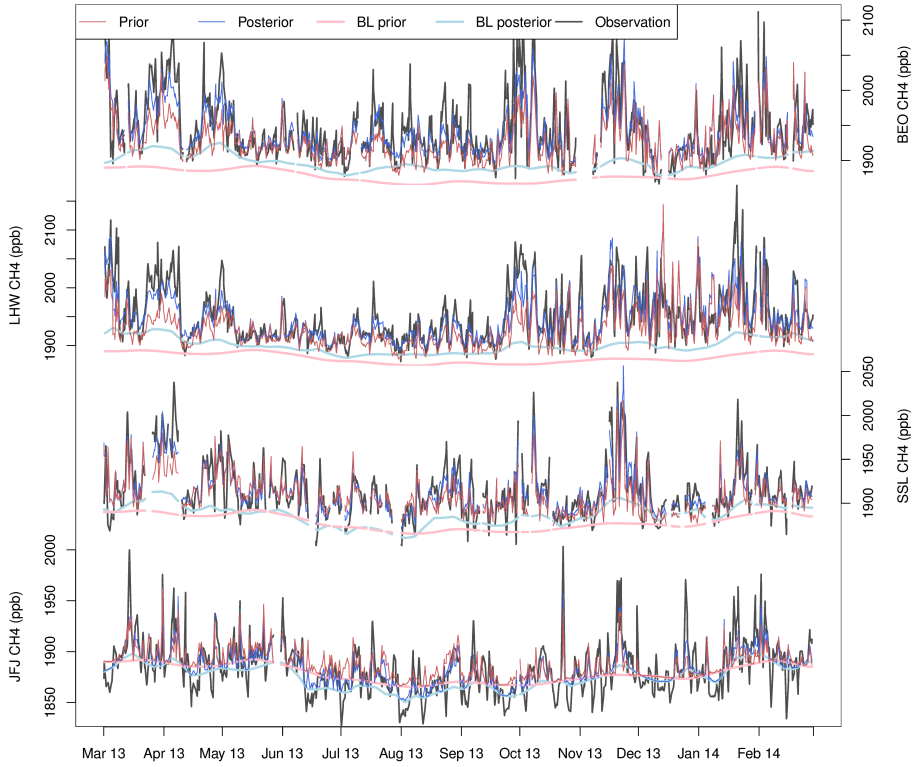

Figure 3. Observed (black) and simulated (prior: red; posterior: blue) CH_4 time series in the base inversion with low release heights (B low) at sites used in the inversion. Also given are the baseline mole fractions as used in the simulations (prior: light red; posterior: light blue). Note that the y axes were scaled for each site separately. All data represent 3-hourly averages.

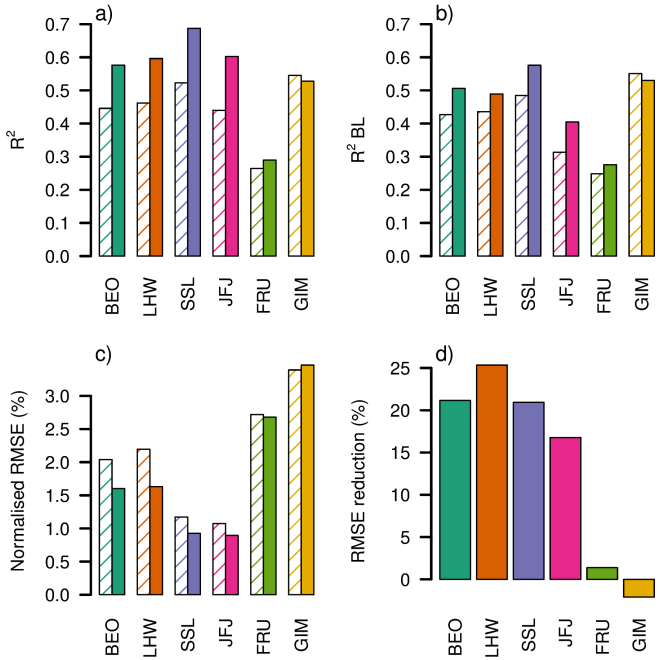

Figure 4. Model performance parameters for simulated time series at all sites for the base inversion with low particle release heights (B low): prior (shaded) and posterior (filled). **(a)** coefficient of determination (R^2) for complete signal and **(b)** above baseline signal, **(c)** normalised RMSE and **(d)** reduction of RMSE between prior and posterior. Note that the FRU and GIM sites were only used for validation but not in the inversion. All comparison statistics are based on 3-hourly averages.

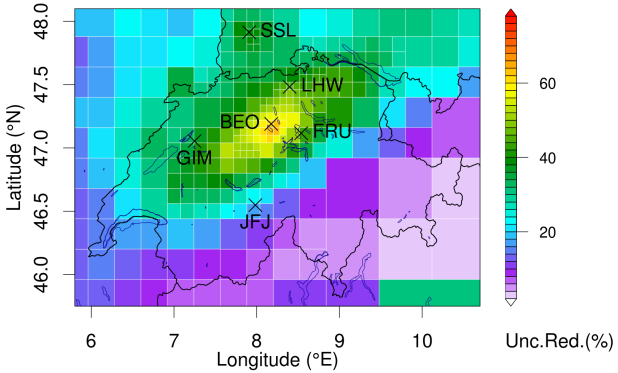

Figure 5. Uncertainty reduction between prior and posterior fluxes given in % relative to prior uncertainty ($1 - \sigma_B/\sigma_A$) for the base inversion with low partice release height.

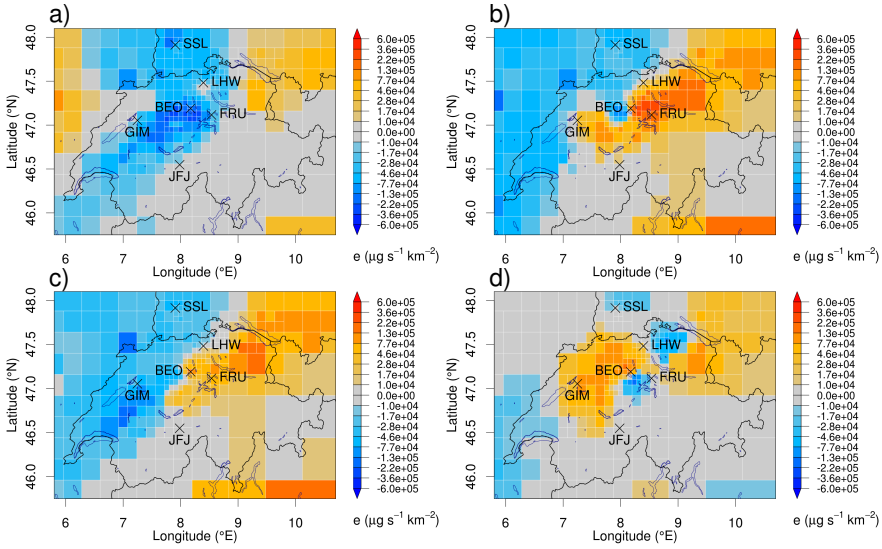

Figure 6. Absolute difference between posterior minus prior emission fluxes for seasonal inversion. **(a)** December, January, February, **(b)** March, April, May, **(c)** June, July, August, **(d)** September, October, November.

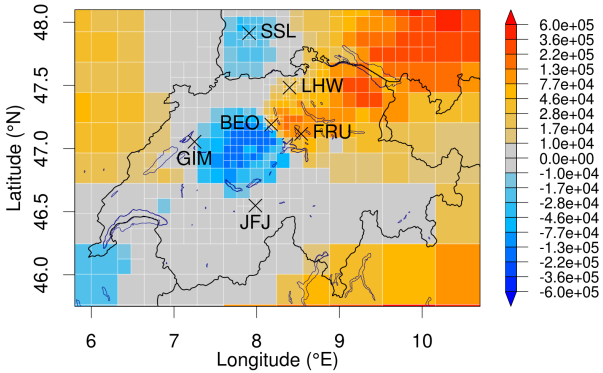

Figure 7. Absolute difference between posterior minus prior emission fluxes as obtained from extended Kalman filter inversion with low particle releases.

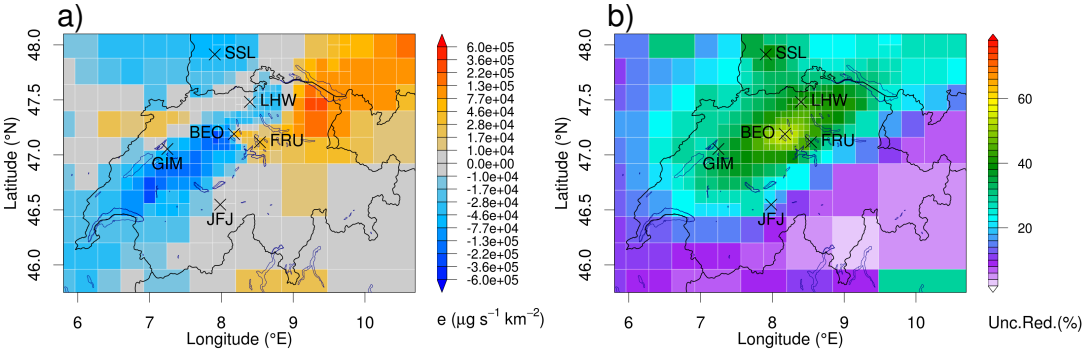

Figure 8. (a) Absolute difference between posterior minus prior emission fluxes for S-EC with low particle release height. **(b)** Uncertainty reduction between prior and posterior fluxes given in % relative to prior uncertainty ($1 - \sigma_B/\sigma_A$).

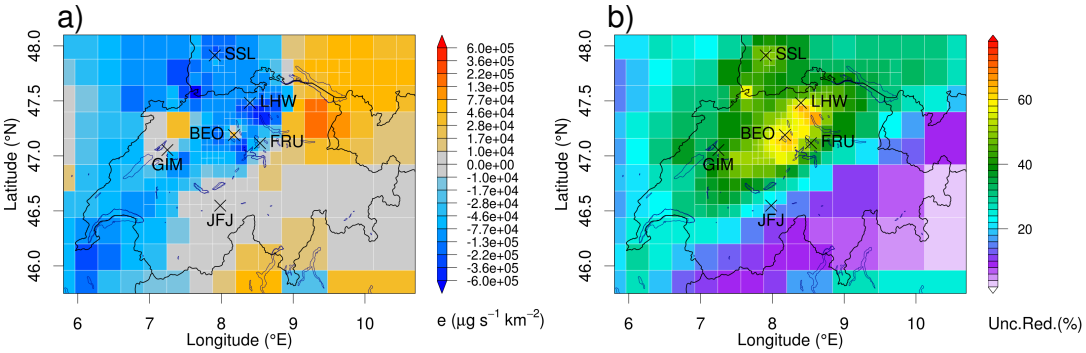

Figure 9. Absolute difference between posterior minus prior emission fluxes when using EDGAR instead of MAIOLICA prior fluxes.

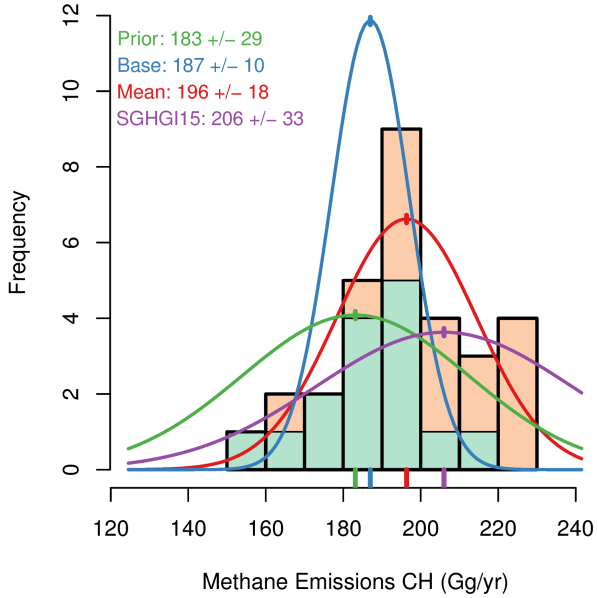

Figure 10. Histogram of total Swiss CH_4 emissions taken from all individual sensitivity inversions: low (light green) and high (light orange) particle releases. The base inversion prior (green) and posterior (blue) estimate as well as the average over all sensitivity inversions (red) and the ~~FOEN2015~~ SGHGI 2015 estimate (purple) are indicated by their Gaussian probability density functions.